A constitutive theory for high rate multiaxial deformation of snow
by Andrew Christian Hansen

A thesis submitted in partial fulfillment of the requirements for the degree of Doctor of Philosophy in Mechanical Engineering
Montana State University

Abstract:
The mechanical properties of snow under high strain rates and finite deformation are highly nonlinear and rate dependent. Unlike most geologic materials, snow can undergo substantial volumetric strains which are irreversible. Pressures may increase by orders of magnitude as snow is compressed from initially low densities of 100 kg/m^3 to densities beyond 500 kg/m^3. At the same time, the shearing stiffness can increase dramatically.

One of the most difficult problems encountered when trying to quantify snow mathematically is to account for the microstructure of the material. Naturally occurring snow generally has a complex microstructure which varies dramatically depending on the weather conditions to which it is subjected. The microstructural properties of snow have a significant impact on its mechanical properties.

In this thesis, a constitutive theory is developed to describe the mechanical properties of snow at finite strain under high rate multiaxial deformation. The theory is based on nonequilibrium thermodynamics with internal state variables. The internal variable approach is based on the view that the state of the material at any given time in a deformation process is adequately determined by the strain, internal energy, and a finite collection of internal state variables. The state variables may be thought of as characterizing the extent of microstructural rearrangement within a sample. This approach is appealing in that it incorporates parameters reflecting the microstructure of snow, while at the same time essentially remaining a continuum theory.

Results are presented for low to medium density snow subjected to a variety of multiaxial loading conditions. Volumetric strains in excess of 100 percent are considered. The theory is shown to reflect mechanical properties of snow such as rate dependence, stress relaxation, and strain recovery.

The constitutive theory is significant in that it is consistent with the first and second laws of thermodynamics as well as satisfying the principle of. material frame indifference. Equally significant is the inclusion of microstructural properties in the formulation. The internal state variable approach provides a powerful method of incorporating the microstructure of snow in a precise mathematical fashion.

A CONSTITUTIVE THEORY FOR HIGH RATE MULTIAXIAL DEFORMATION OF SNOW

by

Andrew Christian Hansen

A thesis submitted in partial fulfillment
of the requirements for the degree

of

Doctor of Philosophy

in

Mechanical Engineering

MONTANA STATE UNIVERSITY
Bozeman, Montana

December 1985

APPROVAL

of a thesis submitted by

Andrew Christian Hansen

This thesis has been read by each member of the thesis committee and has been found to be satisfactory regarding content, English usage, format, citation, bibliographic style, and consistency, and is ready for submission to the College of Graduate Studies.

12/2/85
Date

R L Brown
Chairperson, Graduate Committee

Approved for the Major Department

12/2/85
Date

Head, Major Department

Approved for the College of Graduate Studies

12-4-85
Date

Graduate Dean

STATEMENT OF PERMISSION TO USE

In presenting this thesis in partial fulfillment of the requirements for a doctoral degree at Montana State University, I agree that the Library shall make it available to borrowers under rules of the Library. I further agree that copying of this thesis is allowable only for scholarly purposes, consistent with "fair use" as prescribed in the U.S. Copyright Law. Requests for extensive copying or reproduction of this thesis should be referred to University Microfilms International, 300 North Zeeb Road, Ann Arbor, Michigan 48106, to whom I have granted "the exclusive right to reproduce and distribute copies of the dissertation in and from microfilm and the right to reproduce and distribute by abstract in any format."

Signature Andrew C Hansen

Date 12/2/85

ACKNOWLEDGMENTS

This research was funded by the U.S. Army Research Office, Grant No. DRXRO-18730-GS. I would like to express my appreciation to the Army Research Office for their support.

I would also like to thank Dr. Robert L. Brown for his guidance and the many useful discussions concerning the project. It has been a real pleasure to work with Dr. Brown.

Finally, I would like to express a special thank you to my wife Patty for her support and patience.

TABLE OF CONTENTS

TABLE OF CONTENTS—Continued

TABLE OF CONTENTS—Continued

LIST OF TABLES

LIST OF FIGURES

Figures

Appendix Figures

ABSTRACT

The mechanical properties of snow under high strain rates and finite deformation are highly nonlinear and rate dependent. Unlike most geologic materials, snow can undergo substantial volumetric strains which are irreversible. Pressures may increase by orders of magnitude as snow is compressed from initially low densities of 100 kg/m^3 to densities beyond 500 kg/m^3. At the same time, the shearing stiffness can increase dramatically.

One of the most difficult problems encountered when trying to quantify snow mathematically is to account for the microstructure of the material. Naturally occurring snow generally has a complex microstructure which varies dramatically depending on the weather conditions to which it is subjected. The microstructural properties of snow have a significant impact on its mechanical properties.

In this thesis, a constitutive theory is developed to describe the mechanical properties of snow at finite strain under high rate multiaxial deformation. The theory is based on nonequilibrium thermodynamics with internal state variables. The internal variable approach is based on the view that the state of the material at any given time in a deformation process is adequately determined by the strain, internal energy, and a finite collection of internal state variables. The state variables may be thought of as characterizing the extent of microstructural rearrangement within a sample. This approach is appealing in that it incorporates parameters reflecting the microstructure of snow, while at the same time essentially remaining a continuum theory.

Results are presented for low to medium density snow subjected to a variety of multiaxial loading conditions. Volumetric strains in excess of 100 percent are considered. The theory is shown to reflect mechanical properties of snow such as rate dependence, stress relaxation, and strain recovery.

The constitutive theory is significant in that it is consistent with the first and second laws of thermodynamics as well as satisfying the principle of material frame indifference. Equally significant is the inclusion of microstructural properties in the formulation. The internal state variable approach provides a powerful method of incorporating the microstructure of snow in a precise mathematical fashion.

CHAPTER 1

INTRODUCTION

Snow is a geologic material which dominates the polar climates and intermittently covers a much larger portion of the earth. Historically, it has received little attention from the rheological community. This is primarily because problems requiring knowledge of its material properties have been limited in the past. However, polar and alpine climates are receiving much more attention and use in recent years. Recreational use in the alpine back-country has increased dramatically. Polar regions are now being explored heavily for oil and natural gas reserves. Finally, recognition of the significance of snow from a military standpoint has increased.

Most of the past work in characterizing the material properties of snow has involved snow under low strain rates. However, the properties of snow are strongly rate dependent and there are a number of classical problems which require knowledge of the high rate properties of snow. Probably the most publicized is that of the snow avalanche. When an avalanche occurs in an area developed by man, the results are often disastrous. A recent example of this was the total destruction of the lift lodge and death of seven people at Alpine Meadows, California in March 1982.

Stress waves are another aspect of snow which require knowledge of its high rate properties. For example, snow has the ability to absorb a great deal of energy through material compaction resulting in tremendous attenuation rates for stress waves. Studies indicate that most of the energy produced by a classical one kilogram explosive is dissipated within a meter of the bomb sight. This becomes a significant problem when trying to initiate avalanches or clear mine fields covered by snow with explosives.

Vehicle mobility in alpine and polar terrain also requires knowledge of the high rate properties of snow. A snow cover has two degrading effects on the performance of a vehicle. First, large volumetric deformations occur from compaction by the wheels or tracks of the vehicle. This has the effect of reducing the total amount of energy available to propel the vehicle forward. Brown (1979b) has studied this problem and found that for some tracked military vehicles traveling at 20 mph in medium density snow (300-400 kg/m^3), the power absorbed by the snow cover can exceed 40 percent of the available engine power.

The second degrading effect of snow on vehicle performance is the loss of traction and danger in becoming stuck. This problem is much more difficult to analyze since slippage involves both deviatoric and volumetric deformations. Little success in characterizing this type of multiaxial deformation has been obtained.

The use of snow as a protective material has recently received attention from the field of penetration mechanics. Experimental evidence indicates snow is very effective at retarding projectile penetration (Aitken, 1978). At the same time, artillery shells tend to exhibit a delayed fuse action when impacting a snow cover. This dramatically decreases the effectiveness of the explosive since most of the energy is absorbed in the snow. Knowledge of the high rate multiaxial properties of snow would yield a better understanding of both of these phenomena.

Finally, although this dissertation is directed towards an investigation of snow, a valid constitutive law would represent a significant advancement in the theory of rate dependent deformation of granular materials under finite strain. This includes many geologic materials such as cohesive and cohesionless soils. The theory is also applicable to the field of high temperature powder metallurgy.

Some Unique Properties of Snow

Among all geologic materials, snow may be regarded as one of the most difficult to quantify mathematically. Naturally occurring snow generally has a complex stratigraphy which varies dramatically depending on the conditions it is subjected to while on the ground. These include rain, wind, extreme temperatures, melt-freeze cycles, and temperature gradient effects. The large variation in microstructure precludes modeling the snow as a simple collection of spheres or ellipses.

The reasons for the complex characteristics of a natural snow cover are two fold. First, the material is thermodynamically active because its natural state generally lies close to its melting point. Also, the material is highly porous with the ice phase typically occupying 5 to 50 percent of the material volume. These factors make the structure of snow susceptible to change resulting from changes in the weather. For instance, the ground temperature under a seasonal snow cover typically lies very close to 0°C. If this coincides with cooler ambient air conditions the snow is subjected to a vertical temperature gradient.[1] Under the influence of a temperature gradient, a mass flux of vapor from the zone of high vapor pressure deeper in the pack to the zone of low vapor pressure occurs. This facilitates the development of faceted crystals near the top of an air pore as water vapor is subliminated off the surfaces in the lower regions. Also, the bonds deteriorate most readily, causing an overall weakening of the snow cover. This process, known as temperature gradient metamorphism, has a dramatic effect on the properties of snow.[2]

Figure 1 shows the variation in compressive strength of four 0.1-m-thick layers of snow subjected to a constant temperature gradient. Notice the drastic loss of strength in the lower layers.

---

[1] This situation may also exist on temperate glaciers or polar ice which has been warmed during the summer.

[2] Adams and Brown (1983) review temperature gradient metamorphism.

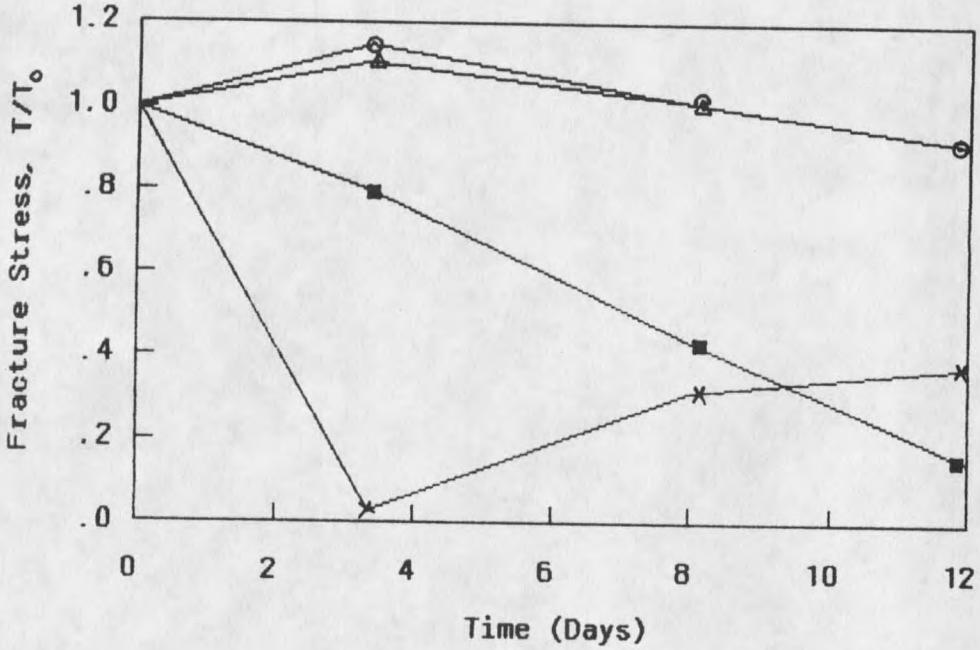

Figure 1. Characteristic reduction in strength in 0.4-m deep snow due to temperature gradient metamorphism (Bradley et al., 1977). T = 9500 Pa, $d\theta/dz$ = -50 K/m, (X) bottom layer, (■) second layer, (△) third layer, (○) top layer, ρ = 180 kg/m^3.

The high porosity of snow is also responsible for the complex deformation mechanisms observed in snow. Bond growth, bond fracture, pressure melting, and intergranular glide all contribute to the total deformation making modeling the deformation process difficult. These factors are compounded even further by the nonlinear rheological properties of the matrix material, ice. For instance, under compression ice is known to behave as an elastic-rate-sensitive plastic material. Under high rate deformation, the rate effects are pronounced.

Finally, snow has been shown to have the ability to rapidly heal itself giving it a limited memory of its past. This is primarily due to sintering of the ice grains. Sintering is the process by which a collection of loose particles form permanent bonds at their points of contact forming a solid framework. This process occurs more readily at temperatures near to, but still below the melting point. Studies indicate that for ice grains, a bond of measurable strength can form within minutes (Hobbs, 1974). Also, deformation induced cracks are thought to heal due to diffusion of vapor and sintering effects.

The driving force for the material rearrangement in sintering is supplied by a surplus of energy associated with the excess of free surface area in the material. Hence, the sintering process is intricately related to the microstructural properties of the material, specifically the mean surface area per unit volume and mean curvature (Reid, 1984). Furthermore, the sintering process significantly alters the microstructural state of the snow resulting in an overall strengthening of the snow cover.

Approach

In light of the above discussion, it is not surprising that previous efforts at characterizing the thermomechanical properties of snow have met with limited success. This is because the microstructural properties of snow are important in characterizing the material response. These properties vary dramatically depending on the weather conditions the snow is subjected to while on the ground. Therefore, the approach taken here is to formulate a continuum theory which incorporates parameters reflecting the microstructure of the snow.

The constitutive theory developed is designed to characterize the properties of snow under high rate multiaxial deformation. The theory is based on non-equilibrium thermodynamics with internal state variables. The internal variable approach is based on the view that the state of a material at any given time in the deformation process is adequately

determined by the strain, internal energy, and a finite collection of state variables. The state variables may be thought of as characterizing the extent of microstructural rearrangement within the sample. Furthermore, at any point in the deformation process, the variables may be fixed in theory, if not in principle, through imposition of appropriate constraints. In this manner, the deformation may be viewed as a series of constrained equilibrium states. The relation between the state variables and other state properties such as stress is then determined by the fictitious state of thermodynamic equilibrium referred to as the accompanying state.

The internal state variables identified in this work are of the "averaging" type on the granular level. By the term "averaging," it is meant that the variables refer to average characteristics of the structural rearrangements taken over all operative sites within the system. With some noted exceptions, this approach follows a formulation by Rice (1971) who developed a theory to describe the constitutive relations for metal plasticity using internal state variables at the microstructural level, e.g., crystalline slip, phase transformations, diffusional transport, etc.

Finally, the theory presented represents a significant deviation from classical plasticity. First, in classical plasticity, volumetric strains are purely elastic. This is hardly the case for snow which may undergo density changes of an order of magnitude under compression. The internal variable approach readily accommodates this property. Furthermore, unlike classical plasticity, the theory is rate dependent through the internal state variables which are governed by temporal evolution equations. This is extremely important for snow which has been shown to have strong rate dependent properties.

Results

Results of the constitutive theory are presented for uniaxial confined compression tests and combined compression and shear tests for multiple strain rates and volumetric strains exceeding 100 percent. The theory is shown to be capable of modeling phenomological properties of snow such as rate dependence, stress relaxation, and limited creep recovery.

CHAPTER 2

OVERVIEW

In this chapter, a general overview of the problems associated with characterizing the rheological properties of snow under high rate deformation and finite strain is given. First, a review of previous investigations on the high rate properties of snow is presented including experimental and analytical results. This is followed by a discussion of previous investigations of general thermomechanical constitutive relations. Included in this discussion is the internal state variable approach as well as other theories which may be applicable to snow. Finally, a description of the proposed problem is presented along with some of the important properties which should be incorporated into the constitutive theory.

It should be noted that the literature review presented is by no means exhaustive and is merely intended to provide a basis for subsequent work performed in this study. For an extensive review of snow research, the reader is referred to review articles by Mellor (1974, 1977). Also, an excellent foundation for studying thermomechanical constitutive relations can be found in Truesdell and Noll (1965).

Previous Investigations on the High Rate Properties of Snow

Much of the laboratory experimental work on high rate deformation of snow under finite strain was done by Napadenski (1964), Abele and Gow (1975, 1976), and Wakahama and Sato (1977). Napadenski's work was concerned with the response of snow subjected to high intensity shock waves. These experiments were conducted by accelerating a metal plate into a snow sample with the use of explosives. A streak camera was used to record the plastic wave speed and particle velocity at the shock front. This data was then used to

determine the shock adiabat (Hugoniot) for the snow sample using hydrodynamic theory. The shock adiabat is useful in that it defines an upper limit to the compressibility of snow for a given pressure. For an extensive review of hydrodynamic theory, the reader is referred to Duvall and Fowles (1963).

To this day the stress wave experiments performed by Napadenski provide the only Hugoniot data for snow. The snow samples for her work ranged from 390 to 530 kg/m^3 and are significantly higher than those normally encountered in a seasonal snow cover. However, a current set of shock tube experiments is being conducted at Los Alamos National Laboratory in conjunction with the United States Army Cold Regions Research and Engineering Laboratory (USACRREL). This should provide much needed information on the response of low density snow to shock waves.

Stress wave data for solid ice is also important to the field of snow mechanics. This has particular relevance to projectile penetration. For instance, inert steel and aluminum projectiles fired at velocities of around 10 m/s into snow with densities of 400 to 500 kg/m^3 are deformed plastically (Swinzow, 1972). These materials had yield stresses of $5(10)^2$ and $3(10)^2$ MPa respectively which are approaching the shock adiabat for ice. To this end, the works of Anderson (1968) and Gaffney (1985) on the shock adiabat of ice are cited.

Abele and Gow (1975, 1976) performed an extensive set of uniaxial compression tests on virgin and precompressed snow. Their work was primarily concerned with investigating the effects of temperature, initial density, and rate of deformation on the stresses produced. The tests were conducted with a 10,000 kg load capacity servo-controlled MTS machine with an environmental test chamber capable of maintaining temperatures down to -50°C. The cross head speeds ranged from 0.1 to 0.4 cm/s while the stresses produced ranged from 0.1 to 75 bar. To supplement this data, some microstructural analysis of the snow before and after the test was made. This was accomplished by preparing thin sections

of the snow and making photomicrographs. Full details of this technique are given in Gow (1969).

Wakahama and Sato (1977) studied the response of snow to a plastic wave by dropping a 1 kg mass 2 meters to a block of snow. The plastic wave speed was monitored using a high speed camera and the results were compared for snow whose initial density ranged from 170 to 460 kg/m^3 and free-water content from 0 to 17 percent. Changes in the snow structure were also studied using thin sections.

A number of field experiments have been conducted to supplement data taken in the laboratory. Stress wave studies using exposives have been conducted by numerous investigators. A review of work previous to 1965 is given by Mellor (1965). Albert (1983) provides still another review of more recent work. Brown and Hansen (1985) have conducted research on the significance of the pore pressure to the overall plastic wave. Studies indicate that the pore pressure is very significant to the overall response. Hansen and Brown (1985) have also analyzed the energy dissipation caused by ice fracture in a plastic wave. The results indicate that at least for pressures up to one MPa, energy dissipation by ice fracture is negligible.

The vast majority of analytical work on the constitutive properties of snow under high rate deformation has been done by Brown (1979a, 1980a). Brown (1979a) formulated a volumetric constitutive law for medium to high density snow based on a pore collapse model put forth by Carroll and Holt (1972). The model consists of spherical pores in a matrix of ice subjected to a hydrostatic pressure. A second volumetric constitutive law based on neck growth of grain bonds was formulated by Brown (1980a) for low density snow. This formulation is significant in that it successfully incorporates microstructural parameters for snow such as bond radius and bond length. Brown (1979b, 1980b,c,d; 1981a,b) has used these equations to study a number of significant problems including vehicle mobility and stress wave propagation.

As mentioned previously, the microstructure of snow plays an important role in the rheological characteristics of the material. Therefore, the study of the structure of snow has received a considerable amount of attention. Kry (1975a) has made an analysis of grain bonds in snow using quantitative stereology. Using this analysis, Kry (1975b) followed the evolution and subsequent effect of grain bonds on material properties under quasi-static uniaxial compression. Gubler (1978) has made significant advances in determining the mean number of bonds per snow grain using stereology. This is a very difficult problem to solve using only two-dimensional information. Finally, Good (1974) has developed a set of numerical parameters to identify the structure of snow.

In closing, there are numerous gaps in the knowledge of the material properties of snow under high rate deformation. This is particularly true for multiaxial states of stress where both experimental and theoretical results are scarce.

Principles of Thermomechanical Constitutive Theories

In describing the dynamic behavior of a continuum, there are three general principles which govern the material response (Truesdell and Noll, 1965). The principles of determinism and local action collectively state that the stress at a point in the body is determined by the history of an arbitrarily small neighborhood of the particle. The principle of material frame indifference states that the response of the material is independent of the observer. These principles are applicable to all classical work in continuum mechanics.

The difference in material response is governed by the specific constitutive assumptions made for the material. These assumptions can be mathematically stated using the principles of determinism and local action. The principle of frame indifference can then be used to place restrictions on the assumptions.

By introducing the thermodynamics of a continuum, an additional set of restrictions can be developed by application of the Second Law. This law takes the form of the

Clasius-Duhem inequality. The inequality implies there is internal entropy production in any irreversible process. Coleman and Noll (1963) present logical consequences of this law for a particular class of materials. These results have since become standard in making thermodynamic arguments.

One specific approach to describing the response of a material is put forth by Coleman and Noll (1960, 1961) in which the principle of fading memory is postulated.[3] This theory assumes that the entire past history of strain influences the stress. The principle is a smoothness postulate which requires the stress to be more sensitive to strains in the recent past as opposed to the distant past. Coleman (1964) developed a general theory of thermodynamics of simple materials with fading memory. Here, he assumed the stress was a function of the past history of the deformation gradient, temperature, and temperature gradient. The article is primarily concerned with restrictions placed on this type of material using the Second Law.

An alternative approach to the principle of fading memory is to postulate the existence of a set of internal state variables which characterize the state of the material at any given time and whose rate of change is governed by a set of temporal evolution equations. Coleman and Gurtin (1967) provide a detailed analysis of the thermodynamics of internal state variables. In this work no attempt is made to identify the specific nature of the variables as they are treated as abstract quantities. However, restrictions on the form of the state variables are developed based on the principle of material frame indifference.

Rice (1971) developed a general internal variable thermodynamic formalism for a class of solids at finite strain exhibiting inelasticity due to specific structural rearrangements on the microscale. In particular, he applied the theory to metals deforming plastically through dislocation motions. Specific kinetic relations for the rate of change of the

[3] This principle was later developed from a set of elementary axioms by Coleman and Mizel (1966).

state variables are postulated and discussed. Rice (1975) discusses the relation between macroscopic deformation and inelastic structural rearrangements which operate on the microscale. These microstructural changes include crystalline slip, diffusion, phase changes, and Griffith cracks. The thermodynamics of internal state variables is further investigated by Bataille and Kestin (1979). Finally, Lubliner (1972) examines evolution equations for internal variables yielding descriptions of viscoelastic, viscoplastic, and plastic behavior.

The work of Valanis (1966; 1971a,b) closely paralleled that of Coleman and Gurtin. Valanis (1966) applied the theory of irreversible thermodynamics to large deformation of viscoelastic materials. In this work he referred to the internal state variables as "hidden" coordinates and shows them to be scaler functionals of the history of the deformation. Valanis (1971a,b) used an internal variable formalism to describe the theory of viscoplasticity without a yield surface. To describe materials of this type he introduced an intrinsic time scale which is related to the external or real time through scaler material properties. As a result, he coined the term, "endochronic" theory.

Numerous papers have been written on the use of endochronic theory in geologic materials. Valanis and Read (1980) provide a brief review of endochronic theory including thermodynamics while introducing a new endochronic model for soils. Read et al. (1981) introduced an inelastic constitutive model for soils based on endochronic theory which incorporates critical state soil mechanics. A review of critical state soil mechanics can be found in Schofield and Wroth (1960). Harrison and Berger (1975, 1976) discuss the possible application of critical state theory to snow mechanics.

Finally, some recent theories of granular materials have shown promise for snow. Specifically, the pioneering work of Goodman (1969) and Goodman and Cowin (1972) are noted. In this theory, the bulk density of a granular material is written as the product of two scalers consisting of the matrix density and a volume distribution function. The

latter may be thought of as characterizing the spatial and time dependence of the porosity. By breaking the bulk density into two parts, an additional degree of freedom in describing the kinematics of the deformation has been introduced. This results in an additional balance equation known as the balance of equilibrated stress. Goodman (1969) shows that the equilibrated stress can represent a center of compression or dilatation in the material.

The theory of Goodman and Cowin has been expanded by Passman (1974, 1977) and Nunziato and Walsh (1980) by treating the volume fraction of each constituent of a mixture as an independent kinematical quantity.[4] This gives rise to additional balance laws describing the microstructural material response.

Description of the Problem

Most engineering materials, including a large class of geologic materials such as sand and many soils are largely incompressible with volumetric strains being small and elastic. By contrast, snow can undergo substantial volumetric strains under compression which are irreversible. Pressures may increase by orders of magnitude as snow is compressed from initially low densities of 100 kg/m^3 to densities beyond 500 kg/m^3. At the same time, the shearing stiffness may increase dramatically. The problem of characterizing the response of snow is further complicated by the material properties of ice which is the matrix material. Ice is a nonlinear, rate dependent material and these properties must be incorporated into the constitutive law.

During plastic deformation, the granular properties of the snow structure change dramatically as the microstructure adjusts to the applied loads. Under compression, the intergranular slip distances close as grains and grain bonds fracture, thereby allowing the grains to reorganize. At the same time, pressure sintering causes new bonds to be formed and "neck growth" in old bonds. Therefore, it is not sufficient to describe the state of the

[4] An extensive review of mixture theory is given by Bowen (1976).

material in terms of density alone. The introduction of internal state variables then provides a means of characterizing the plastic state of the material much more accurately.

As mentioned previously, I am concerned with the material response of snow to high rate deformation. However, only states of stress which produce a mean compressive state in addition to shearing will be considered. A mean tensile stress would simply fracture the material since snow behaves in a brittle fashion under this type of loading.

Finally, the constitutive theory developed should satisfy the following guidelines which are considered important in the modern theory of constitutive relations.

1. The constitutive law should satisfy the principle of material frame indifference.[5] This implies the constitutive equations are invariant under changes of frame of reference. That is, the response of a body to an applied load is independent of the observer.

   Frame indifference is extremely important when dealing with large deformation theory. Many constitutive equations developed in the past do not satisfy this condition. Such a shortcoming can produce erroneous results, particularly when finite rotations are involved.

2. The constitutive law should be consistent with the first and second laws of thermodynamics. In this manner, some knowledge of energy dissipation rates and recoverable energy can be obtained. Furthermore, the Second Law provides valuable restrictions on constitutive assumptions.

3. The constitutive law should be partially defined by the structural properties of the material.

4. The constitutive law should reflect the dominant deformation mechanisms for the material. For snow, some of the mechanisms considered are bond fracture and intergranular glide, and pressure sintering.

---

[5] Malvern (1969) provides an indepth discussion of frame indifference.

A constitutive theory based on the above criteria will by nature be very complex. However, the complex properties of snow require a formulation which is very general and requires few specific assumptions regarding material response. Some simplification to the resulting theory can be obtained by examining specific stress states.

CHAPTER 3

KINEMATICS, BASIC PRINCIPLES

In this chapter, the kinematics and basic thermomechanical principles of the dynamic behavior of a continuum are laid down. These include the balance of mass and momentum as well as the first and second laws of thermodynamics. The equations are developed within the context of large deformation theory.

Notation

Before proceeding with the theory, a brief discussion of the notation is presented. Unless otherwise noted, all work is referred to a general curvilinear coordinate system. Second order tensors will be represented by a subscripted tilde while first order tensors will be underlined. Dot and double dot products represent first and second order contractions of tensors. The transpose and inverse properties of a second order tensor will be denoted with the superscripts T and -1 respectively. Finally, the identity tensor will be denoted by $\underset{\sim}{1}$.

The following examples serve to clarify the notation discussed.

$$\underset{\sim}{A} = A^{ij}\,(\underline{g}_i\underline{g}_j) \quad ; \quad \underset{\sim}{B} = B_{ij}\,(\underline{g}^i\underline{g}^j) \quad ; \quad \underline{u} = u^i\underline{g}_i$$

$$\underset{\sim}{A}:\underset{\sim}{B} = A^{ij}\,B_{ij} = \mathrm{tr}(\underset{\sim}{A}^T\underset{\sim}{B}),$$

where tr denotes the trace (first invariant) of a second order tensor defined by

$$\mathrm{tr}(\underset{\sim}{T}) = T^k{}_k\,.$$

$$\underset{\sim}{A}\cdot\cdot\,\underset{\sim}{B} = A^{ij}\,B_{ji} = \mathrm{tr}(\underset{\sim}{A}\,\underset{\sim}{B})$$

$$\underset{\sim}{B}\,\underline{u} = B_{ij}\,u^j \underline{g}^i$$

$$\underset{\sim}{B}\,\underline{u} = \underline{u}\,\underset{\sim}{B}^T$$

The reader is referred to Malvern (1969) for an in-depth review of tensor algebra and tensor calculus.

Kinematics

A "body" β is a three-dimensional differential manifold, whose elements are called particles. The particles are denoted simply by X. If the particles at any instant occupy the region B, then B is called a "configuration."[6]

Normally, some configuration is chosen as one which is used to refer back to. This is called the "reference configuration," B_r. The body may be referred to a system of coordinates in this configuration which establishes a relationship between particles and triples of real numbers.

$$\underline{X} = \kappa\,(X) \tag{1}$$

where $\underline{X} = (X^1, X^2, X^3)$

The X^I are referred to as the material coordinates of the particle X. This relationship is one-to-one so there is an inverse relationship.

$$X = \kappa^{-1}\,(\underline{X})\,. \tag{2}$$

As the body is deformed, an entire family of configurations B are formed. Therefore, the position of a particle X changes with time. This can be expressed by the following relationship.

$$\underline{x} = \underline{\phi}\,(X, t) \tag{3}$$

The point $\underline{x} = \underline{\phi}\,(X, t)$ is the position occupied by the particle X at time t.

---

[6] A body β is invariant. The region it occupies is not.

There are four approaches to describing the motion of a continuum in common use. These are the material, referential, spatial, and relative descriptions (Truesdell, 1965). Malvern (1969) provides a brief discussion of each of these approaches. The intent here is to provide a basis for the work which follows. Therefore, only the referential and spatial descriptions will be discussed as the others do not appear in any of the discussions.

The referential description is the preferred approach in elasticity where it is assumed the body will return to its natural state when unloaded. This will be the approach followed. However, under finite deformation it is often difficult to attach physical significance to some of the variables in the referential description. In contrast, the physical significance of variables in the deformed configuration is much clearer. Furthermore, the basic principles which govern the dynamic behavior of a continuum are usually derived in the deformed configuration and then transferred back to the reference configuration when necessary. Therefore, a discussion of the spatial description is also provided.

Referential Description

The referential description refers the motion of the body to a reference configuration in which the particle X occupies the position $\underline{X}$. I will define the reference position to be the position occupied at t=0. This is often referred to as the Lagrangian description.

Recall the following relationships.

$$\underline{X} = \kappa\,(X) \quad ; \quad X = \kappa^{-1}\,(\underline{X})$$

$$\underline{x} = \underline{\phi}\,(X, t)$$

where $\underline{x}$ = the position of the particle X in the deformed configuration,

and $\underline{X}$ = the position of the particle X in the reference configuration.

The spatial position can be put in terms of the reference configuration through the inverse mapping κ^{-1}.

$$\underline{x} = \underline{\phi}\,(\kappa^{-1}\,(\underline{X}), t) = \underline{\chi}\,(\underline{X}, t) \tag{4}$$

The velocity of the particle X which occupies the position $\underline{X}$ in B_r is then

$$\underline{V} = \dot{\underline{x}} = \frac{\partial \underline{\chi}(\underline{X}, t)}{\partial t} = \frac{d\underline{\chi}(\underline{X}, t)}{dt} \tag{5}$$

since $\underline{X}$ is not a function of time. Similarly, the acceleration of the particle X is given by

$$\underline{A} = \ddot{\underline{x}} = \frac{\partial^2 \underline{\chi}(\underline{X}, t)}{\partial t^2} = \frac{d^2 \underline{\chi}(\underline{X}, t)}{dt^2} \tag{6}$$

More generally, if $\Psi(\underline{X}, t)$ is any scaler, vector, or tensor valued property of the material, the material time derivatives of Ψ are just

$$\dot{\Psi} = \frac{d\Psi(\underline{X}, t)}{dt} \quad \text{and} \quad \Psi^{(n)} = \frac{d^n\Psi(\underline{X}, t)}{dt^n} \tag{7}$$

Spatial (Eulerian) Description

The spatial description focuses attention on a given region of space as opposed to a given body of matter. Hence, the kinematics are described in terms of the instantaneous position $\underline{x}$. This can be accomplished since the relation

$$\underline{x} = \underline{\chi}(\underline{X}, t)$$

is assumed to be invertable, i.e., one can write

$$\psi(\underline{x}, t) = \Psi(\underline{\chi}^{-1}(\underline{x}, t), t), \tag{8}$$

where ψ may be any scaler, vector, or tensor valued property of the material.

Derivatives of $\psi(\underline{x}, t)$ must take into account the fact that $\underline{x}$ is now a function of time. Therefore, the material derivative of $\psi(\underline{x}, t)$ is

$$\frac{d\psi}{dt} = \frac{\partial \psi(\underline{x}, t)}{\partial t} + (\psi \overleftarrow{\underline{\nabla}}_x)\frac{d\underline{x}}{dt}$$

$$= \frac{\partial \psi(\underline{x}, t)}{\partial t} + (\psi \overleftarrow{\underline{\nabla}}_x)\underline{v} \tag{9}$$

where $\frac{\partial \psi}{\partial t}$ = local rate of change,

and $(\psi \overleftarrow{\underline{\nabla}}_x)\,\underline{v}$ = convected rate of change.

In the above, $(\psi \overleftarrow{\underline{\nabla}}_x)$ is the gradient of ψ with respect to spatial coordinates. This can be distinguished from the gradient $(\Psi \overleftarrow{\underline{\nabla}})$ with respect to material coordinates by the subscript x. Hence, I adopt the following notation.

$$(\psi \overleftarrow{\underline{\nabla}}_x) = \underline{g}^i \frac{\partial \psi}{\partial x^i}$$

$$(\Psi \overleftarrow{\underline{\nabla}}) = \underline{G}^I \frac{\partial \Psi}{\partial X^I}$$

The distinction between the two sets of coordinates is further emphasized by the use of capital letters for coordinates and indices referred to the reference configuration.

As an example of the material derivative in spatial coordinates, the acceleration is just

$$\underline{a} = \frac{\partial \underline{v}}{\partial t} + (\underline{v} \overleftarrow{\underline{\nabla}}_x)\,\underline{v}\,, \tag{10}$$

where $(\underline{v} \overleftarrow{\underline{\nabla}}_x) = v^i|_j\,(\underline{g}_i \underline{g}^j)$,

and $v^i|_j$ are the covariant derivatives of the vector $\underline{v}$.

Large Deformation Theory

Due to the large deformations encountered when snow is loaded, the distinction between the deformed and undeformed states becomes significant. Therefore, it is necessary to develop the theory in terms of a finite deformation measure. This is much more difficult to use than the infinitesimal theory commonly used in engineering since additive decomposition of the displacement gradient into the sum of a pure rotation and pure strain is no longer possible.

Deformation Gradient

There are several different approaches to characterizing finite deformation using the Lagrangian description. The most fundamental approach is the deformation gradient. During a deformation, the following function is defined as a smooth mapping.

$$\underline{x} = \underline{\chi}\,(\underline{X}, t)\,,$$

where $\underline{X} = \kappa\,(X)$.

Given the above deformation, the "deformation gradient" is a second order tensor field with the form

$$\underset{\sim}{F} = (\underline{x}\,\overleftarrow{\underline{\nabla}}) = (\underline{\chi}\,(\underline{X}, t)\,\overleftarrow{\underline{\nabla}})\,. \tag{11}$$

Hence, it is the gradient of the current position with respect to a reference configuration.

As defined, the deformation gradient is a tensor with the following component form.

$$\underset{\sim}{F} = x^{i}|_{J}\,(\underline{g}_i\,\underline{G}^J)\,, \tag{12}$$

where $x^{i}|_{J}$ are the covariant derivatives of the vector components of $\underline{x}$.

This is a mixed tensor in the sense that the basis for $\underset{\sim}{F}$ consists of $\underline{g}_i$ in the deformed configuration and $\underline{G}^J$ in the reference configuration.

For a physical interpretation, the deformation gradient maps neighborhoods of a particle X in B_r into neighborhoods of X in B, Figure 2. More precisely, $\underset{\sim}{F}$ is a linear mapping which operates on an arbitrary infinitesimal vector $d\underline{X}$ at $\underline{X}$ to associate with it a vector $d\underline{x}$ at $\underline{x}$.

$$d\underline{x} = \underset{\sim}{F}\,d\underline{X} \tag{13}$$

This result comes directly from the definition of the gradient of a vector.

Consider any vector field $\underline{v}\,(\underline{X})$.

$$\underline{v}\,(\underline{X} + \underline{u}) = \underline{v}(\underline{X}) + \underline{v}'\,(\underline{X}, \underline{u}) + \underline{\epsilon}\,(\underline{X}, \underline{u}) \tag{14}$$

The Frechet derivative $\underline{v}'(\underline{X}, \underline{u})$ is given by

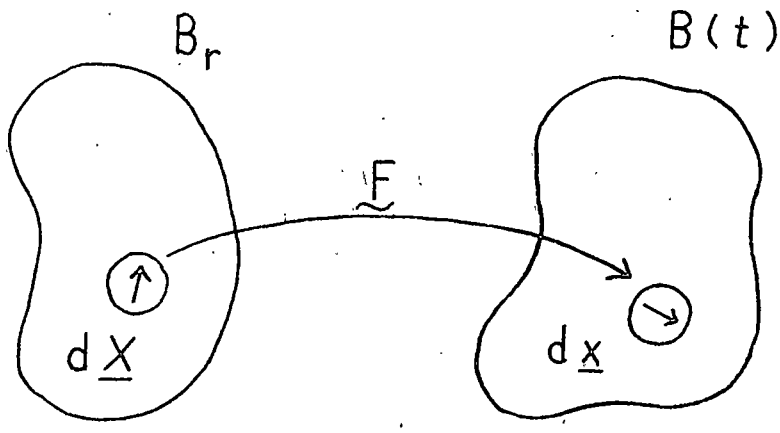

Figure 2. The mapping of the deformation gradient.

$$\underline{v}'(\underline{X}, \underline{u}) = (\underline{v}\overleftarrow{\underline{\nabla}})\underline{u} . \tag{15}$$

Therefore,

$$\underline{x}(\underline{X} + \underline{u}) = \underline{x}(\underline{X}) + (\underline{x}\overleftarrow{\underline{\nabla}})\underline{u} + \underline{\epsilon}(\underline{X}, \underline{u}) . \tag{16}$$

Setting $\underline{u} = \Delta\, \underline{X}$ and letting $\Delta\, \underline{X} \to 0$ gives

$$d\underline{x} = (\underline{x}\overleftarrow{\underline{\nabla}})d\underline{X} = \underset{\sim}{F}\, d\underline{X} .$$

The deformation gradient is interesting in that it contains information about the rotation as well as the strain of the body. As a result, constitutive relations employing this tensor must be constructed so as not to predict a stress due to rigid-body rotation. Furthermore, the deformation gradient is not symmetric and can have nine independent components in general.

Strain

A particular finite deformation measure which involves only the strain of the material vector $d\underline{X}$ is given by the Lagrangian strain tensor $\underset{\sim}{E}$. This tensor is defined so that it gives the change in the squared length of the material vector $d\underline{X}$ as follows.

$$(ds)^2 - (dS)^2 = 2\, d\underline{X} \cdot \underset{\sim}{E} \cdot d\underline{X}\,, \tag{17}$$

where $(ds)^2$ = the squared length of the material vector in the deformed configuration,

and $(dS)^2$ = the squared length of the material vector in the reference configuration.

The Lagrangian strain tensor may be expressed in terms of the deformation gradient as follows.

$$(ds)^2 = d\underline{x} \cdot d\underline{x} = (d\underline{X}\, \underset{\sim}{F}^T) \cdot (\underset{\sim}{F}\, d\underline{X}) = d\underline{X}\, (\underset{\sim}{F}^T \underset{\sim}{F})\, d\underline{X} \tag{18}$$

Therefore,

$$(ds)^2 - (dS)^2 = d\underline{X}(\underset{\sim}{F}^T \underset{\sim}{F})\, d\underline{X} - d\underline{X}\, \underset{\sim}{1}\, d\underline{X} = d\underline{X}\, (\underset{\sim}{F}^T \underset{\sim}{F} - \underset{\sim}{1})\, d\underline{X}\,. \tag{19}$$

Comparing the above results there follows,

$$\underset{\sim}{E} = \frac{1}{2}(\underset{\sim}{F}^T \underset{\sim}{F} - \underset{\sim}{1})$$

$$= \frac{1}{2}(\underset{\sim}{C} - \underset{\sim}{1})\,, \tag{20}$$

where $\underset{\sim}{C} = \underset{\sim}{F}^T \underset{\sim}{F}$ is defined as the Green deformation tensor.

For a comparison with the classical infinitesimal strain tensor one can write

$$x_i = X_I + u_I\,.$$

Substituting the above into Equation 20 and using rectangular Cartesian coordinates there follows,

$$E_{IJ} = \frac{1}{2}\left(\frac{\partial u_I}{\partial X^J} + \frac{\partial u_J}{\partial X^I} + \frac{\partial u_k}{\partial X^I}\frac{\partial u_k}{\partial X^J}\right). \tag{21}$$

This shows that if the partial derivatives of the displacement gradients U_I with respect to the material coordinates are small compared to unity, the second order terms may be neglected. This results in the infinitesimal strain tensor often used in engineering and classical elasticity.

It is interesting to note that the finite strain components of $\underset{\sim}{E}$ involve only linear and quadratic terms in the components of the displacement gradients. However, this is a complete finite strain tensor and not merely a second order approximation to it.

Finally, there are numerous other finite strain measures which can be referred to the reference configuration. In particular, multiplicative decompositions of the deformation gradient into a stretch and rotation tensor are common. However, I intend to develop the theory in terms of the Lagrangian strain and alternate strain definitions will no longer be considered.

General Mechanical Principles

In the following section, equations will be derived which give additional information on the way stress and deformation can vary in the neighborhood of a point with time. These equations express locally the conservation of mass and the balance of linear and angular momentum respectively. The equations are derived from integral forms of balance equations which express fundamental postulates of continuum mechanics and are therefore valid for any continuous medium.

The equations presented are usually expressed in terms of spatial coordinates and are well documented in this form. In contrast, the Lagrangian forms of these principles appear much less frequently. It is for this reason that the derivation of these equations is presented.

Conservation of Mass

Consider a body β and an arbitrary part $\mathcal{P}$ of β, Figure 3. The body β occupies the regions B_r in the reference configuration and B(t) in the configuration $\underline{x} = \underline{\chi}(\underline{X}, t)$. $\mathcal{P}$ occupies the region P_r in the reference configuration and P(t) in the spatial configuration. The boundaries of B and P are denoted respectively by $\partial B(t)$, $\partial P(t)$.

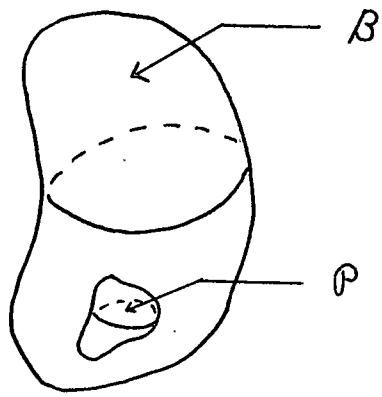

Figure 3. The body β and an arbitrary part $\mathcal{P}$ of β.

The principle of conservation of mass states that for any part $\mathcal{P}$ of β, there corresponds a positive number, $\mathcal{M}(\mathcal{P})$, called the *mass of part* $\mathcal{P}$, which remains invariant from one configuration to another. The mass is assumed to be smooth enough to permit the existence of a *mass density function*, $\rho_\chi(\underline{x}, t)$, such that

$$\mathcal{M}(\mathcal{P}) = \int_{P(t)} \rho_\chi(\underline{x}, t)\, dV . \tag{22}$$

Since the mass is independent of the configuration; if $\underline{\chi}(\underline{x}, t)$ and $\underline{\psi}(\underline{x}, t)$ are two different possible configurations, then there follows,

$$\mathcal{M}(\mathcal{P}) = \int_{P_\chi} \rho_\chi(\underline{x}, t)\, dV = \int_{P_\psi} \rho_\psi(\underline{x}, t)\, dV . \tag{23}$$

P_χ and P_ψ are just the two regions occupied respectively by the configurations $\underline{\chi}$ and $\underline{\psi}$. Unless there is a need, the subscripts for ρ will be dropped, i.e.,

$$\rho_\chi(\underline{x}, t) = \rho(\underline{x}, t) .$$

The one exception to this is the mass density in the reference configuration. In this case the notation $\rho_o(\underline{X})$ will be used and one can write

$$\mathcal{M}(\mathcal{P}) = \int_{P_r} \rho_o(\underline{X})\, dV_o = \int_{P(t)} \rho(\underline{x}, t)\, dV . \tag{24}$$

The above is a global statement of the principle of conservation of mass. Now put this in local form in terms of the Lagrangian coordinates. Malvern (1969) provides the following kinematic relationship between the deformed volume and the reference volume.

$$dV = \det(\underset{\sim}{F})\, dV_o \tag{25}$$

Using this expression, the spatial form of the mass measure may be referred back to the reference configuration.

$$\int_{P(t)} \rho(\underline{x}, t)\, dV = \int_{P_r} \rho(\underline{\chi}(\underline{X}, t), t) \det(\underset{\sim}{F})\, dV_o \tag{26}$$

Combining the above result with Equation 24 and collecting terms gives

$$\int_{P_r} [\rho_o(\underline{X}) - \rho(\underline{\chi}(\underline{X}, t), t) \det(\underset{\sim}{F})]\, dV_o = 0 . \tag{27}$$

This equation is valid for any part of the body β. This then requires

$$\rho_o(\underline{X}) - \rho(\underline{x}, t) \det(\underset{\sim}{F}) = 0 ;$$

or $$\frac{\rho_o}{\rho} = \det(\underset{\sim}{F}) . \tag{28}$$

This expression is the Lagrangian form of the principle of conservation of mass.

Balance of Momentum

For the momentum balance laws, two types of forces are considered.

a. *Surface forces* are forces distributed over the boundary of $\mathcal{P}$ and are caused by contact with other parts of β or other foreign bodies.

b. *External body forces* are forces distributed over the interior and are caused by the effects of an external body.

In the case of surface forces, it is assumed there exists a vector valued function, $\underline{t}_n(\underline{x}, t)$, called the *stress traction* which gives a measure of the force intensity transmitted across the surface (force/unit area) of ∂P. The total resultant of this is

$$\underline{P} = \int_{\partial P(t)} \underline{t}_n dS . \tag{29}$$

The stress traction may be expressed in terms of the Cauchy stress tensor, $\underset{\sim}{t}$, by the following.

$$\underline{t}_n = \underline{n}\,\underset{\sim}{t} = \underset{\sim}{t}^T \underline{n}\,, \tag{30}$$

where $\underset{\sim}{t} = t^{ij}\,(\underline{g}_i \underline{g}_j)$,

and the ith superscript represents the face acted on while the jth superscript represents the direction.

In a similar manner, a vector valued function $\underline{b}(\underline{x}, t)$ called the *body force density* (force/unit mass) is assumed to exist such that the total body force is

$$\underline{P} = \int_P \underline{b}(\underline{x}, t)\, \rho\,(\underline{x}, t)\, dV\,. \tag{31}$$

The momentum principle states that the time rate of change of the total momentum of a collection of particles equals the vector sum of all external forces acting on the particle. This fundamental postulate takes the form of the following axioms in continuum mechanics.

(M_1) Balance of Linear Momentum

$$\int_{\partial P(t)} \underline{t}_n dS + \int_{P(t)} \underline{b}(\underline{x}, t)\, \rho\,(\underline{x}, t)\, dV = \frac{d}{dt} \int_{P(t)} \underline{v}(\underline{x}, t)\, \rho\,(\underline{x}, t)\, dV \tag{32}$$

(M_2) Balance of Angular Momentum

$$\int_{\partial P(t)} (\underline{x} - \underline{x}_o) \times \underline{t}_n\,(\underline{x}, t) dS + \int_{P(t)} (\underline{x} - \underline{x}_o) \times \underline{b}(\underline{x}, t)\, \rho\,(\underline{x}, t)\, dV$$

$$= \frac{d}{dt} \int_{P(t)} (\underline{x} - \underline{x}_o) \times \underline{v}(\underline{x}, t)\, \rho\,(\underline{x}, t)\, dV \tag{33}$$

where $\underline{x}_o$ is some fixed point of a part $\mathcal{P}$ of β.

Consider the balance of linear momentum. Using the Reynold's Transport Theorem, axiom (M_1) may be rewritten as

$$\int_{\partial P(t)} \underline{t}_n dS + \int_{P(t)} \underline{b}(\underline{x}, t)\, \rho(\underline{x}, t)\, dV$$

$$= \int_{P(t)} \underline{a}(\underline{x}, t)\, \rho(\underline{x}, t)\, dV \,. \tag{34}$$

Now transform this expression to the reference configuration. Using conservation of mass there follows,

$$\int_{P(t)} \rho(\underline{x}, t)\, \underline{b}(\underline{x}, t)\, dV = \int_{P_r} \rho(\underline{\chi}(\underline{X}, t), t)\, \underline{b}(\underline{\chi}(\underline{X}, t)\, dV_o$$

$$= \int_{P_r} \underline{B}(\underline{X}, t)\, \rho_o\, dV_o \,. \tag{35}$$

Likewise, for the acceleration,

$$\int_{P(t)} \rho\, \underline{a}(\underline{x}, t)\, dV = \int_{P_r} \rho_o\, \underline{A}(\underline{X}, t)\, dV_o \,. \tag{36}$$

For the surface integral, define the force across the surface dS by $d\underline{P}$.

$$d\underline{P} = \underline{t}_n dS = \underline{n}\, \underset{\sim}{t}\, dS = (\underline{n}\, dS)\, \underset{\sim}{t} \tag{37}$$

The areas dS_o in B_r and dS in B(t) are related by the following expression (Malvern, 1969).

$$\underline{n}\, dS = \underline{N}\, \underset{\sim}{F}^{-1} \frac{\rho_o}{\rho}\, dS_o \tag{38}$$

where $\underline{n}$ is the unit normal in the deformed configuration,

and $\underline{N}$ is the unit normal in the reference configuration.

Using the above result, the force $d\underline{P}$ may be expressed as

$$d\underline{P} = (\underline{N}\, dS_o\, \underset{\sim}{F}^{-1} \frac{\rho_o}{\rho}\, \underset{\sim}{t}) = \underline{N}\, \underset{\sim}{T}\, dS_o \,, \tag{39}$$

where $\underset{\sim}{T} = \frac{\rho_o}{\rho} \underset{\sim}{F}^{-1} \underset{\sim}{t}$ is defined as the first Piola-Kirchhoff stress tensor.

Therefore, using Gauss's theorem,

$$\int_{\partial P(t)} \underline{n}\, \underset{\sim}{t}\, dS = \int_{P_r} \underline{N}\, \underset{\sim}{T}\, dS_o = \int_{P_r} \vec{\underline{\nabla}} \cdot \underset{\sim}{T}\, dV_o \,. \tag{40}$$

Combining Equations 32, 33 and 36 the balance of linear momentum acquires the form

$$\int_{P_r} [\vec{\underline{\nabla}} \cdot \underset{\sim}{T} + \rho_o \underline{B} - \rho_o \underline{A}] dV_o = 0 . \tag{41}$$

Since P is arbitrary, this requires

$$\vec{\underline{\nabla}} \cdot \underset{\sim}{T} + \rho_o \underline{B} = \rho_o \underline{A} . \tag{42}$$

The above is the equation of motion in the Lagrangian description. This is contrasted to the equation of motion in the Eularian description shown below.

$$\vec{\underline{\nabla}}_x \cdot \underset{\sim}{t} + \rho \underline{b} = \rho \underline{a} \tag{43}$$

For non-polar materials, the Cauchy stress tensor is symmetric, i.e.,

$$\underset{\sim}{t}^T = \underset{\sim}{t} . \tag{44}$$

This is actually the local form of the balance of angular momentum in spatial coordinates. In contrast, the first Piola-Kirchhoff stress tensor is non-symmetric in general. Therefore, often a second Piola-Kirchhoff stress tensor is introduced which is symmetric. This is given by

$$\underset{\sim}{S} = \frac{\rho_o}{\rho} \underset{\sim}{F}^{-1} \underset{\sim}{t} F^{-1T} . \tag{45}$$

The equation of motion using this tensor is given by

$$\vec{\underline{\nabla}} \cdot (\underset{\sim}{S} \underset{\sim}{F}^T) + \rho_o \underline{B} = \rho_o \underline{A} . \tag{46}$$

The physical relationships between the three stress tensors is shown in Figure 4. The Cauchy stress tensor gives the force transmitted across the area dS when operated on the unit normal, $\underline{n}$.

$$d\underline{P} = \underline{n} \underset{\sim}{t} \, dS \tag{47}$$

The first Piola-Kirchhoff stress tensor also gives the force transmitted across the area dS, but it does it with respect to the undeformed area.

$$d\underline{P} = \underline{N} \underset{\sim}{T} \, dS_o = \underline{n} \underset{\sim}{t} \, dS \tag{48}$$

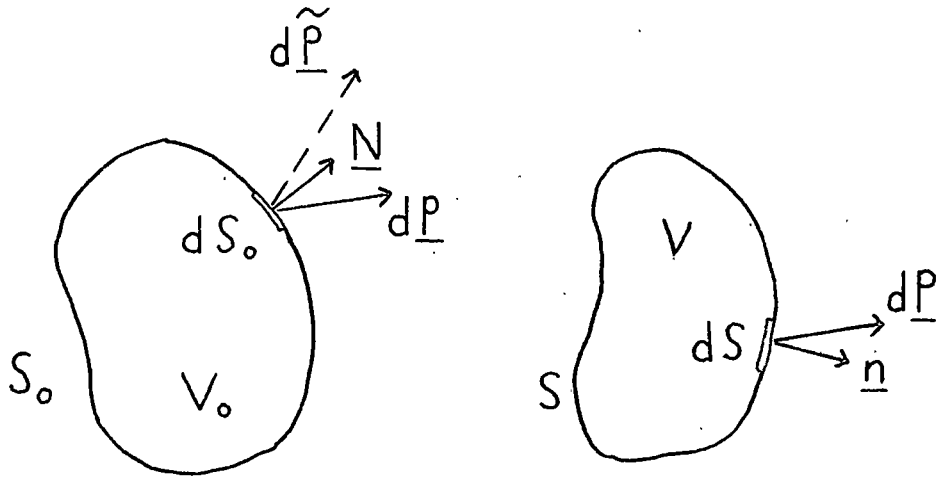

Figure 4. The relationship between the Cauchy stress tensor and the Piola-Kirchhoff stress tensors (Malvern, 1969).

In contrast, the second Piola-Kirchhoff stress tensor gives a force $d\tilde{\underline{P}}$ which is related to the force $d\underline{P}$ by the inverse of the deformation gradient.

$$d\tilde{\underline{P}} = \underline{N}\,\underset{\sim}{S}\,dS_o = \underset{\sim}{F}^{-1}\,d\underline{P} \tag{49}$$

Hence, the physical significance of the second Piola-Kirchhoff stress is often difficult to interpret.

Thermodynamics

Here the fundamental laws of thermodynamics are laid down as they apply to a continuum. The First Law provides a basis for determining the proper thermodynamic conjugate to be used with an associated choice of strain. The Second Law produces valuable mathematical restrictions on the constitutive assumptions.

First Law

The First Law requires that for any thermomechanical process, all energy exchanges within a body or a part of it must be accounted for. The global form of this law is given by

$$\frac{d}{dt}\int_{P(t)}(u+\frac{1}{2}\,\underline{v}\cdot\underline{v})\,\rho\,dV = \int_{\partial P(t)}[\underline{t}_n\cdot\underline{v}-\underline{q}\cdot\underline{v}]\,dS$$

$$+\int_{P(t)}[\rho r+\rho\,\underline{b}\cdot\underline{v}]\,dV \tag{50}$$

In the above expression:

u = the specific internal energy of the body. (This includes things such as strain energy, thermal energy, surface energy, etc.),

$\frac{1}{2}\underline{v}\cdot\underline{v}$ = the specific kinetic energy,

$\underline{q}$ = the heat flux vector,

and r = the heat supply.

The First Law states that the rate of change of energy (both internal and kinetic) is equated to the sum of:

1. The rate of work of boundary forces
2. The flux of heat across the boundary
3. Heat sources such as radiation
4. The rate of work of body forces

Using the Reynold's Transport Theorem and Gauss's Theorem, the global form of the First Law becomes,

$$\int_{P(t)}[\rho\,\dot{u}+\rho\,\underline{a}\cdot\underline{v}]\,dV$$

$$=\int_{P(t)}[\vec{\underline{\nabla}}_x\cdot(\underset{\sim}{t}\,\underline{v})-\vec{\underline{\nabla}}_x\cdot\underline{q}+\rho r+\rho\,\underline{b}\cdot\underline{v}]\,dV\,. \tag{51}$$

Now note the following identity.

$$\vec{\underline{\nabla}}_x\cdot(\underset{\sim}{t}\,\underline{v}) = (\vec{\underline{\nabla}}_x\cdot\underset{\sim}{t})\,\underline{v} + \mathrm{tr}(\underset{\sim}{t}\,\underset{\sim}{D})\,, \tag{52}$$

where $\underset{\sim}{D}$ is the rate of deformation tensor.

$$\underset{\sim}{D} = \frac{1}{2}(\underline{v}\,\overleftarrow{\underline{\nabla}}_x+\vec{\underline{\nabla}}_x\,\underline{v}) \tag{53}$$

Substituting Equation 52 into the First Law and collecting terms gives

$$\int_{P(t)} [\rho \underline{a} - \rho \underline{b} - \vec{\underline{\nabla}}_x \cdot \underset{\sim}{t}] \cdot \underline{v} + \rho \dot{u} - tr(\underset{\sim}{t}\, \underset{\sim}{D}) - \rho r + \vec{\underline{\nabla}}_x \cdot \underline{q}]\, dV = 0 . \tag{54}$$

The first term in the above expression is simply the equation of motion in spatial coordinates and is equal to zero. Therefore, one is left with

$$\int_{P(t)} [\rho \dot{u} - tr(\underset{\sim}{t}\, \underset{\sim}{D}) - \rho r + \vec{\underline{\nabla}}_x \cdot \underline{q}]\, dV = 0 . \tag{55}$$

Now express the above result in the reference configuration. Consider the stress power defined by $tr(\underset{\sim}{t}\, \underset{\sim}{D})$. The rate of deformation tensor is related to the time rate of change of the Lagrangian strain tensor by the following.

$$\underset{\sim}{D} = \underset{\sim}{F}^{-1T} \dot{\underset{\sim}{E}}\, \underset{\sim}{F}^{-1} \tag{56}$$

Using the above the stress power can be written as

$$tr(\underset{\sim}{t}\, \underset{\sim}{D}) = tr(\underset{\sim}{t}\, \underset{\sim}{F}^{-1T} \dot{\underset{\sim}{E}}\, \underset{\sim}{F}^{-1})$$

$$= tr((\underset{\sim}{F}^{-1}\, \underset{\sim}{t}\, \underset{\sim}{F}^{-1T})\, \dot{\underset{\sim}{E}}) = \frac{\rho}{\rho_o}\, tr(\underset{\sim}{S}\, \dot{\underset{\sim}{E}}) . \tag{57}$$

The divergence of the heat flux may be expressed in the reference configuration as follows.

$$\int_{P(t)} \vec{\underline{\nabla}}_x \cdot \underline{q}\, dV = \int_{\partial P(t)} \underline{n} \cdot \underline{q}\, dS$$

$$= \int_{\partial P_r} \frac{\rho_o}{\rho}\, \underline{N}\, \underset{\sim}{F}^{-1}\, \underline{q}\, dS = \int_{P_r} \frac{\rho_o}{\rho}\, \vec{\underline{\nabla}} \cdot (\underset{\sim}{F}^{-1}\, \underline{q})\, dV_o \tag{58}$$

Using Equations 57 and 58 the global form of the First Law in the reference configuration becomes

$$\int_{P_r} [\rho_o \dot{U} - tr(\underset{\sim}{S}\, \dot{\underset{\sim}{E}}) + \rho_o R + \frac{\rho_o}{\rho} \vec{\underline{\nabla}} \cdot (\underset{\sim}{F}^{-1}\, \underline{q})]\, dV_o = 0 . \tag{59}$$

Since the above integral is equal to zero for all parts P_r there follows,

$$\rho_o \dot{U} = tr(\underset{\sim}{S}\, \dot{\underset{\sim}{E}}) + \rho_o R + \frac{\rho_o}{\rho} \vec{\underline{\nabla}} \cdot (\underset{\sim}{F}^{-1}\, \underline{q}) . \tag{60}$$

Equation 60 is the local form of the First Law in the reference configuration. This shows that the second Piola-Kirchhoff stress tensor is the thermodynamic conjugate of the rate of change of the Lagrangian strain. In a similar manner, it can be shown that the first Piola-Kirchhoff stress tensor is conjugate to the rate of change of the deformation gradient.

Second Law

The Second Law is based on the observation that energy is dissipated in an irreversible process. The law postulates the existence of entropy as a state function and that internal entropy production is the result of dissipative irreversible processes. Further, the internal entropy production is zero for reversible processes. Hence, the Second Law requires

Rate of Entropy Increase $\geqslant$ Entropy Input Rate .

This may be expressed in a continuum form as follows.

$$\frac{d}{dt}\int_{P(t)} \rho\,\eta\, dV \geqslant \int_{P(t)} \frac{\rho r}{\theta}\, dV + \int_{\partial P(t)} \frac{-\underline{q}\cdot\underline{n}}{\theta}\, dS \tag{61}$$

where η is the specific entropy,

and θ is the temperature.

Again, using the transport theorem and Gauss's Theorem,

$$\int_{P(t)} [\rho\,\dot{\eta} - \frac{\rho r}{\theta} + \vec{\underline{\nabla}}_x \cdot (\frac{\underline{q}}{\theta})]\, dV \geqslant 0 \tag{62}$$

In terms of the reference configuration, Equation 62 becomes

$$\int_{P_r} [\rho_o \dot{H} - \frac{\rho_o R}{\Theta} + \frac{\rho_o}{\rho} \vec{\underline{\nabla}} \cdot (\frac{\underset{\sim}{F}^{-1}\,\underline{q}}{\Theta})]\, dV_o \geqslant 0 \tag{63}$$

This requires

$$\rho_o \dot{H} - \frac{\rho_o R}{\Theta} + \frac{\rho_o}{\rho} \vec{\underline{\nabla}} \cdot (\frac{\underset{\sim}{F}^{-1}\,\underline{q}}{\Theta}) \geqslant 0 \tag{64}$$

The above is known as the Clasius-Duhem inequality and is the local form of the Second Law. The divergence term can be expanded to give

$$\rho_o \dot{H} - \frac{\rho_o R}{\Theta} + \frac{\rho_o}{\rho}\frac{1}{\Theta}\vec{\underline{\nabla}} \cdot (\underset{\sim}{F}^{-1}\,\underline{q}) - \frac{1}{\Theta^2}\underset{\sim}{F}^{-1}\,\underline{q} \cdot \vec{\underline{\nabla}}\,\Theta \geqslant 0\,. \tag{65}$$

Now substitute the energy equation into the above to eliminate R and $\vec{\underline{\nabla}} \cdot \underset{\sim}{F}^{-1}\,\underline{q}$.

$$\rho_o \Theta \dot{H} - \rho_o \dot{U} + \mathrm{tr}(\underset{\sim}{S}\,\dot{\underset{\sim}{E}}) - \frac{1}{\Theta}\underset{\sim}{F}^{-1}\,\underline{q} \cdot \vec{\underline{\nabla}}\,\Theta \geqslant 0 \tag{66}$$

This expression is an alternate form of the Second Law. Finally, introduce the Helmholtz free energy, Φ, defined by

$$\Phi = U - \Theta H \tag{67}$$

This quantity represents the recoverable strain energy in the body. The material time derivative of the free energy is given by

$$\dot{\Phi} = \dot{U} - \dot{\Theta} H - \Theta \dot{H} \tag{68}$$

Substituting the above expression into Equation 66 provides still another form of the Second Law.

$$-\rho_o \dot{\Phi} - \rho_o H \dot{\Theta} + \mathrm{tr}(\underset{\sim}{S}\,\dot{\underset{\sim}{E}}) - \frac{1}{\Theta}\underset{\sim}{F}^{-1}\,\underline{q} \cdot \vec{\underline{\nabla}}\,\Theta \geqslant 0 \tag{69}$$

CHAPTER 4

GENERAL CONSTITUTIVE THEORY

A general constitutive theory for a class of inelastic materials at finite strain is presented within the framework of non-equilibrium thermodynamics. Specific constitutive relations are postulated and restrictions on their form are developed from the Second Law. General restrictions on the form of the evolution equations for the internal state variables are also explored. Finally, a brief description of the inverted form of the constitutive law is presented.

Constitutive Assumptions

I begin by assuming the existence of a caloric equation of state such that,

$$U = U(\underset{\sim}{E}, H, \underline{\xi}), \tag{70}$$

where U = the internal energy per unit *reference mass*,

H = the entropy per unit reference mass,

$\underset{\sim}{E}$ = the Lagrangian strain tensor,

and $\underline{\xi}$ = a finite collection of internal state variables characterizing the current pattern of structural arrangement on the granular level.

Hence, the internal state vector may be thought of as characterizing the plastic state of the material.

Restrictions on the form of $\underline{\xi}$ have been found by Coleman and Gurtin (1967) based on the principle of objectivity. They show that $\underline{\xi}$ cannot represent a vector of dimension three transforming as a spatial position vector under a change of frame, i.e.,

$$\underline{\xi}^* = \underset{\sim}{Q}(t)\,\underline{\xi}\,, \tag{71}$$

where $\underline{\xi}^*$ = the internal state vector in the starred reference frame,

$\underline{\xi}$ = the internal state vector in the unstarred reference frame,

and $\underset{\sim}{Q}(t)$ = any time dependent orthogonal tensor relating the motion of the two frames.

$\underline{\xi}$ can however represent a set of N-tuple scalers, each of which remains invariant under a change of frame. The state vector then transforms similar to an objective scalar, i.e.,

$$\underline{\xi}^* = \underline{\xi}\,. \tag{72}$$

Thus the only restriction on the internal state variables is that they be objective scalers.

It is often convenient to transform Equation 70 into a form where the independent variable of temperature (Θ) replaces the entropy. This is accomplished by introducing the Helmholtz free energy $\Phi\,(\underset{\sim}{E}, \Theta, \underline{\xi})$ defined earlier as

$$\Phi = U - H\Theta\,. \tag{67}$$

Assuming equipresence of the constitutive variables, there follows,

$$\Phi = \Phi(\underset{\sim}{E}, \Theta, \underline{\xi})\,,$$

$$H = H(\underset{\sim}{E}, \Theta, \underline{\xi})\,,$$

$$S = S(\underset{\sim}{E}, \Theta, \underline{\xi})\,,$$

$$\underset{\sim}{F}^{-1}\,\underline{q} = \underline{q}_r = \underline{q}_r(\underset{\sim}{E}, \Theta, \underline{\xi})\,,$$

and $$\dot{\underline{\xi}} = \dot{\underline{\xi}}\,(\underset{\sim}{E}, \Theta, \underline{\xi}) \tag{73}$$

Restrictions Based on the Second Law

The second law of thermodynamics was given a precise mathematical meaning by the postulate of internal entropy production. This law can now be used to place valuable mathematical restrictions on the constitutive assumptions. For convenience, the law is shown below in terms of the free energy.

$$-\rho_o \dot{\Phi} - \rho_o H \dot{\Theta} + \mathrm{tr}(\underset{\sim}{S}\, \dot{\underset{\sim}{E}}) - \frac{1}{\Theta} \underset{\sim}{F}^{-1} \underline{q} \cdot \vec{\underline{\nabla}} \Theta \geqslant 0 \tag{69}$$

From Equation 73, the time derivative of the free energy is given by

$$\dot{\Phi} = \frac{\partial \Phi}{\partial \underset{\sim}{E}} : \dot{\underset{\sim}{E}} + \frac{\partial \Phi}{\partial \Theta} \dot{\Theta} + \frac{\partial \Phi}{\partial \underline{\xi}} \cdot \dot{\underline{\xi}} \,. \tag{74}$$

Substituting the above equation into Equation 69 and collecting terms gives

$$\mathrm{tr}\left(\left(\rho_o \frac{\partial \Phi}{\partial \underset{\sim}{E}} - \underset{\sim}{S}\right) \dot{\underset{\sim}{E}}\right) - \rho_o \left(H + \frac{\partial \Phi}{\partial \Theta}\right) \dot{\Theta}$$

$$- \rho_o \frac{\partial \Phi}{\partial \underline{\xi}} \cdot \dot{\underline{\xi}} - \frac{1}{\Theta} \underset{\sim}{F}^{-1} \underline{q} \cdot \vec{\underline{\nabla}} \Theta \geqslant 0 \,. \tag{75}$$

By standard thermodynamic arguments, the entropy inequality above could be violated for a particular jump in strain or temperature unless,

$$\frac{\partial \Phi}{\partial \underset{\sim}{E}} = \frac{1}{\rho_o} \underset{\sim}{S} \quad \text{and} \quad H = - \frac{\partial \Phi}{\partial \Theta} \,. \tag{76}$$

The Second Law then reduces to

$$- \rho_o \frac{\partial \Phi}{\partial \underline{\xi}} \cdot \dot{\underline{\xi}} - \frac{1}{\Theta} \underset{\sim}{F}^{-1} \underline{q} \cdot \vec{\underline{\nabla}} \Theta \geqslant 0 \,. \tag{77}$$

Under isothermal conditions, the entropy inequality may be reduced even further to

$$\frac{\partial \Phi}{\partial \underline{\xi}} \cdot \dot{\underline{\xi}} \leqslant 0 \,. \tag{78}$$

The above result provides a restriction on the relation between the time rate of change of the internal state vector and its representative thermodynamic conjugate.

General Stress-Strain Law

In the previous discussion, the constitutive theory has been formulated with strain as the independent variable. However, a significant advantage can be obtained by formulating

the strain as a function of stress. This is due to the fact that the strain can be separated into an elastic part and a plastic part respectively.

The change in independent variables can be accomplished by introducing the complementary energy, Ψ, defined by the following Legendre transformation.

$$\Psi(\underset{\sim}{S}, \Theta, \underline{\xi}) = \frac{1}{\rho_o} \underset{\sim}{S} : \underset{\sim}{E} - \Phi . \tag{79}$$

Differentiating the above expression there follows,

$$d\Psi = \frac{1}{\rho_o} d\underset{\sim}{S} : \underset{\sim}{E} + \frac{1}{\rho_o} \underset{\sim}{S} : d\underset{\sim}{E} - \frac{\partial \Phi}{\partial \underset{\sim}{E}} : d\underset{\sim}{E} - \frac{\partial \Phi}{\partial \Theta} d\Theta - \frac{\partial \Phi}{\partial \underline{\xi}} \cdot d\underline{\xi} . \tag{80}$$

Recall from the Second Law,

$$\frac{\partial \Phi}{\partial \underset{\sim}{E}} = \frac{1}{\rho_o} \underset{\sim}{S} .$$

Therefore,

$$d\Psi = \frac{1}{\rho_o} \underset{\sim}{E} : d\underset{\sim}{S} - \frac{\partial \Phi}{\partial \Theta} d\Theta - \frac{\partial \Phi}{\partial \underline{\xi}} \cdot d\underline{\xi} . \tag{81}$$

Clearly, if Ψ is to be a function of $\underset{\sim}{S}$, Θ, and $\underline{\xi}$, then

$$\frac{1}{\rho_o} \underset{\sim}{E} = \frac{\partial \Psi}{\partial \underset{\sim}{S}} , \frac{\partial \Psi}{\partial \Theta} = - \frac{\partial \Phi}{\partial \Theta} , \frac{\partial \Psi}{\partial \underline{\xi}} = - \frac{\partial \Phi}{\partial \underline{\xi}} . \tag{82}$$

From Equation 82 it follows that the strain has a constitutive relation of the form why?

$$\underset{\sim}{E} = \underset{\sim}{E}(\underset{\sim}{S}, \Theta, \underline{\xi}) . \tag{83}$$

A slight perturbation in the strain from the current thermodynamic state leads to the differential expression

$$d\underset{\sim}{E} = \frac{\partial \underset{\sim}{E}}{\partial \underset{\sim}{S}} : d\underset{\sim}{S} + \frac{\partial \underset{\sim}{E}}{\partial \Theta} d\Theta + \frac{\partial \underset{\sim}{E}}{\partial \underline{\xi}} \cdot d\underline{\xi} . \tag{84}$$

I require that changes in $\underset{\sim}{E}$ at fixed $\underline{\xi}$ induce a purely elastic response (Rice, 1971). This is physically reasonable since by fixing $\underline{\xi}$, the plastic state of the material remains

unchanged. Similarly, changes in $\underset{\sim}{E}$ holding $\underset{\sim}{S}$ and Θ fixed results in inelastic deformation. Therefore, the total strain increment may be written as

$$d\underset{\sim}{E} = d^e\underset{\sim}{E} + d^P\underset{\sim}{E} , \tag{85}$$

where $d^e\underset{\sim}{E}$ = the elastic strain increment,

and $d^P\underset{\sim}{E}$ = the inelastic strain increment.

The inelastic portion of the strain increment is given by

$$d^P\underset{\sim}{E} = \frac{\partial \underset{\sim}{E}}{\partial \underline{\xi}} \cdot d\underline{\xi} . \tag{86}$$

Now consider the complementary energy, Ψ. Define the thermodynamic conjugate to the internal state vector as

$$\underline{f} = \rho_o \frac{\partial \Psi}{\partial \underline{\xi}} . \tag{87}$$

Taking cross derivatives of Ψ with respect to $\underline{\xi}$ and $\underset{\sim}{S}$ there follows,

$$\frac{\partial^2 \Psi}{\partial \underline{\xi}\, \partial \underset{\sim}{S}} = \frac{\partial}{\partial \underline{\xi}} \left(\frac{\partial \Psi}{\partial \underset{\sim}{S}}\right) = \frac{1}{\rho_o} \frac{\partial \underset{\sim}{E}}{\partial \underline{\xi}} ,$$

and $$\frac{\partial^2 \Psi}{\partial \underset{\sim}{S}\, \partial \underline{\xi}} = \frac{\partial}{\partial \underset{\sim}{S}} \left(\frac{\partial \Psi}{\partial \underline{\xi}}\right) = \frac{1}{\rho_o} \frac{\partial \underline{f}}{\partial \underset{\sim}{S}} . \tag{88}$$

Hence, the following Maxwell relation holds.

$$\frac{\partial \underline{f}}{\partial \underset{\sim}{S}} = \frac{\partial \underset{\sim}{E}}{\partial \underline{\xi}} \tag{89}$$

Noting the above and expressing $\underset{\sim}{E}$ in terms of the potential Ψ gives

$$d\underset{\sim}{E} = \underset{\approx}{M} : d\underset{\sim}{S} + \underset{\sim}{A}\, d\Theta + \frac{\partial \underline{f}}{\partial \underset{\sim}{S}} \cdot d\underline{\xi} , \tag{90}$$

where $\underset{\approx}{M} = \dfrac{1}{\rho_o} \dfrac{\partial^2 \Psi}{\partial \underset{\sim}{S}\, \partial \underset{\sim}{S}}$,

and $$\underset{\sim}{A} = \frac{1}{\rho_o} \frac{\partial^2 \Psi}{\partial \underset{\sim}{S} \, \partial \Theta} .$$

The rate of change of the internal state vector must now be formulated as a function of stress rather than strain. This may be accomplished in principle since,

$$\dot{\underline{\xi}} = \dot{\underline{\xi}} (\underset{\sim}{E} (\underset{\sim}{S}, \Theta, \underline{\xi}), \Theta, \underline{\xi}) = \dot{\underline{\xi}} (\underset{\sim}{S}, \Theta, \underline{\xi}) . \tag{91}$$

Equation 90 has been shown to satisfy the principle of material frame indifference.[7] This is of particular significance since I am dealing with a large deformation theory.

In dealing with the constitutive theory shown in Equation 90, one must determine how $\underset{\approx}{M}$, $\underset{\sim}{A}$, $\underline{f}$, and $\dot{\underline{\xi}}$ depend on $\underset{\sim}{S}$, Θ, and $\underline{\xi}$. This equation may be simplified by considering isothermal processes only, i.e., $\dot{\Theta} = 0$, $\vec{\underline{\nabla}} \Theta = \underline{0}$. Hence, I am dealing with a purely mechanical theory of the form

$$\dot{\underset{\sim}{E}} = \underset{\approx}{M} : \dot{\underset{\sim}{S}} + \frac{\partial \underline{f}}{\partial \underset{\sim}{S}} \cdot \dot{\underline{\xi}} . \tag{92}$$

It should be noted that isothermal processes do not preclude accounting for temperature effects in a mechanical theory. For instance, the temperature may appear as a parameter in the evolution equations of the internal state vector. This can have significant effect on the resulting constitutive law.

Complementary Energy Expansion

In order to determine the compliance tensor, $\underset{\approx}{M}$, it is necessary to generate an expansion for the complementary energy. This can be used in conjunction with the Second Law to determine the functional form of $\underset{\approx}{M}$.

Recall Ψ is a state function of the material. Hence, under isothermal conditions one can write

---

[7] Appendix A.

$$\Psi = \Psi(\underset{\sim}{S}, \underline{\xi}) . \tag{93}$$

Furthermore, the constitutive theory is restricted by requiring the material response to be elastic if no microstructural rearrangements take place while changes in $\underset{\sim}{E}$ holding $\underset{\sim}{S}$ fixed results in inelastic deformation.

Under finite strain, the elastic contribution to the strain is small compared to the plastic deformation and therefore may be assumed to be linear in stress. This implies $\underset{\approx}{M} = \underset{\approx}{M}(\underline{\xi})$ only. Hence, $\underset{\approx}{M}$ is determined by the current microstructural makeup of the material.

Assuming the compliance tensor is a function of the internal state vector only, Equation 90 allows one to write

$$\underset{\sim}{E} = \underset{\approx}{M} : \underset{\sim}{S} + \underset{\sim}{E}^P(\underset{\sim}{S}, \underline{\xi}) . \tag{94}$$

Therefore, in terms of the potential Ψ there follows,

$$\rho_o \frac{\partial \Psi}{\partial \underset{\sim}{S}} = \underset{\approx}{M} : \underset{\sim}{S} + \underset{\sim}{E}^P(\underset{\sim}{S}, \underline{\xi}) . \tag{95}$$

Integrating the above expression gives

$$\rho_o \Psi = -\Phi^\circ(\underline{\xi}) + \int \underset{\sim}{E}^P(\underset{\sim}{S}, \underline{\xi}) : d\underset{\sim}{S} + \frac{1}{2} \underset{\sim}{S} : (\underset{\approx}{M}(\underline{\xi}) : \underset{\sim}{S}) . \tag{96}$$

Rice (1975) refers to $-\Phi^\circ(\underline{\xi})$ as the locked in free energy. Physically this term is related to the excess surface area in a granular material.

Equation 96 can be used in conjunction with the Second Law to determine the functional form of the compliance tensor. The details of this are left to Chapter 6.

Evolution Equations

The development of the evolution equations is of primary importance in the formulation of this constitutive theory. Brown (1981a) has shown that kinetic relations can be developed for internal state variables at the granular level. These equations were developed

for high rate volumetric deformations of snow and were base on a specific "neck growth" model. I would like to expand the general applicability of these equations to include high rate deviatoric strains while possibly including new internal state variables. However, before choosing the specific state variables, I shall discuss further limitations the equations must have based on material isotropy.

Snow is assumed to take on isotropic characteristics in the undeformed state. This is due largely to the granular properties of snow and the random orientation of specific structural parameters. However, under applied loads, the resulting deformation may introduce anisotropy into the material.

Many geologic materials can be modelled to a great extent even when stress and strain anisotropies are neglected. Furthermore, for the problem of high rate deformation of snow considered here, I am primarily concerned with a single loading of the material, e.g., shock waves, vehicle mobility, penetration mechanics, etc. Hence, the anisotropic properties become even less significant. Therefore, I will consider snow to behave isotropically throughout the deformation process.

Recall the following constitutive relation was assumed for the time rate of change of the state variables under isothermal conditions.

$$\dot{\xi}_a = \dot{\xi}_a(\underset{\sim}{S}, \underline{\xi}) \tag{97}$$

Furthermore, the vector $\underline{\xi}$ is invariant under a change of frame, i.e.,

$$\underline{\xi}^* = \underline{\xi} \ .$$

Hence, under changes of reference frame, $\dot{\xi}_a$ may be considered to be a scaler valued function of the symmetric tensor $\underset{\sim}{S}$. Truesdell and Noll (1965) show that a scaler valued tensor function $\epsilon(\underset{\sim}{A})$ of one symmetric variable is invariant (isotropic) if and only if it can be expressed as a function of the principle invariants of A.[9]

[9] An alternative to the principle invariants would be the first three moments of $\underset{\sim}{A}$ given on the next page.

Therefore the kinetic relations must be expressible in the form,

$$\dot{\xi}_a = \dot{\xi}_a(I_s, II_s, III_s, \underline{\xi}) \tag{99}$$

Alternate Constitutive Form

The general inverted form of the constitutive law can readily be shown to be,

$$\dot{\underset{\sim}{S}} = \underset{\approx}{L} : \dot{\underset{\sim}{E}} + \underset{\sim}{B}\,\dot{\Theta} + \frac{\partial \underline{g}}{\partial \underset{\sim}{E}} \cdot \dot{\underline{\xi}}, \tag{100}$$

where $\underset{\approx}{L} = \dfrac{1}{\rho_o} \dfrac{\partial^2 \Phi}{\partial \underset{\sim}{E}\, \partial \underset{\sim}{E}}$,

$\underset{\sim}{B} = \dfrac{1}{\rho_o} \dfrac{\partial^2 \Phi}{\partial \underset{\sim}{E}\, \partial \Theta}$,

and $g = \dfrac{\partial \Phi}{\partial \underline{\xi}}$.

Under isothermal deformation the above reduces to the following.

$$\dot{\underset{\sim}{S}} = \underset{\approx}{L} : \dot{\underset{\sim}{E}} + \frac{\partial \underline{g}}{\partial \underset{\sim}{E}} \cdot \dot{\underline{\xi}} \tag{101}$$

Using this form of the constitutive theory requires one to deal with the free energy rather than the complementary energy. However, as in the previous section, a similar set of thermodynamic restrictions for the free energy expansion can be developed.

A significant aspect of the alternate form given by Equations 100 and 101 is that the evolution equations must now be developed as a function of strain rather than stress. This precludes any simple inversion of one form of the constitutive law to obtain the other. Hence, one must choose the desired form of the constitutive law at the onset and stick with it.

$\epsilon(\underset{\sim}{A}) = \epsilon(\bar{I}_{1A}, \bar{I}_{2A}, \bar{I}_{3A})$

where $\bar{I}_{kA} = \mathrm{tr}(\underset{\sim}{A}^k)\,; k = 1, 2, 3.$

CHAPTER 5

THE GRANULAR STRUCTURE OF SNOW

In this chapter, a statistical model characterizing the granular structure of snow is developed using quantitative stereology. The model is based on specific parameters (e.g., bond radius, grain size, etc.) which may take the form of internal state variables in a constitutive theory for high rate deformation of snow. In addition to parameters developed by other authors in previous investigations, a new parameter characterizing the mean bond length is developed. More significantly, general relations are derived for the mean number of bonds per grain and mean number of grains per unit volume without making any assumptions regarding the shapes or sizes of the ice grains, or their respective distributions.

It should be noted that not all parameters developed here will be used as internal state variables. This would be extremely difficult as a large number of parameters will be discussed. Furthermore, the set of parameters discussed are not linearly independent. Finally, some variables may appear as constants in the evolution equations of the state variables by assuming they are not a function of the deformation process. This does not imply they have no effect on the deformation.

Selection of the Structural Parameters

The variables selected must describe the current microstructural state of the material and be capable of representing average measures of the structural rearrangements taking place within the snow cover. The variable selection process attempted to include the most significant aspects of the granular structure as well as considering the dynamic environment of the material under high rate deformation.

The variables chosen should be able to characterize the dominant deformation mechanisms for high rates such as bond fracture and the resulting intergranular glide and neck growth at the bonds (pressure sintering). Furthermore, they must account for various phenomena known to occur under compressive loadings such as:

1. the effects of pore pressure,
2. a locking mechanism for grains during intergranular glide,
3. coupling the deviatoric and volumetric responses,
4. work hardening, and
5. local inertial effects.

Finally, the variables must be chosen so as to make measuring them a feasible task.

Before proceeding with the selection of the variables it is necessary to clarify the notation to be used. When discussing the behavior of dry snow in the general macroscopic sense the material is considered to be a multiphase mixture consisting of an ice phase and an air phase. Each phase is denoted by a subscript as follows.

a: air phase

i: ice phase

This convention is in accordance with that used in mixture theory studies of mechanical properties of snow.

An alternative approach will be used when measuring the state variables in the snowpack at the granular level. Here the snow is considered to be a three phase material consisting of an ice grain phase, ice neck phase, and air phase. The three phases are denoted by the following Greek subscripts.

α: ice grain phase

β: ice neck phase

γ: air phase

In the following discussions, no attempt is made to state which of the two previous approaches is being used since the subscripts are self explanatory. Finally, in quantitative stereology it is necessary to differ between length, area, and volume measurements. Therefore, let the following capitalized subscripts denote this difference.

L: length measurement

A: area measurement

V: volume measurement

Taking into account the desired properties of the state variables, the following parameters were chosen to formulate the statistical model for snow. A discussion of their significance and measurability is given later.

1. $\alpha = \rho_i/\rho$ — density ratio
2. r — mean bond radius
3. h — mean bond (neck) length
4. λ — mean intergranular slip distance
5. L — mean intercept length (grain size)
6. $\overline{n}_3$ — mean number of bonds per grain
7. $N_{\alpha V}$ — mean number of grains per unit volume
8. V — mean volume of a single grain
9. S — mean surface area per unit volume

Measuring the State Variables

Before discussing each state variable it is necessary to describe the stereological measurements which are required to obtain the desired information. The necessary assumption which allows results from one section plane to give three-dimensional information is randomness of location and orientation of the structural features of the three-dimensional

network. Kry (1975a) has shown that this is satisfied to within ±10 percent even after 30 percent uniaxial plastic deformation.

As mentioned previously, snow at the granular level is considered to be a three phase material consisting of ice grains, ice necks, and air. Kry (1975a) has developed an operational definition to identify grain bonds in a two-dimensional surface section. If a grain bond is cut by a section plane it will appear as a line connecting opposite edges of the ice. Three criteria are required to identify these bonds.

1. A minimum constriction in the ice must exist on the plane of the section.
2. Both edges of the ice must show the constriction.
3. The notches on each edge must point approximately towards each other.

The neck region of a grain bond is defined as that area surrounding the bond where the grain goes from convex to concave with respect to the outward normal. Figure 5 shows an image enhanced snow sample which deliminates the three phases of interest.

Using the enhanced image the following measurements can now be made. The code contained within the parentheses indicates the method of analysis, e.g., visual count (VC) or computerized image analysis (IA).

P_α Area fraction of points falling in the ice grain phase (IA).

P_β Area fraction of points falling in the ice neck phase (IA).

P_γ Area fraction of points falling in the air phase (IA).

$\bar{E} = \overline{(1/d_2)}$ Harmonic mean of lines representing grain bonds in the surface section (IA).

$N_{\alpha L}$ Number of interceptions of ice grains in the microstructure per unit length of a random test line (IA). (See Figure 6.)

N_α Number of grains in the test area (VC).

N_β Number of bonds in the test area (VC).

$f_2(n)$ Probability distribution of the number of bonds per grain cut by the section plane (VC).

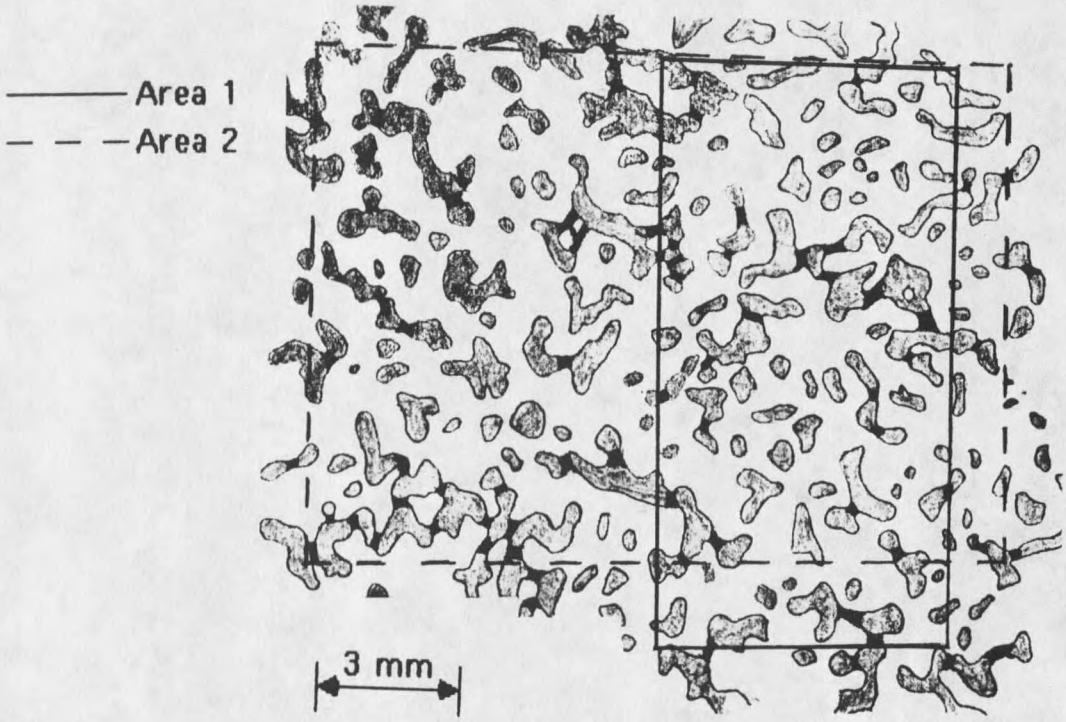

Figure 5. Image enhanced surface section showing the three phases of interest. The solid and dashed lines indicate respective areas of analysis.

It should be noted that all measurements which require a visual count can be performed on the order of minutes. The time consuming portion of the analysis will be in the area of image enhancement.

At this point one can proceed with a discussion of each of the state variables.

Density Ratio (a)

The density ratio is defined by the following expression.

$$a = \rho_i/\rho \tag{102}$$

where ρ_i = density of ice,

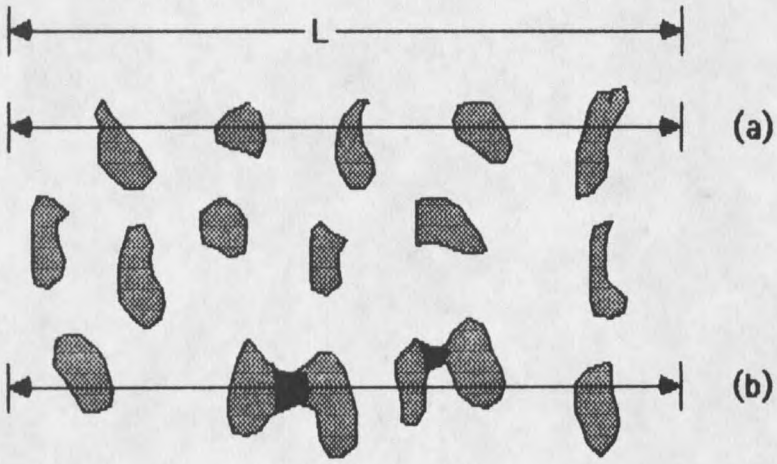

Figure 6. Counting relationship for $N_{\alpha L}$. (a) $N_{\alpha L} = 5/L$, (b) $N_{\alpha L} = 6/L$.

and ρ = density of snow

The density of snow has been the primary measure of the "state" of the material in many of the past investigations of the mechanical behavior of snow. This is primarily because of the ease and quickness of density measurement in the field. However, recent papers have shown that density alone cannot adequately describe the state of the material under certain conditions. This is especially true at low densities where the impact of other state variables is more significant. However, the importance of density increases as α approaches unity.

The value of the density ratio obtained in the field may be cross checked using the following stereological relationship.

$$\alpha = 1 / (P_\alpha + P_\beta) \tag{103}$$

This equation neglects the mass of the air phase.

Mean Bond Radius (r)

The mean 3-dimensional bond radius is a significant parameter of pressure sintering as well as bond strength and resistance to fracture. Brown (1980a) used this parameter in a volumetric constitutive law based on neck growth. Fullman (1953) derived the necessary relations for the assumption that the grain bonds are circular disks. Kry (1975a) has shown that this idealization yields self-consistent results.

The governing equation for the mean bond radius as derived by Fullman is

$$r = \pi/(4\,\bar{E}) \tag{104}$$

Mean Bond Length (L)

The mean bond length is also a significant parameter for modeling pressure sintering. This was used in Brown's "neck growth" volumetric constitutive law. However, until now I am unaware of any attempts to evaluate this parameter stereologically. The statistical model of bond length is developed by idealizing the necks of grains to be cylinders. This is based on the fact that self-consistent results have been obtained by idealizing the grain bonds as disks. Clearly the neck regions of an ice grain are not perfectly cylindrical. However, the definition still provides a meaningful relationship when comparing differing types of snow in that it is a consistent measure of bond length. Fullman (1953) has derived a relationship for the number of bonds per unit volume based on knowledge of the number of bonds per unit area. This relationship is

$$N_{\beta V} = 8\,\bar{E}\,N_{\beta A}/\pi^2\,, \tag{105}$$

where $N_{\beta V}$ = the number of bonds per unit area.

Underwood (1970) has shown that a statistically exact equation for determining the volume fraction of the αth constituent is given by

$$V_\alpha = P_\alpha\,. \tag{106}$$

Therefore, by introducing the neck region of an ice grain as a separate phase, one can determine the volume fraction of the necks. The idealized bond length can then be determined by the following expression.

$$h = P_\beta / (N_{\beta V} \pi r^2) \tag{107}$$

Mean Intergranular Slip Distance (λ)

The mean intergranular slip distance is of major importance for characterizing intergranular glide. As this distance decreases, viscous deformation becomes increasingly difficult in the deformation process. Furthermore, this parameter must be inherently related to the locking phenomenon of intergranular glide. The stereological relationship as defined by Fullman (1953) is given by

$$\lambda = (a - 1) / (a\, N_{aL}) \tag{108}$$

This equation is valid regardless of size, shape, or the respective distributions of the grains.

Mean Intercept Length (L)

The mean intercept length provides a measure of the grain size and as a result complements the mean intergranular slip distance. The combination of these two parameters should provide a physical basis for determining a critical "locking" density for grains during intergranular glide.

The mean intercept length as derived by Underwood (1970) is given by the following.

$$L = (P_a + P_\beta) / N_{aL} \tag{109}$$

Again this equation makes no assumptions about the shape, size, or distribution of the grains.

Remaining State Variables

The remaining internal state variables must be discussed together because of their close dependence on each other. The variables are given by:

1. Mean number of grains per unit volume. (N_{av})
2. Mean number of bonds per grain. ($\overline{n}_3$)
3. Mean volume of a single grain. (V)
4. Mean surface area per unit volume (S)

The mean number of bonds per grain is a strong measure of the degree of grain mobility and fracture strength. The number of grains per unit volume and the mean volume of a grain are important terms for modeling intergranular glide including local inertial effects. Finally, the mean surface area per unit volume is important for computing energy absorption by ice fracture in snow during high rate deformation. Under high strain rates, the snow will undergo brittle fracture at the grain bonds. This causes an increase in the surface area which in turn is directly related to the free energy.

Until recently, no method was available for determining the mean number of bonds per grain from a section plane. Gubler (1978) has derived a technique for determining this value based on comparing a theoretical distribution of the number of bonds per grain, $f_2(n)$, seen in a section plane with the actual distribution. This paper appears to be a pioneering effort in this area. The technique involves calculating the probability, p, that if a grain with a coordination number n=1 is cut by a section plane, its bond also appears in the section plane. The bond areas are assumed to be random and isotropically distributed on the grain surface. Furthermore, the bonds are considered to be small compared to the grain surface. This is consistent with Kry's (1975a) definition of a bond.

Unfortunately, Gubler's approach contains one significant weakness in that the stereological relationship used to obtain the number of grains per unit volume is based on all grains being the same size *and* shape. This is hardly the case for alpine snow, as highly faceted crystals as well as rounded grains may appear throughout the snowpack in all sizes.

The problem of accurately determining the number of grains per unit volume from surface sections for a collection of particles of arbitrary size and shape is extremely difficult.

Most authors have assumed the particles to be all one size and shape for which many solutions are known. Some solutions are also known for particles of one shape which obey a log normal distribution in size. DeHoff (1964, 1965) has provided solutions for this case for some simple shapes. Finally, Hilliard (1968) has developed a technique for determining N_{av} for an arbitrary collection of sizes and shapes provided the relative frequency of the various shapes is known. Unfortunately, his theory is unable to produce specific results since shape factors necessary to apply the theory have not been developed.

The approach taken here to determine N_{av} will avoid any specific identification of grain shape as this is virtually impossible for alpine snow. The formulation follows Gubler's approach with some noted exceptions.

To begin, the probability of finding a grain with a coordination number between n and n+dn as derived by Gubler (1978) is given by

$$f_3(n) = N_3 n^{3i-1} \exp(-\xi n^{2i}) , \tag{110}$$

where n = the 3-dimensional coordination number,

N_3 = a normalizing constant,

i = a free parameter of the distribution,

and $$\xi = \left[\frac{2}{\sqrt{\pi}} \frac{1}{\bar{n}_3} \Gamma \left(\frac{3}{2} + \frac{1}{2i}\right)\right]^{2i}$$

The normalizing constant may be determined numerically by requiring

$$\sum_{n=1}^{12} f_3(n) = 1 . \tag{111}$$

This is based on the premise that each ice grain in a snow cover has at least one bond and at most twelve bonds, as in the case for ice.

The resulting two-dimensional probability distribution as derived by Gubler is given by the following.

$$f_2(l) = N_2 \sum_{k=1}^{12} \binom{k}{\ell} p\,(1-p)^{k-\ell} f_3(k)\,, \tag{112}$$

where p is defined as the probability that, if a grain with a coordination number n=1 is cut by a section, its bond also appears in the section,

and N_2 is a normalizing constant.

The normalizing constant N_2 does not appear in Gubler's work. The reason for inserting this is as follows. Equation 112 without N_2 represents a binomial distribution of the probability p multiplied by the three-dimensional probability distribution $f_3(k)$. Therefore, the following equality holds.

$$\sum_{\ell=0}^{12} f_2(l) = 1 \tag{113}$$

However, when cutting a section of ice with grains having a coordination number of 12, it is physically possible to cut at most 6 bonds. Hence, one can require

$$\sum_{\ell=0}^{6} f_2(l) = 1\,. \tag{114}$$

The probability p is given by the following (Gubler, 1978).

$$p = s_\beta / s_k \tag{115}$$

where $s_\beta = \pi N_{aL} b / N_{av}$,

$s_k = 4 N_{aL} / N_{av}$,

$b = 2\,(r^2 - (\bar{d}_2/2)^2)^{1/2}$,

and $\bar{d}_2$ = mean intersection length of bonds appearing in the surface section.

Notice that p is a function of the number of grains per unit volume, N_{av}. It is at this point where all previous investigations assume specific shape and size distributions and where this theory deviates.

To begin, one must digress somewhat. Underwood (1970) has provided a table for determining $N_{\alpha V}$ for particles of one size and shape. This is the approach followed by Gubler. The general equation is given by

$$N_{\alpha V} = C\,(N^2_{\alpha A} / N_{\alpha L}) \,, \tag{116}$$

where C is a coefficient depending only on shape. It is interesting to note that C takes on a fairly narrow range of values for a wide variety of shapes, typically ranging from 0.4 to 0.8 for shapes pertinent to alpine snow. Therefore, one can use Equation 116 to obtain a *first estimate* of $N_{\alpha V}$. This in turn fixes the probability, p, as defined in Gubler's paper.

Now recall an earlier relationship derived by Fullman (1953) for the number of bonds per unit volume.

$$N_{\beta V} = 8\,\bar{E}\,N_{\beta A} / \pi^2 \tag{105}$$

The above equation is based on the assumption that the bonds may be considered to be a polydispersed system of thin disks. This is precisely what has been assumed throughout this paper. Using this result, the mean number of bonds per grain is then *fixed* by the equation

$$\bar{n}_3 = 2\,N_{\beta V} / N_{\alpha V} \,. \tag{117}$$

By neglecting this equation and allowing n to vary, Gubler has an underconstrained system. This could lead to uniqueness problems and produce erroneous results.

By invoking Equation 105 the parameters $N_{\alpha V}$ and i are varied rather than $\bar{n}_3$ and i to determine the proper theoretical density distribution $f_2(n)$. Hence, a method has been developed for determining $N_{\alpha V}$ without specific consideration of the individual grain shapes and sizes other than to obtain a first guess.

Once $N_{\alpha V}$ is determined, the mean volume of a single grain including the "necks" is given by

$$V = (P_\alpha + P_\beta) / N_{\alpha V} \tag{118}$$

The neck regions in this variable are included since the neck is assumed to become an integral part of the grain when a bond fractures. Furthermore, the neck volume is typically on the order of 5 percent or less of the total grain volume. Therefore, any errors caused by this assumption are small.

The mean surface area per unit volume can be derived by considering each of the grains as being detached from their neighbors and then subtracting off the surface area contained by the grain bonds. Underwood (1970) has derived an expression for the surface area for a system of detached grains given by

$$S = 4 N_{aL} \quad . \tag{119}$$

Therefore, subtracting the area contained by the grain bonds from the above expression gives the correct surface area per unit volume.

$$S = 4 N_{aL} - 2 \pi r^2 \overline{n}_3 N_{aV} \tag{120}$$

Application

The theory presented above has been written into a computer code which uses a high speed image analyzer located at Montana State University. The image analyzer is capable of digitizing a photograph of a section into approximately 300,000 points and assigning each point one of 256 possible gray levels. The digitized section is then image enhanced and stored on a floppy disk for future analysis.

By using the image analyzer, exact point counts and extremely accurate length measurements can be made very quickly. This allows large areas of a section containing numerous grains to be analyzed which increases the statistical accuracy.

The following data is an example of the application of the theory using the image analyzer. A surface section was taken from a sample of alpine snow stored in a cold room at -12°C over the summer at Montana State University. Details of the section preparation

are given in Appendix B. Also, Perla (1982) provides an in-depth discussion of surface section techniques.

Two areas of the surface section were analyzed using the image analyzer. The areas of analysis are shown by the dashed and solid lines in Figure 5 respectively. The two areas overlap and hence are not statistically independent. However, the larger area does provide a check on the statistical accuracy of the smaller area. The data taken from the image analysis of the two areas is shown in Table 1. The data generated by the image analysis of the surface section is very close for both areas analyzed. This indicates the smaller area was representative of the overall properties of the section.

Table 1. Image Analysis Data Taken from the Surface Section Shown in Figure 5.

	Area 1	Area 2
Area of analysis:	65.5 mm^2	133.9 mm^2
Ice grain area fraction:	0.350	0.363
Ice neck area fraction:	0.038	0.043
Air phase area fraction:	0.612	0.594
Mean 2-D bond length:	0.307 mm	0.331 mm
Harmonic mean of 2-D bond length:	3.42 mm^{-1}	3.30 mm^{-1}
Number of grains per unit length of a random test line:	0.803 mm^{-1}	0.776 mm^{-1}

Using the above information the two dimensional theoretical probability distribution for grain coordination numbers can be computed. The results for each area analyzed along with the measured distributions are shown in Table 2.

The theoretical distributions for the number of bonds per grain as seen in the section plane compare very favorably with the measured distributions. For the larger area of analysis the error is approximately one percent for grains with 0,1, or 2 bonds respectively. These grains account for approximately 95 percent of the grains in the section analyzed.

Using the theoretical data generated above in conjunction with the previous information determined by image analysis, the internal state variables may be readily computed. These are given in Table 3.

Table 2. Comparison of the Measured versus Theoretical Two-Dimensional Probability Distributions for the Surface Section Shown in Figure 5.

No. of Bonds	Measured Distribution	Theoretical Distribution
	Area 1	
n = 0	0.518	0.515
n = 1	0.291	0.313
n = 2	0.139	0.102
n ⩾ 3	0.052	0.080
	Area 2	
n = 0	0.490	0.489
n = 1	0.327	0.327
n = 2	0.112	0.111
n ⩾ 3	0.071	0.073

Table 3. Internal State Variables Generated by Image Analysis of the Surface Section Shown in Figure 5.

	Area 1	Area 2
Density Ratio:	2.58	2.46
Mean 3-D Bond Radius:	0.230 mm	0.238 mm
Mean 3-D Bond Length:	0.193 mm	0.182 mm
Mean Intergranular Slip Distance:	0.762 mm	0.766 mm
Mean Intercept Length:	0.484 mm	0.523 mm
Mean Number of Bonds per Grain:	2.04	2.26
Mean Number of Grains per Unit Volume:	1.16 mm^{-3}	1.17 mm^{-3}
Mean Grain Volume:	0.334 mm^3	0.345 mm^3
Mean Surface Area per Unit Volume:	2.43 mm^{-1}	2.16 mm^{-1}

The repeatability of the data for the internal state variables for the two areas analyzed is quite strong with the difference between the two typically being on the order of 10 percent or less. Also, the density ratio determined by a field measurement of this particular snow sample was 2.29. This differs from the stereological measurements by 13 percent and 7 percent respectively for Areas 1 and 2. It is not surprising that the field measured density was slightly higher than that determined by image analysis since some compaction of the snow will occur when taking field data.

Conclusions

A statistical model for snow based on internal state variables of the "averaging" type has been developed. The model yields self consistent results and is feasible to apply in a constitutive theory since all of the parameters can be easily computed experimentally using image analysis techniques.

A new stereological relation has been developed to characterize the mean three-dimensional length of a bond. This is a significant parameter for modeling viscous deformation.

The number of grains per unit volume and the number of bonds per grain, both of which are significant parameters in characterizing the granular structure of snow are derived while making no assumptions on shape, size, or distribution of the grains. As a consequence of this, values for the mean surface area per unit volume, and mean volume of an ice grain are developed. Many of these parameters will make significant contributions to a constitutive theory based on internal state variables.

CHAPTER 6

PARTICULARS OF THE CONSTITUTIVE THEORY

In Chapter 4, the general framework of a constitutive theory for rate dependent inelastic materials at finite strain was presented. The constitutive equation developed is represented in the form

$$\dot{\underset{\sim}{E}} = \underset{\approx}{M} : \dot{\underset{\sim}{S}} + \frac{\partial \underline{f}}{\partial \underset{\sim}{S}} \cdot \dot{\underline{\xi}} \tag{121}$$

where $\underset{\sim}{E}$ = the Lagrangian strain,

$\underset{\sim}{S}$ = the second Piola-Kirchhoff stress,

$\underset{\approx}{M}$ = the compliance,

$\underline{\xi}$ = an internal state vector,

and $\underline{f}$ = the thermodynamic conjugate to the state vector.

Chapter 5 was devoted to identifying possible internal state variables for snow based on the microstructure at the granular level.

In this chapter, the details of the constitutive theory are presented. In particular, specific internal state variables are selected for the state vector. Also, relationships for $\underset{\approx}{M}$, $\underline{f}$, and $\dot{\underline{\xi}}$ as functions of the stress and the state vector are presented. This will make the formulation complete.

The complexity of the theory necessitates a numerical solution. Therefore, some of the discussion in this chapter will involve numerical approximations. In particular, let Ψ represent any scalar, vector, or tensor valued function of the material. Then Ψ_i is taken to mean the approximate value of Ψ at the ith time step, i.e.,

$$\Psi_i = \Psi(t_i) .$$

Finally, in using this constitutive theory to solve specific boundary value problems, it is often desirable to solve the stress given the strain or strain rate as input. Therefore, the solution technique will be based on prescribing the deformation.

Selection of the State Variables

The specific internal state variables chosen for the constitutive theory are the mean intergranular slip distance, λ, and the mean grain size, L. These are the variables that will explicitly appear in Equation 121. However, evolution equations will also be written for the mean bond radius, r, and mean bond length, h, since the mean grain size is a function of these parameters. Hence the internal state vector takes the form

$$\underline{\xi} = (\lambda, L; r, h) . \tag{122}$$

In addition, there may be other variables discussed in Chapter 5 which appear as parameters in the theory. However, evolution equations will only be written for those variables given in Equation 122.

The Dependence of the Conjugate Force ($\underline{f}$) on the Stress Tensor ($\underset{\sim}{S}$)

The physical meaning of the thermodynamic conjugate force ($\underline{f}$) is very difficult to interpret. Furthermore, the dependence of $\underline{f}$ on the Piola stress $\underset{\sim}{S}$ is even more obscure. However, the relationship becomes much clearer by considering the Maxwell relation given by Equation 89 and repeated below for convenience.

$$\frac{\partial \underline{f}}{\partial \underset{\sim}{S}} = \frac{\partial \underset{\sim}{E}}{\partial \underline{\xi}} \tag{123}$$

This relationship shows that if the dependence of strain on the state vector can be established, the dependence of the conjugate $\underline{f}$ on the stress $\underset{\sim}{S}$ is also known.

From Equation 121, the plastic strain rate is given by

$$\dot{\underset{\sim}{E}}^P = \frac{\partial \underline{f}}{\partial \underset{\sim}{S}} \cdot \dot{\underline{\xi}} = \frac{\partial \underset{\sim}{E}}{\partial \underline{\xi}} \cdot \dot{\underline{\xi}} \ . \tag{124}$$

Expanding Equation 124 in terms of the specific internal state variables gives

$$\dot{\underset{\sim}{E}}^P = \frac{\partial \underset{\sim}{E}}{\partial \lambda} \dot{\lambda} + \frac{\partial \underset{\sim}{E}}{\partial L} \dot{L} \ . \tag{125}$$

Also, combining Equation 103 and 108-109 from quantitative stereology provides the following expression for the density ratio in terms of the state vector.

$$a = \frac{\lambda + L}{L} \tag{126}$$

Noting this result, Equation 125 may be expressed as

$$\dot{\underset{\sim}{E}}^P = \frac{\partial \underset{\sim}{E}}{\partial a}\left(\frac{\partial a}{\partial \lambda} \dot{\lambda} + \frac{\partial a}{\partial L} \dot{L}\right) = \frac{\partial \underset{\sim}{E}}{\partial a} \dot{a} \ . \tag{127}$$

Comparing Equations 125 and 127 gives

$$\frac{\partial \underset{\sim}{E}}{\partial \underline{\xi}} = \frac{\partial \underset{\sim}{E}}{\partial a} \frac{\partial a}{\partial \underline{\xi}} = \underline{k}_\xi \dot{\underset{\sim}{E}}^P \ , \tag{128}$$

where $\underline{k}_\xi$ is a vector of constants of proportionality given by

$$\underline{k}_\xi = \frac{1}{\dot{a}} \frac{\partial a}{\partial \underline{\xi}} \ . \tag{129}$$

Substituting Equation 126 into Equation 129 to solve for $\underline{k}_\xi$ gives

$$k_\lambda = \frac{1}{\dot{a} L} \ ,$$

and $$k_L = -\frac{\lambda}{\dot{a} L^2} \ , \tag{130}$$

where k_λ and k_L are the scaler valued components of the vector $\underline{k}_\xi$.

Finally, plastic deformation accounts for nearly all of the deformation of snow under finite strain. Hence, the plastic strain rate is approximately given by

$$\dot{\underset{\sim}{E}}^P \cong \dot{\underset{\sim}{E}} \ . \tag{131}$$

At high densities this relationship may break down. However, $\dot{\underset{\sim}{E}}^P$ may still be closely approximated by

$$\dot{\underset{\sim}{E}}^P_{i+1} = \dot{\underset{\sim}{E}}_{i+1} - \underset{\approx}{M}_i : \dot{\underset{\sim}{S}}_i \tag{132}$$

Therefore, the dependence of $\underline{f}$ on $\underset{\sim}{S}$ has been explicitly determined by Equations 128–130.

Determining the Compliance ($\underset{\approx}{M}$)

In what follows, a set of two equations are developed to determine the compliance tensor. The formulation is an approximate one since one of the equations developed is an inequality which places bounds on the rate of change of the compliance.

Recall the elastic response is small and is therefore assumed to be linear in stress. This implies the compliance is a function of the state vector only. Also, the material is assumed to behave isotropically throughout the deformation. This is reasonable due to the random orientation of the microstructural properties of snow. Furthermore, only a single loading of the material is being considered. Based on this assumption, the most general fourth-order isotropic tensor M_{IJRS} symmetric with respect to IJ or RS has the following rectangular Cartesian coordinate form.

$$M_{IJRS} = U(\underline{\xi})\,\delta_{IJ}\,\delta_{RS} + V(\underline{\xi})(\delta_{IR}\,\delta_{JS} + \delta_{IS}\,\delta_{JR}) \tag{133}$$

where δ_{IJ} denotes the Kronecker delta.

Now recall the following entropy inequality from the second law of thermodynamics.

$$\frac{\partial \Psi}{\partial \underline{\xi}} \cdot \dot{\underline{\xi}} \geqslant 0 \tag{134}$$

Furthermore, integration of Equation 94 results in the following expression for the complementary energy.

$$\rho_o \Psi = -\Phi^\circ(\underline{\xi}) + \int \underset{\sim}{E}^P(\underset{\sim}{S}, \underline{\xi}) : d\underset{\sim}{S} + \frac{1}{2}\,\underset{\sim}{S} : (M(\underline{\xi}) : \underset{\sim}{S}) \tag{135}$$

The integral in the above expression cannot be evaluated *a priori* since the constitutive law is not fully defined.

The term $-\Phi^{\circ}(\underline{\xi})$ in Equation 135 is referred to as the locked in free energy of the body. For snow, this term is related to the surface energy caused by an excess of surface area. This energy is negligible compared to the strain energy developed during deformation.

Neglecting the locked in free energy, Equation 135 may be separated into an elastic and plastic contribution to the complementary energy as follows.

$$\rho_o \Psi = \rho_o \Psi^e + \rho_o \Psi^P, \tag{136}$$

where $$\rho_o \Psi^e = \frac{1}{2} \underset{\sim}{S} : (\underset{\approx}{M}(\underline{\xi}) : \underset{\sim}{S}), \tag{137}$$

and $$\rho_o \Psi^P = \int \underset{\sim}{E}^P (\underset{\sim}{S}, \underline{\xi}) : d\underset{\sim}{S} . \tag{138}$$

It should be noted that changes in Ψ^e do not necessarily represent an elastic process since changes in $\underset{\approx}{M}(\underline{\xi})$ are irreversible.

An expression for the change in $\underset{\approx}{M}(\underline{\xi})$ can be developed by imposing a stricter inequality than Equation 134. Specifically, I require

$$\Gamma_e = \frac{\partial \Psi^e}{\partial \underline{\xi}} \cdot \dot{\underline{\xi}} \geqslant 0 \tag{139}$$

where Γ_e represents entropy production resulting from irreversible changes in the compliance tensor.

This approach is similar to that of Truesdell and Noll (1965) in which they propose a stronger form of the classical entropy inequality, requiring separately

$$\gamma_{loc} = \dot{\eta} - \frac{r}{\theta} + \frac{1}{\rho\theta} \vec{\underline{\nabla}} \cdot \underline{q} \geqslant 0,$$

and $$\gamma_{con} = -\frac{1}{\rho\theta^2} \underline{q} \cdot \vec{\underline{\nabla}} \theta \geqslant 0, \tag{140}$$

where γ_{loc} = the local entropy production,

and γ_{con} = entropy production by heat conduction.

This can be compared with the classical entropy inequality given by

$$\gamma = \dot{\eta} - \frac{r}{\theta} + \frac{1}{\rho\theta} \vec{\nabla} \cdot \underline{q} - \frac{1}{\rho\theta^2} \underline{q} \cdot \vec{\nabla} \theta \geqslant 0 . \tag{141}$$

Substituting Equations 122 and 137 into Equation 139 and noting Equation 133 gives

$$\Gamma_e = \left(\frac{\partial U}{\partial \lambda} \dot{\lambda} + \frac{\partial U}{\partial L} \dot{L}\right) (\mathrm{tr}\, \underset{\sim}{S})^2 + 2\left(\frac{\partial V}{\partial \lambda} \dot{\lambda} + \frac{\partial V}{\partial L} \dot{L}\right) \mathrm{tr}\, \underset{\sim}{S}^2 \geqslant 0 \tag{142}$$

This equation may be expressed as a function of the density ratio since $a = a(\lambda, L)$. Hence,

$$\Gamma_e = \frac{\partial U}{\partial a} \dot{a} (\mathrm{tr}\, \underset{\sim}{S})^2 + 2 \frac{\partial V}{\partial a} \dot{a}\, \mathrm{tr}\, \underset{\sim}{S}^2 \geqslant 0 \tag{143}$$

By setting the inequality to zero in the above expression, an equation for a bound on change of U and V with respect to changes in the density has been determined.

A second equation for U and V can be obtained by comparing the elastic strains with the known stress-strain data. The general constitutive relation is given by

$$\dot{\underset{\sim}{E}} = \underset{\approx}{M} : \dot{\underset{\sim}{S}} + \frac{\partial \underline{f}}{\partial \underset{\sim}{S}} \cdot \dot{\underline{\xi}} . \tag{121}$$

Now consider an arbitrary loading history where at some time, t_1, the stresses are "instantaneously" reduced to zero. The plastic strain rate immediately goes to zero and one is left with

$$\dot{\underset{\sim}{E}}^e = \underset{\approx}{M} : \dot{\underset{\sim}{S}} = \underset{\approx}{M} : \underset{\sim}{S}\, \delta(t_1) , \tag{144}$$

where $\delta(t_1)$ is the Dirac delta function.

Integrating this expression and taking the trace gives

$$\mathrm{tr}\, (\underset{\sim}{E}^e) = (3U + 2V)\, \mathrm{tr}\, (\underset{\sim}{S}) . \tag{145}$$

Also, for an isotropic elastic material,

$$\mathrm{tr}\,\underset{\sim}{E}^{e} = \frac{1}{3K}\ \mathrm{tr}\,\underset{\sim}{t}\,, \tag{146}$$

where K = the elastic bulk modulus.

Comparing Equations 145 and 146 gives a second relationship for U and V.

$$(3U + 2V)\ \mathrm{tr}(\underset{\sim}{S})\,dt = \frac{1}{3K}\ \mathrm{tr}(\underset{\sim}{t}) \tag{147}$$

Mellor (1974) provides some data for determining elastic material coefficients for snow as a function of density. Equations 143 and 147 provide the necessary relations for estimating the compliance.

The Functional Form of the Stress Tensor

Recall the solution is being developed in terms of inputting the strain rate and solving for the stress. Also, during intense loading of snow the elastic strains are negligible. Hence,

$$\dot{\underset{\sim}{E}} = \frac{\partial \underline{f}}{\partial \underset{\sim}{S}} \cdot \dot{\underline{\xi}} \tag{148}$$

where $\dot{\underline{\xi}} = \dot{\underline{\xi}}(\underset{\sim}{S}, \underline{\xi})$.

At first glance it appears that given $\underset{\sim}{E}$ and $\frac{\partial \underline{f}}{\partial \underset{\sim}{S}}$, Equation 148 can be solved. However, the rate of change of the internal state vector is only a function of the invariants of $\underset{\sim}{S}$ and the specific form of the stress tensor must still be determined.

Recall the complementary energy is a function of the state of stress and the internal state vector.

$$\Psi = \Psi(\underset{\sim}{S}, \underline{\xi}) \tag{149}$$

Furthermore, for an isotropic material, Ψ must be a function of the invariants of $\underset{\sim}{S}$.

$$\Psi = \Psi(\mathrm{tr}\,\underset{\sim}{S}, \mathrm{tr}\,\underset{\sim}{S}^{2}, \mathrm{tr}\,\underset{\sim}{S}^{3}, \underline{\xi}) \tag{150}$$

Therefore, assuming a second order expansion, the most general expression for the complementary energy is given by

$$\Psi = C_0(\underline{\xi}) + C_1(\underline{\xi})(\mathrm{tr}\,\underset{\sim}{S})^2 + C_2(\underline{\xi})\,\mathrm{tr}\,\underset{\sim}{S}^2 . \tag{151}$$

In terms of this expansion, the thermodynamic conjugate $\underline{f}$ is given by

$$\underline{f} = \frac{\partial C_0}{\partial \underline{\xi}} + \frac{\partial C_1}{\partial \underline{\xi}}(\mathrm{tr}\,\underset{\sim}{S})^2 + \frac{\partial C_2}{\partial \underline{\xi}}\,\mathrm{tr}\,\underset{\sim}{S}^2 . \tag{152}$$

Differentiating the above expression with respect to $\underset{\sim}{S}$ gives

$$\frac{\partial \underline{f}}{\partial \underset{\sim}{S}} = 2\frac{\partial C_1}{\partial \underline{\xi}}(\mathrm{tr}\,\underset{\sim}{S})\underset{\sim}{1} + 2\frac{\partial C_2}{\partial \underline{\xi}}\underset{\sim}{S} . \tag{153}$$

Now recall the Maxwell relation given by

$$\frac{\partial \underline{f}}{\partial \underset{\sim}{S}} = \frac{\partial \underset{\sim}{E}}{\partial \underline{\xi}} . \tag{123}$$

Substituting Equation 153 into the above expression and solving for the stress gives

$$\underset{\sim}{S} = d_1(\underline{\xi})\frac{\partial \underset{\sim}{E}}{\partial a} + d_2(\underline{\xi})\,\mathrm{tr}\,\frac{\partial \underset{\sim}{E}}{\partial a}\underset{\sim}{1} , \tag{154}$$

where d_1 and d_2 are scaler functions of the state vector.

Recall I am seeking the functional form of the stress and not the stress itself. Therefore, it is only necessary to determine a relationship for d_2. Furthermore, the coefficients d_1 and d_2 are functions of the state of the material only and do not depend on the stress.

Consider a uniaxial confined compression test as shown in Figure 7. The deformation is given by the following.

$$\begin{aligned} x_1 &= X_1 - X_1 g(t) \\ x_2 &= X_2 \\ x_3 &= X_3 \end{aligned} \tag{155}$$

where $g(t)$ = the dimensionless ratio of the deformation to the sample height.

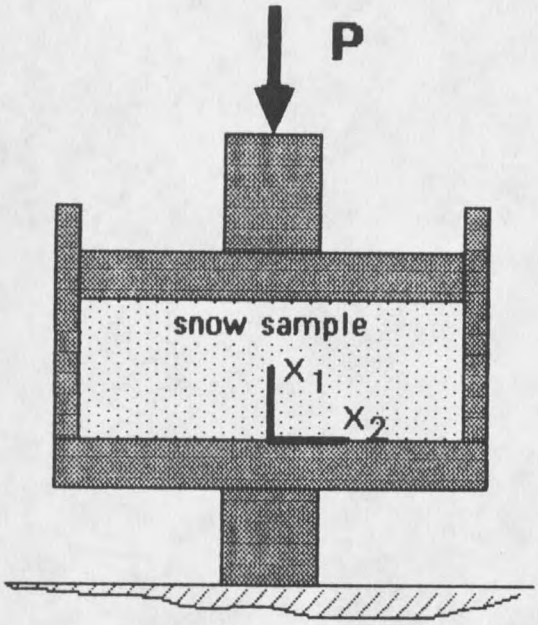

Figure 7. Schematic of a confined uniaxial compression test.

For this type of test, the form of the stress from Equation 154 becomes

$$\underset{\sim}{S} = \frac{a}{a_o} \underset{\sim}{t} = d_1 \begin{bmatrix} (1 + d_2) \dfrac{\partial E_{11}}{\partial a} & 0 & 0 \\ 0 & d_2 \dfrac{\partial E_{11}}{\partial a} & 0 \\ 0 & 0 & d_2 \dfrac{\partial E_{11}}{\partial a} \end{bmatrix} \tag{156}$$

Therefore,

$$t_{11} = \frac{\rho_o}{\rho} d_1 \frac{\partial E_{11}}{\partial a} (1 + d_2) , \tag{157}$$

and $t_{22} = \frac{\rho_o}{\rho} d_1 d_2 \frac{\partial E_{11}}{\partial a}$. (158)

Solving for $d_2(\underline{\xi})$ gives

$$d_2(\underline{\xi}) = \frac{t_{22}}{t_{11} - t_{22}} . \tag{159}$$

This is a significant result in that multiaxial information about the form of the second Piola stress has been obtained from a simple uniaxial test.

The specific form of $d_2(\underline{\xi})$ will have to be determined from test data. However, a great deal of insight into the form of d_2 can be obtained upon closer examination. For instance, d_2 is a dimensionless coefficient. Furthermore, from Equation 154 it is clear that d_2 is related to volumetric effects. In terms of classical isotropic elasticity, the equivalent to d_2 is given by

$$d_{2\,eq} = \frac{\nu}{1 - 2\nu} , \tag{160}$$

where ν is Poisson's ratio.

Figure 8 shows a speculative envelope for a viscous analog of Poisson's ratio for snow (Mellor, 1974). The "curve" is intuitively appealing since $d_2 \to \infty$ as the material approaches solid ice. This is precisely what one would expect, i.e., ice is plastically incompressible, or at least approximately so. Furthermore, the envelope of the data could be explained by considering state variables other than density. For instance, snow which is well sintered should result in a different effective Poisson's ratio than sifted snow of the same density. The internal state variable formulation readily accommodates this feature.

The data provided by Mellor (1974) is not intended to be a substitute for uniaxial test data. However, it does provide a baseline for comparison.

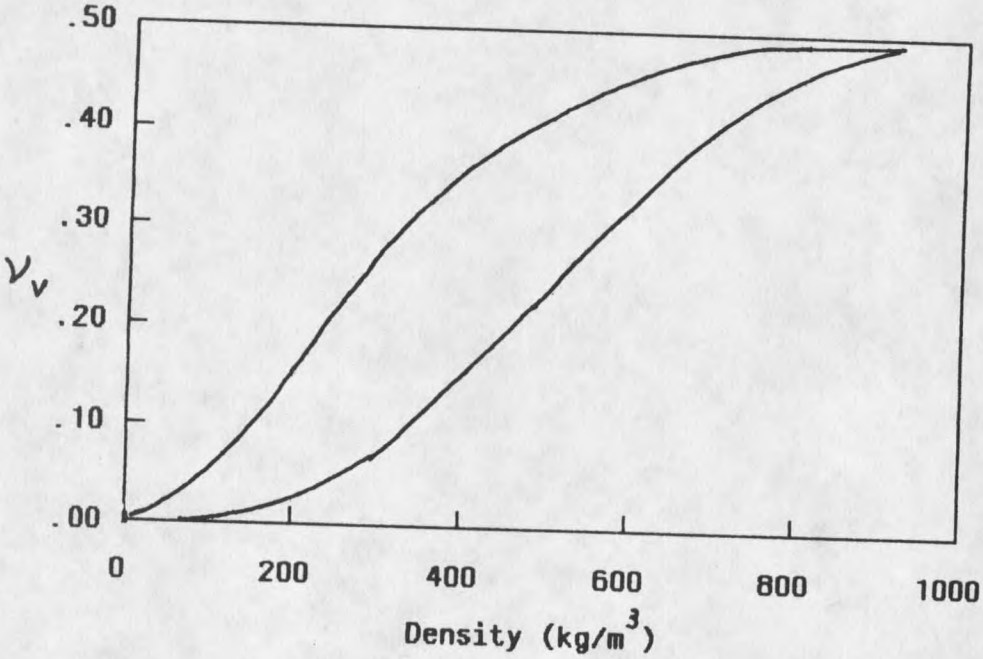

Figure 8. Speculative envelope for a viscous analog of Poisson's ratio (Mellor, 1974).

Evolution Equations

At this point the general framework of a multiaxial constitutive law for snow at finite strain has been developed. The theory is rate dependent through the time evolution of the internal state variables. However, the specific form of the evolution equations will determine whether the behavior is viscoelastic, elastic-viscoplastic, or some combination of these. This will have a pronounced effect on the modelling of various phenomena known to occur in snow such as stress relaxation and limited strain recovery.

The general form of the evolution equations is given by

$$\dot{\underline{\xi}} = \underline{h}(\underset{\sim}{S}, \underline{\xi}) . \tag{161}$$

This equation can be recast in terms of the Cauchy stress as follows.

$$\dot{\underline{\xi}} = \underline{g}(\underset{\sim}{t}, \underline{\xi}) \tag{162}$$

This is far more preferable since the Cauchy stress provides a direct measure of load intensity. Furthermore, this does not affect the generality of the results since the functions $\underline{h}(\underset{\sim}{S}, \underline{\xi})$ and $\underline{g}(\underset{\sim}{t}, \underline{\xi})$ are arbitrary at this point.

Elastic-Viscoplastic Materials

Recall that snow under high rate deformation was assumed to behave as an elastic-viscoplastic material. The defining property of a viscoplastic or plastic material is the existence of a function, G, called the yield function such that no inelastic deformation occurs when $G<0$. I allow G to depend on the stress, stress rate, and the state vector. Hence, G has the form

$$G = G(\underset{\sim}{t}, \dot{\underset{\sim}{t}}, \underline{\xi}) \tag{163}$$

An elastic-viscoplastic material can then be represented as

$$\dot{\underline{\xi}} = \langle G(\underset{\sim}{t}, \dot{\underset{\sim}{t}}, \underline{\xi}) \rangle \, \underline{g}(\underset{\sim}{t}, \underline{\xi}) \tag{164}$$

where $G<0$ implies $\dot{\underline{\xi}} = 0$.

If G is positive semi-definite, the evolution equation represents a viscoelastic material.

It is important to note that including the stress rate in the yield function does not affect any of the thermodynamic restrictions developed from the Second Law, where it was assumed

$$\dot{\underline{\xi}} = \underline{g}(\underset{\sim}{t}, \underline{\xi}).$$

Hence, the restrictions developed are actually valid for a much larger class of materials.

Finally, from material isotropy, one can express $\dot{\underline{\xi}}$ in terms of the invariants of $\underset{\sim}{t}$. More specifically, I allow the evolution equations to depend on the pressure, P, and the second invariant of the deviatoric stress, J_2, where

$$P = -\frac{1}{3}\,\mathrm{tr}\,\underset{\sim}{t}\,, \tag{165}$$

$$J_2 = \frac{1}{2}\,\mathrm{tr}\,\tau^2\,, \tag{166}$$

and $$\underset{\sim}{\tau} = \underset{\sim}{t} - \frac{1}{3}\,\mathrm{tr}(\underset{\sim}{t})\,\underset{\sim}{1}\,. \tag{167}$$

The pressure can be directly related to volumetric loading while J_2 provides a measure of the shear intensity. Hence, the general form of the evolution equations becomes

$$\dot{\underline{\xi}} = \langle G(P, \dot{P}, J_2, \dot{J}_2, \underline{\xi}) \rangle\, g(P, J_2, \underline{\xi})\,. \tag{168}$$

It is virtually impossible to *a priori* write correct evolution equations for the internal state variables. This will require an extensive test program to track the changes in the microstructure under various loading conditions. However, one can write evolution equations which are at least functionally correct. These equations can then be checked to see if they qualitatively model the response of snow under a variety of loading conditions.

Deformation Mechanisms

The internal state vector chosen for the constitutive law consisted of the mean intergranular slip distance, λ, and the mean grain size, L. The rate of change of the intergranular slip distance provides a direct measure of intergranular glide. This is believed to be the dominant deformation mechanism in low density snow. The reasoning for this is as follows.

First note some data taken on plate sinkage tests of snow in a snow cover, Figure 9. The data are plots of vertical force versus density ratio. The data suggest that a critical value of density occurs in the range from 400 to 450 kg/m^3. At this point, the force required to produce further deformation increases dramatically. This data is consistent with other observed plate sinkage tests.

In terms of the internal state vector, the critical range is approximately given by

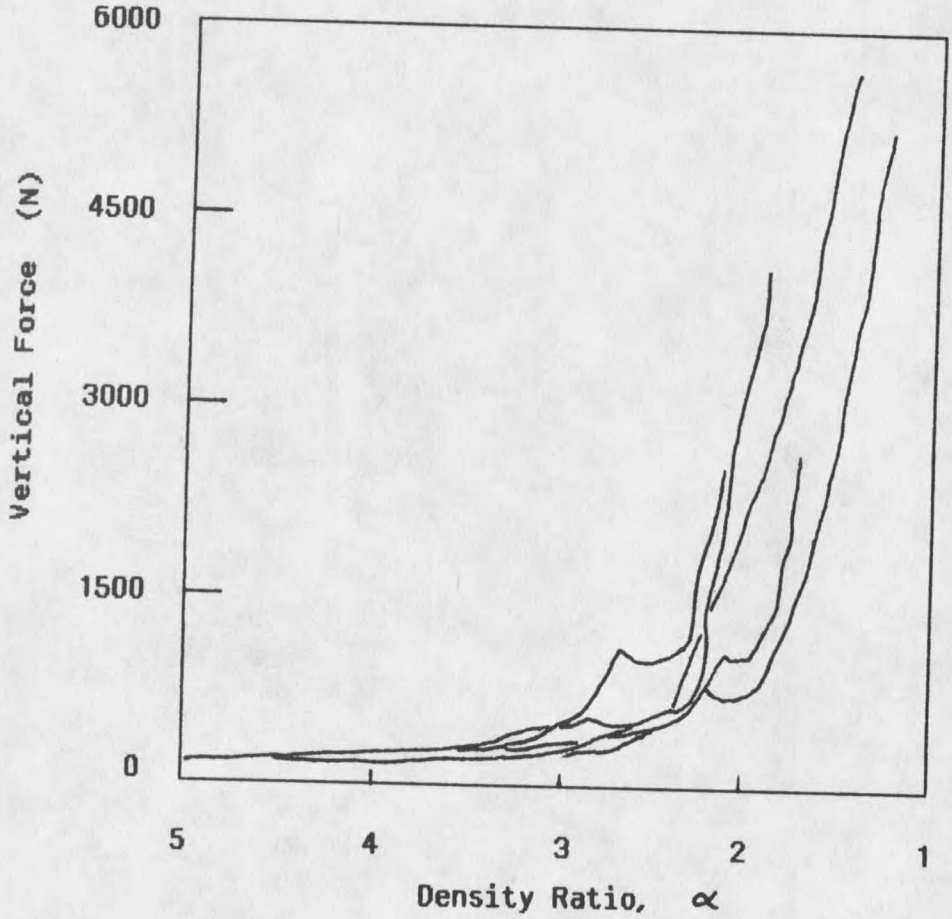

Figure 9. Plate sinkage tests for a snow cover (George L. Blaisdell, CRREL, unpublished data).

$$1.0 < \frac{\lambda}{L} < 1.3 \ .$$

Under applied loads, ice grains fracture and reorganize resulting in intergranular glide. Clearly, as $\lambda \rightarrow L$, the force required to produce intergranular glide must increase dramatically. This is precisely what the data suggests.

As λ approaches L, the significant increase in applied force is believed to be responsible for changes in the mean grain size. This parameter can change as a result of neck growth at grain bonds, shape changes, and pressure sintering of adjacent grains. Under an applied pressure, necks will become shorter and fatter while the shapes of individual

grains tend to become more spherical. This results in an increase in the mean grain size as a spherical shape produces the largest value of grain size for a given volume. Finally, direct pressure sintering of two adjacent grains can eventually result in one large grain.

The density range of 400 to 450 kg/m^3 is believed to be the critical density range for separating the deformation mechanisms. At values below 400 kg/m^3, intergranular glide is assumed to be the dominant deformation mechanism while at values above 400 kg/m^3 intergranular glide and grain size alterations from pressure sintering both contribute to the deformation. However, under very low strain rates, the significance of intergranular glide versus pressure sintering is questionable.

Intergranular Glide

The evolution equation representing intergranular glide is presented purely from a phenomological point of view. First note some uniaxial confined compression data given by Abele and Gow (1975), Figure 10. The figure plots data of the major principal stress versus density for various values of initial density. The tests were conducted at constant cross-head speeds ranging from 0.027 to 27 cm/s. The curves show that the principal stress varies nearly exponentially with density.

Unfortunately, the lateral stress was not measured in these tests so multiaxial data could not be obtained. Brown (1980a) performed a series of experiments to measure the lateral stress under uniaxial confined compression and found in all tests that

$$-0.6\, t_{11} < P < -0.98\, t_{11}\,, \tag{169}$$

where t_{11} = the principal stress,

and $P = -\frac{1}{3}\,\mathrm{tr}\,\underset{\sim}{t}$ = the hydrostatic pressure.

Equation 169 shows that the pressure behaves similarly to the major principal stress.

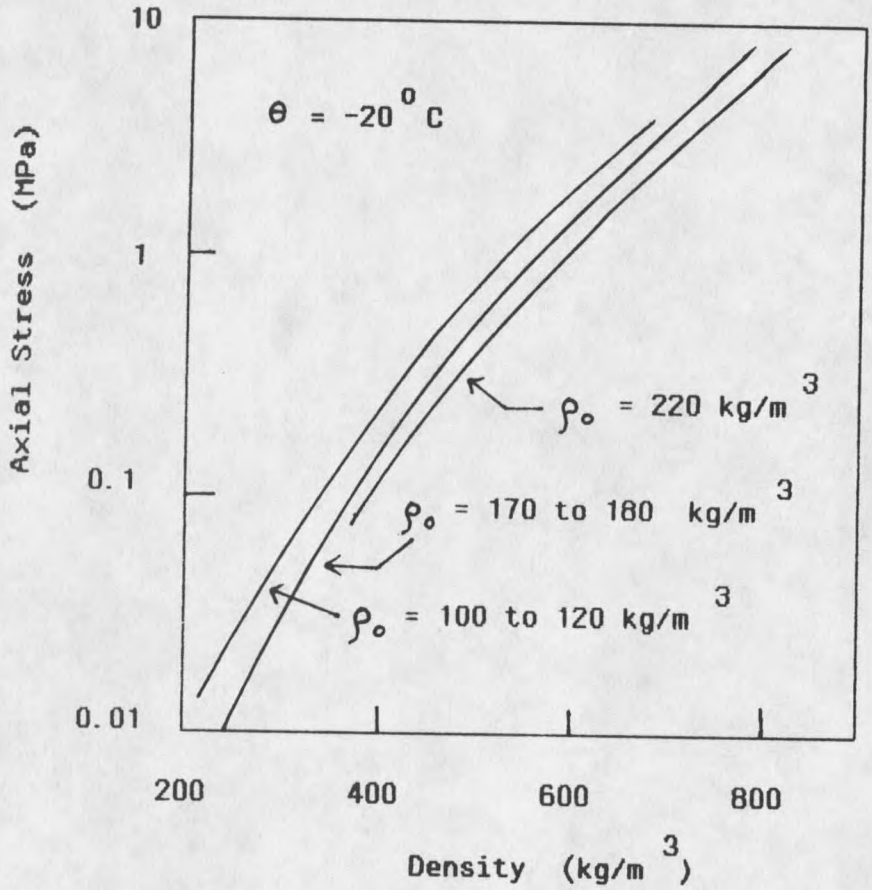

Figure 10. Major principal stress versus density with initial density as a parameter (Abele and Gow, 1975).

Now consider the deformation for a uniaxial confined compression test. From conservation of mass there follows,

$$\det(\underset{\sim}{F}) = 1 - g(t) = \frac{a}{a_o}, \tag{170}$$

where $g(t)$ = the dimensionless ratio of the deformation to the sample height.

Differentiating the above with respect to time gives

$$\dot{g}(t) = -\frac{\dot{a}}{a_o}. \tag{171}$$

This relationship can be expressed in terms of the state vector as follows.

$$\dot{g} = -\frac{1}{a_o}\left(\frac{\dot{\lambda}L - \dot{L}\lambda}{L^2}\right) \tag{172}$$

For low density snow, $\dot{\lambda} \gg \dot{L}$ and Equation 172 reduces to

$$\dot{g} \cong -\frac{\dot{\lambda}}{a_o L}. \tag{173}$$

This equation shows that $\dot{\lambda}$ is approximately constant for low density snow for uniaxial confined compression tests run at constant cross-head rates of deformation.

Based on the previous result, the following form for $\dot{\lambda}$ was assumed.

$$\dot{\lambda} = \langle G \rangle A P \exp(-a_1 (J_2, \theta) \operatorname{erf}(a_2 (J_2, \theta)/\left(\frac{L}{\lambda + L} - \frac{1}{2a_o}\right)) \tag{174}$$

where $\operatorname{erf}(x)$ = the error function defined as

$$\operatorname{erf}(x) = \frac{2}{\sqrt{\pi}} \int_o^x \exp(-t^2)\, dt, \tag{175}$$

and A is a known coefficient determined from initial conditions.

Solving for A gives

$$A = \frac{\dot{\lambda}(o)}{P_Y} \exp(a_1 (J_2, \theta) \operatorname{erf}(a_2 (J_2, \theta)/\left(\frac{L_o}{\lambda_o + L_o} - \frac{1}{2a_o}\right)), \tag{176}$$

where P_Y represents the pressure at initial yield.

Equation 174 may have to be modified for high density snow.

The dependence of the coefficients a_1 and a_2 in Equation 174 on J_2 reflects the dependence of intergranular glide on shearing stresses. It is believed that glide is enhanced with increasing shear intensity. Also, Abele and Gow (1975) show that for pressures above one MPa, the temperature, θ, significantly affects the deformation. The exact form of a_1 and a_2 must be determined from experimental data. Finally, the specific form of the yield function is not specified at this time since this does not affect the behavior of $\dot{\lambda}$ other than to generate an initial condition for yielding.

Mean Grain Size

As mentioned previously, the mean grain size can change as a result of neck growth, shape changes, and pressure sintering of adjacent grains. However, with the exception of extreme pressures at high densities, the dominant mechanism for $\dot{L}$ will be neck growth as the necks are areas of high stress concentrations. Brown (1980a) used a neck growth model to completely model the volumetric deformation of snow.

The change in grain size as a result of neck growth can be developed from quantitative stereology. Underwood (1970) provides the following relation between grain size, surface area, and volume.

$$L\, S_g = 4\, V \tag{177}$$

where S_g equals the mean surface area per grain defined as

$$S_g = \frac{4\,(a-1)}{a\,\lambda}. \tag{178}$$

Differentiating Equation 177 with respect to time and assuming the volume of a single grain remains constant gives

$$L\,\dot{S}_g + \dot{L}\,S_g = 0\,. \tag{179}$$

Now consider a single ice grain with idealized neck regions as shown in Figure 11. The mean surface area of the grain may be expressed as

$$S_g = S_{g_1} + S_{g_2} = S_{g_1} + \pi r h \bar{n}_3 + \pi r^2 \bar{n}_3 , \tag{180}$$

where S_{g_1} = the mean surface area of region one,

and S_{g_2} = the mean surface area of region two.

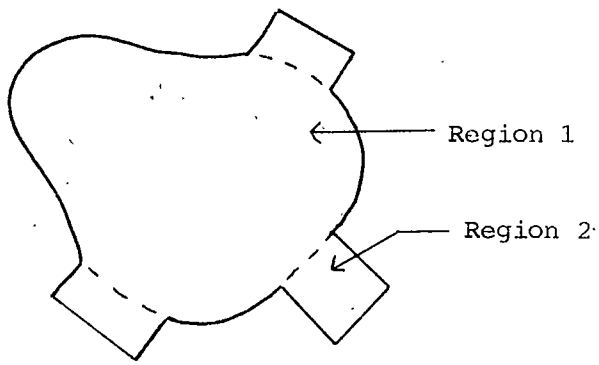

Figure 11. Two dimensional schematic of an ice grain with idealized neck regions.

During the neck growth phase of the deformation, the fundamental shape of region one will not change. Hence, any change in surface area must be accounted for by changes in the neck region. Therefore, differentiating Equation 180 with respect to time gives

$$\dot{S}_g = \bar{n}_3 \pi (\dot{r} h + r \dot{h} + 2 r \dot{r}) . \tag{181}$$

The value of the mean number of bonds per grain, $\bar{n}_3$, is assumed constant during this phase of the deformation. This does not preclude new contact points from forming between adjacent grains. Indeed, the actual number of contacts will increase but this is not a neck growth mechanism. The equation governing L may have to be slightly adjusted to account for this form of direct pressure sintering caused by the formation of new contacts.

Substituting Equation 181 into Equation 179 gives

$$\dot{L} = -\frac{\bar{n}_3 \pi a}{4(a-1)} \lambda L (\dot{r} h + r \dot{h} + 2 r \dot{r}) \tag{182}$$

Now consider the neck region of a specific ice grain. The volume of the neck region is given by

$$V_\beta = \frac{1}{2} \bar{n}_3 \pi r^2 h. \tag{183}$$

Differentiating this expression with respect to time and requiring the neck volume to remain constant provides a kinematic relation between r and h.

$$\dot{h} = -2 \frac{\dot{r}}{r} h \tag{184}$$

Substituting the above expression into Equation 182 gives

$$L = -\frac{\bar{n}_3 \pi a}{4(a-1)} \lambda L (2 r \dot{r} - \dot{r} h) . \tag{185}$$

Equations 184 and 185 define the behavior of L and h in terms of the mean bond radius r and the rate of change $\dot{r}$. To complete the formulation, a kinetic equation for r must be specified. Brown (1980a) has shown that a functionally correct behavior for $\dot{r}$ is given by

$$\dot{r} = \langle G \rangle b_1 \exp(b_2 P a - b_3) , \tag{186}$$

where b_1, b_2, and b_3 are coefficients which depend on the material properties of ice. Equations 184-186 completely define the neck growth model for L.

Finally, it is not necessary for the yield function, G, to be the same for both $\dot{\lambda}$ and $\dot{L}$ since these are independent variables. However, choosing G to be the same is not overly restrictive.

Remarks

The evolution equations presented are merely postulated forms based on the phenomological behavior of snow. However, they do represent functionally correct behavior of the material.

A significant point that was not addressed is the fracturing of ice grains themselves. The current equations readily account for fracture at grain bonds. This is where most of the fracture will take place as the bonds represent weak regions. However, under extremely intense loads, the ice grains themselves will fracture. This will change the complexion of the microstructure since λ, L, and $\overline{n}_3$ will change instantaneously.

The time rate of change of λ representing intergranular glide will not be affected by grain fracture since it is expressed in terms of the ratio of λ/L which remains unchanged. However, the effect of ice fracture on L is more obscure and must be examined more closely.

CHAPTER 7

CONSTITUTIVE BEHAVIOR FOR LOW TO MEDIUM DENSITY SNOW

In this chapter, some theoretical results are presented for snow in the density range from 100 to 400 kg/m^3. The reason for selecting this density range is that intergranular glide can be considered to be the dominant deformation mechanism under high rate deformation. For densities beyond 400 kg/m^3, pressure sintering becomes increasingly important and can no longer be neglected.

Considering only intergranular glide allows some analytical results to be presented. This provides a great deal of insight into the theory as opposed to purely computational results. Also, it should be noted that the density range of 100 to 400 kg/m^3 is actually quite broad and encompasses typical densities found in an alpine snow cover.

The intent of the results is to show that the theory reflects the material response of snow under a variety of loading conditions. Unfortunately, the absence of any multiaxial experimental data which also contains microstructural information limits the comparisons between the theory and actual data. Experimental data is presented in an attempt to show the proper trends.

Specifying a Yield Function and Material Coefficients

Recall the evolution equation governing intergranular glide is given by

$$\dot{\lambda} = \langle G \rangle A P \exp(-a_1 (J_2, \theta)) \operatorname{erf}(a_2 (J_2, \theta) \frac{L}{\lambda + L} - \frac{1}{2a_0}). \tag{174}$$

To complete the formulation a yield function must be specified along with the material coefficients $a_1(J_2, \theta)$ and $a_2(J_2, \theta)$.

Yield Function

Brown (1977) used a thermodynamic formulation based on an expansion of the free energy to develop a fracture criteria for snow. A similar approach could be followed to develop a yield criteria for snow by expressing a critical value of the volumetric complementary energy in terms of the deviatoric complementary energy and microstructural parameters.

The strength of snow is strongly affected by its granular structure. This was graphically demonstrated in Figure 1 where characteristic reductions in strength due to temperature gradient metamorphism were plotted as a function of time. Unfortunately, there is no experimental data characterizing snow strength as a specific function of microstructural parameters. Therefore, in the absence of any experimental data involving strength as a function of microstructure, an empirical yield function will be developed. From Equation 168 the yield function assumes the form

$$G = G(P, \dot{P}, J_2, \dot{J}_2, \underline{\xi}). \tag{187}$$

Now consider the compilation of data relating major principal stress to density under uniaxial strain as shown in Figure 12. Region A shows the stresses required for natural densification of snow and may be thought of as representing a quasi-static yield condition. The large band in the data points out the significance of microstructural parameters other than density. As the stress rate is increased, the data show a jump or discontinuity in the principal stress from that of natural densification. This jump can only be accounted for by a jump in the yield condition.

Based on the data of Figure 12, an approximate yield function is given by

$$G = P - P_1\, 10^{(5.2/\alpha)} - Y + R \text{ MPa}, \tag{188}$$

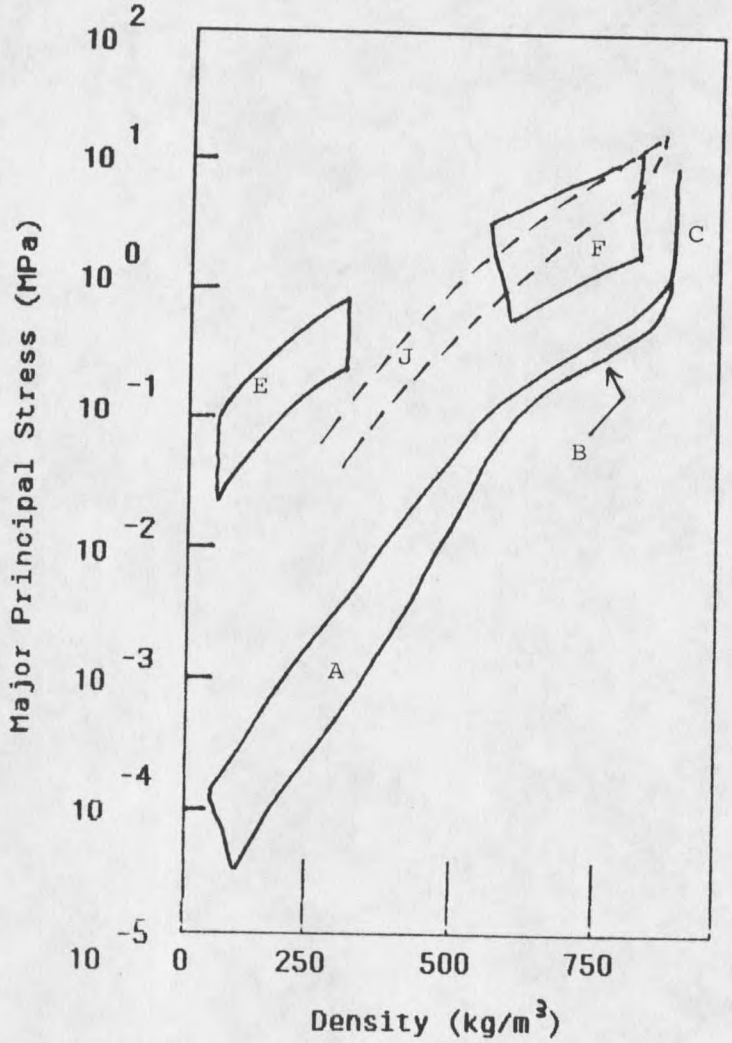

Figure 12. Compilation of data relating major principal stress to bulk density for compression in uniaxial strain at various rates and temperatures (Mellor, 1974). (A) Natural densification of snow deposits, -1° to -48°C. Approximate average loading rates 10^{-5} to 10^{-3} Pa/s (data from depth/density curves for many sites). (B) Slow natural compression of dense firn and porous ice. Approximate loading rates 10^{-5} to 10^{-4} Pa/s (from depth/density curves for polar ice caps). (C) Slow compression of solid ice. (E) Calculated values for plane wave impact at 20-40 m/s (Mellor, 1968). (F) Hugoniot data for explosively generated shock waves (impact velocities 1-12 m/s), -7° to -18°C (data selected from Napadenski, 1964). (J) Compression at approximately constant strain rate, -7° to 18°C. Strain rate = 10^{-4} s^{-1} (Kinosita, 1967).

where $4 < Y < 5$,

$$R = H(\dot{P})\,(\mathrm{erf}(\frac{1}{8}(\log(\frac{\dot{a}}{a_o}) + 1))\,(\frac{2.9}{a} + 3),$$

and $H(\dot{P})$ = the Heavyside function.

Equation 188 with R=0 represents a yield criteria based on natural compression of snow. The value of Y is allowed to vary between 4 and 5 to account for differences in the microstructure at any given density. The coefficient P_1 reflects the fact that the data is given in terms of the major principal stress while the yield function is expressed in terms of the hydrostatic pressure. Equation 169 provides the following empirical bound on P_1.

$$0.6 < P_1 < 0.98$$

Ideally, P_1 and Y should be expressed as a function of the microstructure. However, unless otherwise specified, the following values will be assumed for numerical purposes.

$$Y = 4.5 \quad \text{and} \quad P_1 = 0.8$$

The function R represents the jump in yield stress due to rate effects. This function behaves in a manner such that rate effects become less significant as density increases. Also, expressing R as a function of $\dot{a}$ does not violate Equation 187 since $\dot{a}$ is a linear function of P in the elastic range.

A significant aspect of Equation 188 is the absence of deviatoric effects in the yield function. Future theoretical and experimental studies should address this issue.

Material Coefficients

The material coefficients $a_1(J_2, \theta)$ and $a_2(J_2, \theta)$ of Equation 174 must also be specified before explicit results can be presented. To actually determine their dependence on shear intensity and temperature would require an extensive experimental program. In the absence of such data the coefficients will be treated as fixed as opposed to variable.

Equation 174 may be rearranged to express the pressure as a function of λ.

$$P = \frac{\dot{\lambda}}{A} \exp(a_1 \operatorname{erf}(a_2 (\frac{L}{\lambda + L} - \frac{1}{2a_o})) \tag{189}$$

This equation can be used to estimate a_1 and a_2 based on known slope conditions of the stress density curves given in Figure 10. Approximating the slope at densities of 300 kg/m^3 and 400 kg/m^3, the values of the coefficients are given by

$a_1 = 9.5$ and $a_2 = 2.1$.

The values shown above will be used for all of the numerical results generated in this chapter.

Uniaxial Compression

Consider the case of uniaxial confined compression. Figure 7 shows a schematic of this type of test where the deformation is given by Equation 155. Expressing the deformation in terms of the Lagrangian strain gives

$$E_{IJ} = \frac{1}{2} \begin{bmatrix} (1-g)^2 - 1 & 0 & 0 \\ 0 & 0 & 0 \\ 0 & 0 & 0 \end{bmatrix} , \tag{190}$$

where $g(t)$ = the dimensionless ratio of the deformation to the sample height.

For low density snow the constitutive law assumes the form

$$\dot{\underset{\sim}{E}} = \underset{\approx}{M} : \dot{\underset{\sim}{S}} + \frac{\partial f}{\partial \underset{\sim}{S}} \dot{\lambda} , \tag{191}$$

where f is the thermodynamic conjugate to λ.

Under finite strain, the elastic strains may be neglected and Equation 191 reduces to

$$\dot{\underset{\sim}{E}} = \frac{\partial f}{\partial \underset{\sim}{S}} \dot{\lambda} . \tag{192}$$

Substituting Equations 131 and 133 into the above expression gives

$$\dot{\underset{\sim}{E}} = (k_\lambda \dot{\lambda}) \dot{\underset{\sim}{E}} , \tag{193}$$

where $k_\lambda = \dfrac{1}{\dot{a} L}$.

This equation requires

$$\dot{\lambda} = \dot{a} L \tag{194}$$

for all time t. Expressing k_λ in terms of the deformation gives

$$\dot{\lambda} = - L a_o \dot{g} . \tag{195}$$

Equation 195 can be used in conjunction with the kinetic evolution equation for λ given by Equation 174 to determine the pressure. It should be noted that the mean grain size, L, need not be specified since it shows up in Equation 174 and 195. Specifically, L appears in the coefficient A of Equation 174 and 176 since

$$\dot{\lambda}(0) = L \dot{a}(0) .$$

It should not be surprising that the solution is independent of L since this parameter is constant throughout the deformation.

Figure 13 shows theoretical results of uniaxial confined compression tests for three different deformation rates ranging over four orders of magnitude. The curves indicate a rate dependent response as expected. Quantitative comparisons of magnitudes are unavailable as Abele and Gow (1975) did not show the specific deformation rates in their data. However, the curves represent qualitatively correct behavior as seen by comparing the data with Figure 12.

Figure 14 shows the pressures generated at a constant rate of $\dot{g}=1\ s^{-1}$ for initial densities ranging from 100 to 250 kg/m^3. The data show that initial density strongly influences the pressure-density relationship. As initial density decreases, the pressures required to produce a given final density increase dramatically. These results are consistent with those of Abele and Gow (1975) as shown in Figure 10.

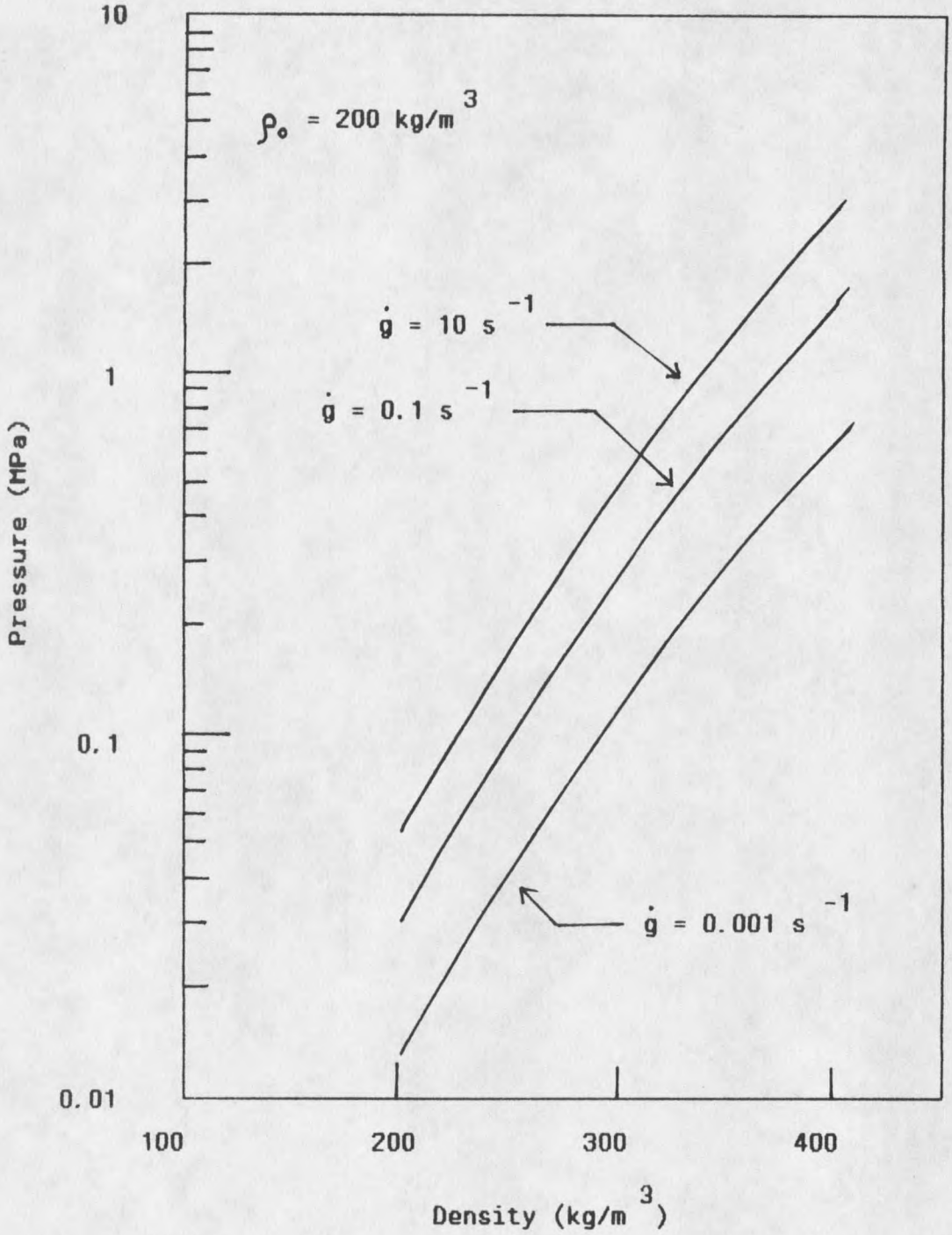

Figure 13. Pressure versus density under uniaxial confined compression with rate of deformation as a parameter (ρ_o = 200 kg/m^3).

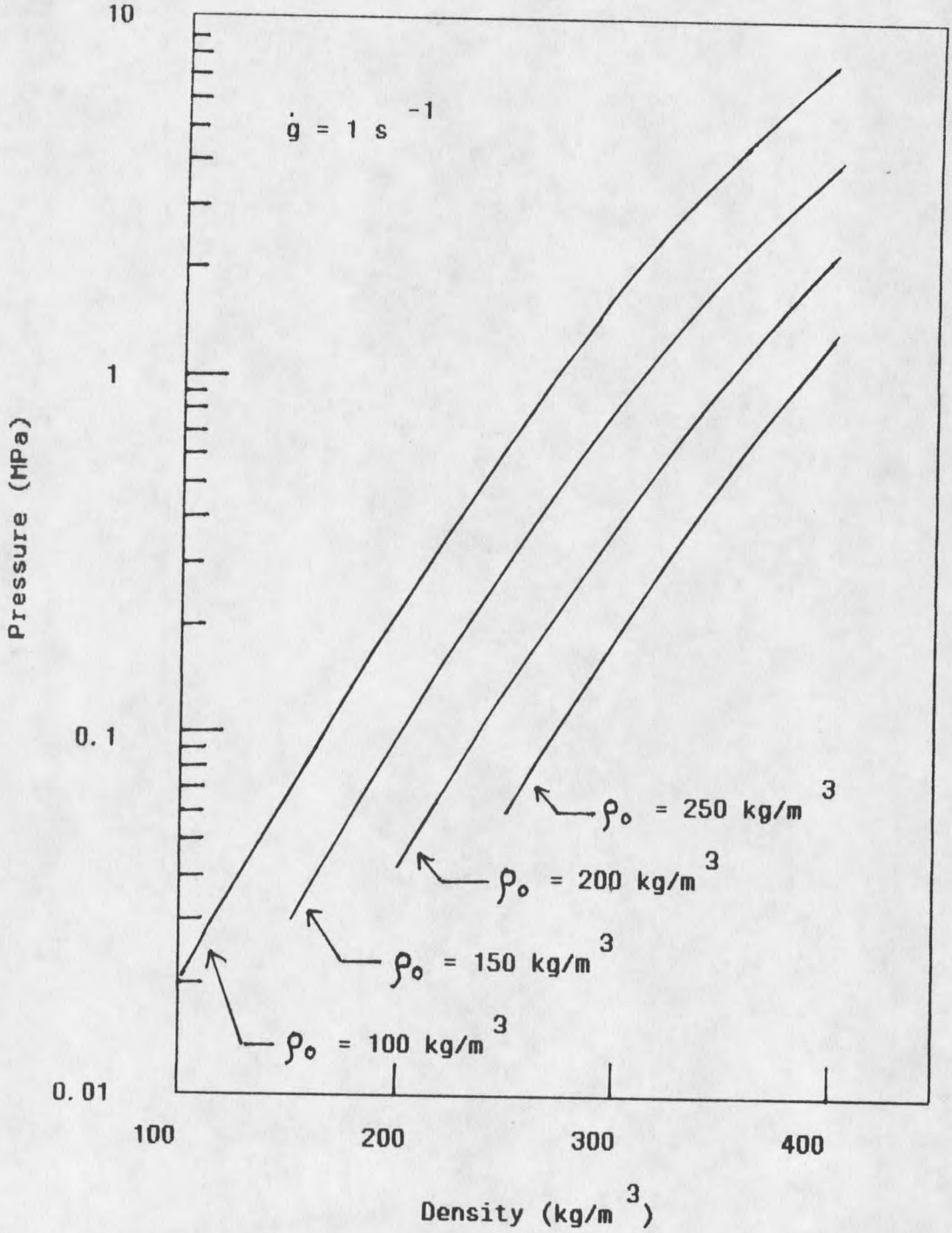

Figure 14. Pressure versus density under uniaxial confined compression with initial density as a parameter ($\dot{g} = 1\ s^{-1}$).

The lateral stress under uniaxial confined compression can be determined in principle from Equation 161.

$$d(\underline{\xi}) = \frac{t_{22}}{t_{11} - t_{22}} \tag{161}$$

In the absence of any experimental data concerning the microstructural behavior of d_2, the following form is assumed.

$$d_2 = \frac{\nu_V}{1 - 2\nu_V} \tag{196}$$

where ν_V = the analog viscous Poisson's ratio.

This particular choice of d_2 is simply the equivalent of d_2 for classical isotropic elasticity where the analog viscous Poisson's ratio has replaced the elastic Poisson's ratio.

From Figure 8, a reasonable form for ν_V is given by

$$\nu_V = 0.73/a - 0.06 \tag{197}$$

This equation simply dissects the envelope of ν_V in the density range from 100 to 400 kg/m^3. The envelope of Figure 8 again points out the significance of microstructure in developing a constitutive theory for snow.

Figure 15 shows the multiaxial stress distribution for a uniaxial confined compression test based on the assumed form of $d_2(\underline{\xi})$. The figure shows that the lateral stress, axial stress, and pressure tend to converge with increasing density. This represents a functionally correct behavior as the stresses will all converge to the same value as the material approaches solid ice.

Strain Recovery

Strain recovery is defined as the amount of strain recovered during a deformation once the stresses are removed. For an elastic response, the strain recovery represents 100 percent of the total strain. However, once a material goes plastic, the strain recovery represents only a fraction of the total strain as the plastic strains are permanent.

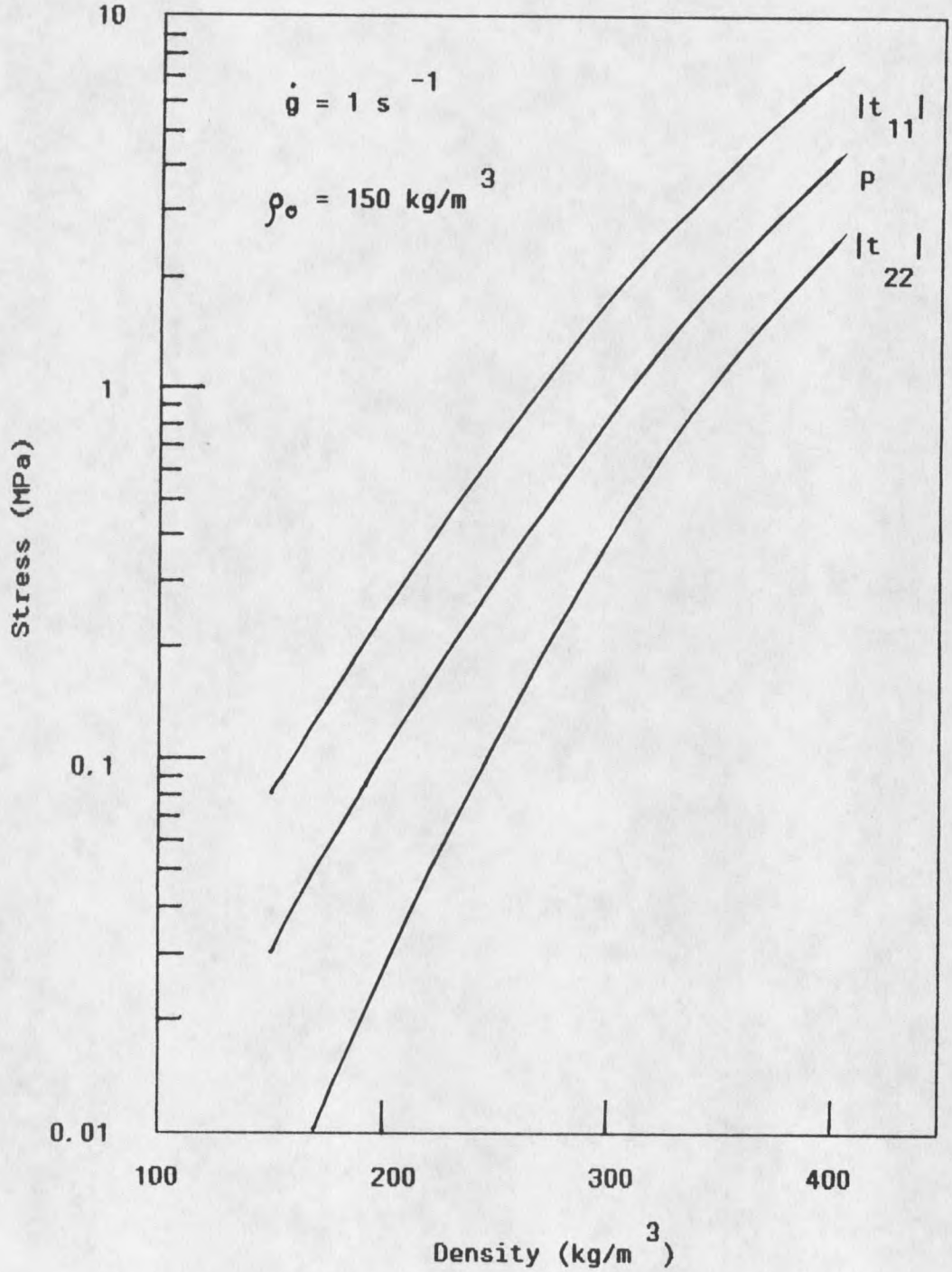

Figure 15. Predicted stress distribution for uniaxial confined compression.

The constitutive theory for snow takes the following form during strain recovery.

$$\dot{\underset{\sim}{E}}_r = \underset{\approx}{M} : \dot{\underset{\sim}{S}} = -\underset{\approx}{M} : \underset{\sim}{S}\ \delta(t_1) \tag{198}$$

where $\delta(t_1)$ = the Dirac delta function,

and $\underset{\sim}{E}_r$ represents the elastic recovery.

Here it is assumed that the stresses are removed instantaneously at time t_1 to prevent further plastic deformation. The equation shows that the strain recovery will be instantaneous or elastic.

The elastic recovery is easily expressed in terms of the Cauchy stress since under uniaxial confined compression,

$$\underset{\sim}{t} = \frac{\rho}{\rho_o}\ \underset{\sim}{S}\ . \tag{199}$$

Differentiating this expression and noting the density is constant during strain recovery gives

$$\dot{\underset{\sim}{t}} = \frac{\rho}{\rho_o}\ \dot{\underset{\sim}{S}}\ . \tag{200}$$

Hence, Equation 198 may be rewritten as

$$\dot{\underset{\sim}{E}}_r = -\underset{\approx}{M}_e : \underset{\sim}{t}\ \ \delta(t_1)\ , \tag{201}$$

where $\underset{\approx}{M}_e$ is the compliance in the deformed configuration.

Integrating this expression gives

$$\underset{\sim}{E}_r = -\underset{\approx}{M}_e : \underset{\sim}{t}\ . \tag{202}$$

Taking the trace of Equation 202 and noting $E_{22} = E_{33} = 0$ gives

$$E_{11_r} = P/K\ , \tag{203}$$

where K = the elastic bulk modulus.

Figure 16 shows the predicted strain recovery characteristics for snow under a constant cross-head rate of deformation. The figure is a plot of axial strain versus characteristic time for an initial density of 200 kg/m^3. The curves are interesting in that they show the elastic recovery decreases as the total strain increases. This is typical of the type of behavior observed for snow. Furthermore, this behavior is exactly the opposite of that predicted by classical plasticity where the elastic recovery increases with increasing strain for a work hardening material. Finally, the strain recovery response also shows that the elastic recovery is rate dependent in that higher rates of deformation result in a larger elastic rebound on unloading.

Stress Relaxation

When a rate dependent material is subjected to a deformation and the deformation is subsequently stopped, the stress in the body tends to relax with time. The rate and degree of relaxation are dependent on the specific material properties. Snow is known to exhibit strong stress relaxation characteristics.

Consider the stress relaxation response as predicted by the constitutive law.

$$\dot{\underset{\sim}{E}} = \underset{\approx}{M} : \dot{\underset{\sim}{S}} + \frac{\partial f}{\partial \underset{\sim}{S}} \dot{\lambda} \tag{191}$$

When the deformation is halted, $\dot{\underset{\sim}{E}} = 0$, and the governing differential equation becomes

$$\underset{\approx}{M} : \dot{\underset{\sim}{S}} = - \frac{\partial f}{\partial \underset{\sim}{S}} \dot{\lambda} . \tag{204}$$

Employing the Maxwell relation given by Equation 123 there follows,

$$\underset{\approx}{M} : \dot{\underset{\sim}{S}} = - \frac{\partial \underset{\sim}{E}}{\partial \lambda} \dot{\lambda} . \tag{205}$$

It is convenient to discuss stress relaxation in terms of the pressure. Therefore, taking the trace of Equation 205 gives, with the use of Equation 133

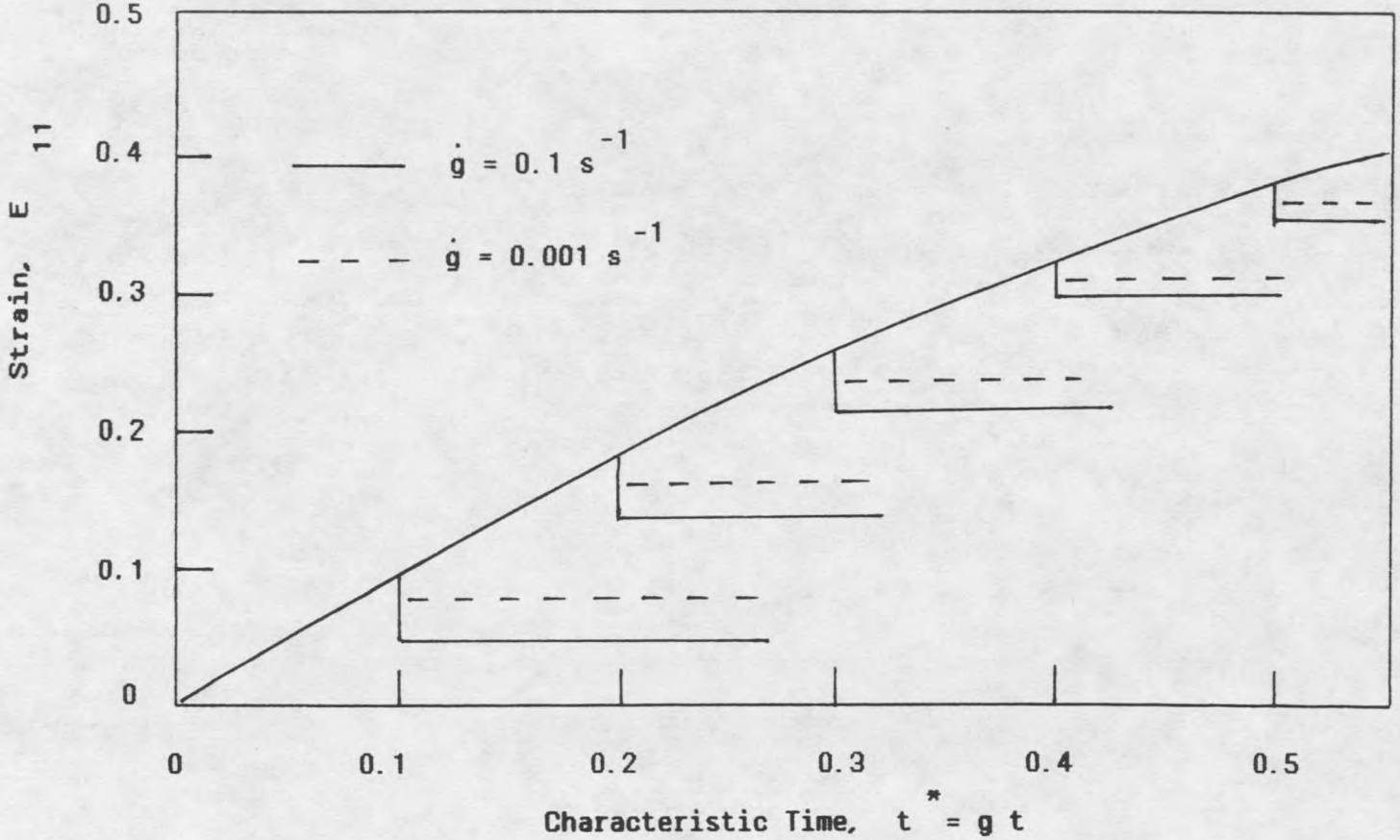

Figure 16. Predicted strain recovery characteristics for snow under uniaxial confined compression.

$$(3U + 2V)\,\mathrm{tr}\,\dot{\underset{\sim}{S}} = -\,\mathrm{tr}\left(\frac{\partial \underset{\sim}{E}}{\partial \lambda}\right)\dot{\lambda}\,. \tag{206}$$

Again, under uniaxial confined compression, the Cauchy stress is related to the second Piola stress by

$$\underset{\sim}{t} = \frac{\rho}{\rho_o}\,\underset{\sim}{S}\,. \tag{199}$$

Noting Equation 147 and the fact that the state of the material is approximately constant during relaxation, the left hand side of Equation 206 may be expressed as

$$(3U + 2V)\,\mathrm{tr}\,\dot{\underset{\sim}{S}} = -\dot{P}/K\,, \tag{207}$$

where P = the hydrostatic pressure,

and K = the elastic bulk modulus.

Equations 128-130 provide an expression for $\frac{\partial \underset{\sim}{E}}{\partial \lambda}$ as follows.

$$\frac{\partial \underset{\sim}{E}}{\partial \lambda} = \frac{1}{\dot{a}L}\,\dot{\underset{\sim}{E}}^{P} \tag{208}$$

Taking the trace of this expression and neglecting elastic strains gives

$$\mathrm{tr}\left(\frac{\partial \underset{\sim}{E}}{\partial \lambda}\right) = \frac{1}{\dot{a}L}\,\mathrm{tr}\,\dot{\underset{\sim}{E}}\,. \tag{209}$$

Again, during the relaxation phase, the plastic state of the material is approximately unchanged. Hence, $\frac{\partial \underset{\sim}{E}}{\partial \lambda}$ may be assumed to be a constant.

Combining Equations 206-207 and 209 gives

$$\dot{P} = K\,\mathrm{tr}\left(\frac{\partial \underset{\sim}{E}}{\partial \lambda}\right)\dot{\lambda}\,. \tag{210}$$

The evolution equation at post yield is given by

$$\dot{\lambda} = P\,A\exp\left(-a_1\,\mathrm{erf}\left(a_2\left(\frac{L}{\lambda + L} - \frac{1}{2a_o}\right)\right)\right), \tag{211}$$

where $A = \frac{\dot{\lambda}(0)}{P_Y} \exp(a_1 \operatorname{erf}(a_2 (\frac{L}{\lambda_o + L} - \frac{1}{2a_o}))$.

Substituting this result into Equation 210 and collecting terms gives

$$\dot{P} = -C P \ , \ (t \geqslant t_1) \tag{212}$$

where $P(t_1) = P^*$ = the stress at time t_1 when the deformation is halted,

and C is a *positive* constant given by

$$C = -K \operatorname{tr} (\frac{\partial \underset{\sim}{E}}{\partial \lambda}) A \exp(a_1 \operatorname{erf}(a_2 (\frac{L}{\lambda + L} - \frac{1}{2a_o})) \ . \tag{213}$$

Equation 212 represents the governing differential equation for stress relaxation in snow. This equation has the following analytical solution.

$$P = P^* \exp[-C(t - t_1)] \ , \ (t \geqslant t_1) \tag{214}$$

where t_1 represents the time when the deformation is halted.

Figure 17 shows the characteristic form of the solution for stress relaxation. The results are encouraging as this is the qualitative relaxation behavior for snow. It should be noted that the stress will not relax completely as Equation 214 ceases to be valid once the stress has fallen below the yield surface.

A quantitative comparison of stress relaxation as well as the prior loading history can be made for the case of uniaxial unconfined compression. A series of these tests have been performed at Montana State University (Brown, private communication).

For comparison purposes, consider the deformation history for the first 25 minutes of test number RC-8-5-08.08.73-10 shown below.

0 - 900 s ; $\dot{g} = 1.11\ (10)^{-3}\ s^{-1}$

900 - 1500 s ; $\dot{g} = 0$

The snow sample in question had an initial density of 350 kg/m^3 and was in the early stages of temperature gradient metamorphism. The environmental temperature was -10°C.

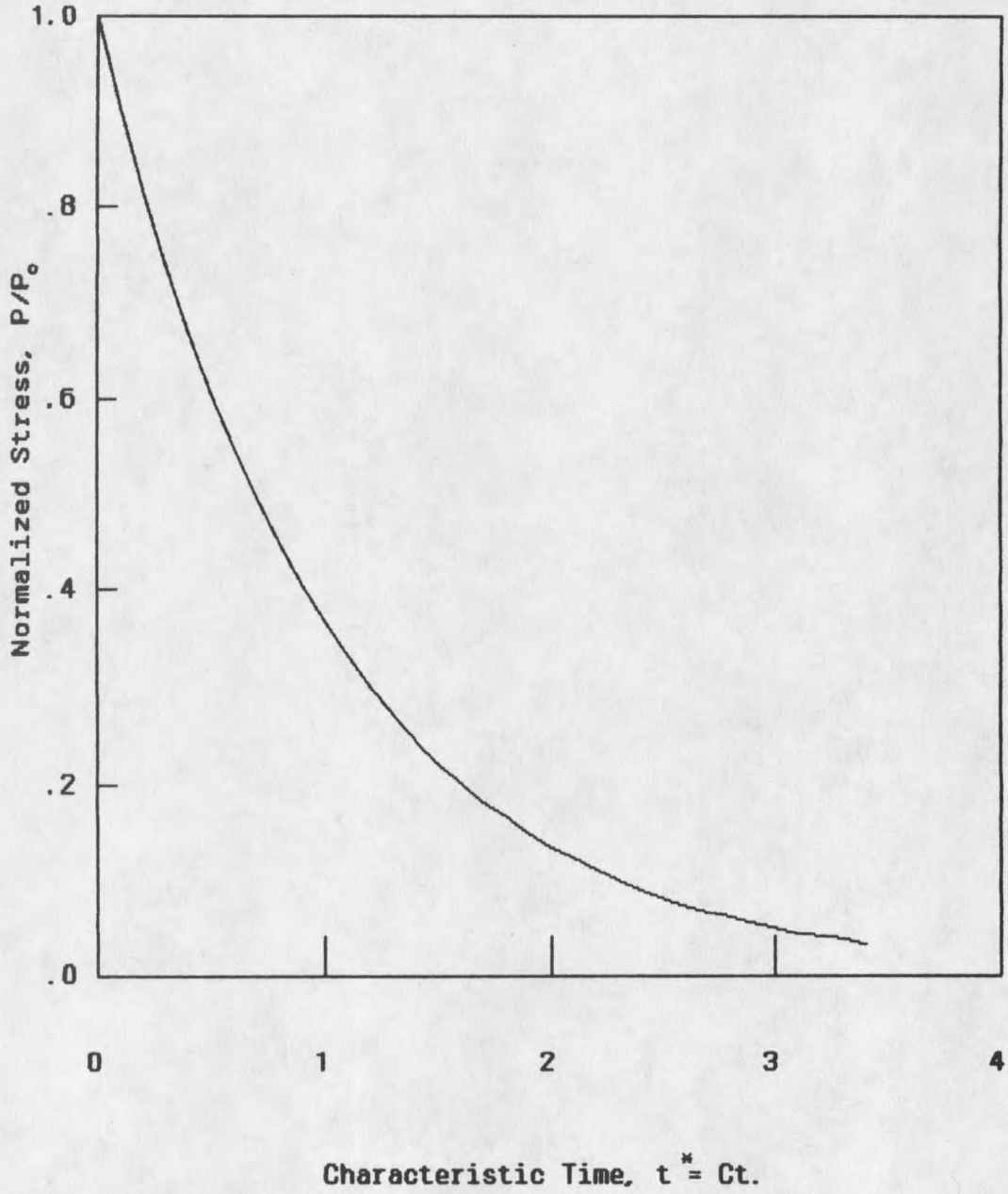

Figure 17. Characteristic solution for stress relaxation.

An extensometer was used to determine the lateral deformation of the sample. Based on this data, an equivalent viscous Poisson's ratio was determined to be $\nu_V = 0.22$. Treating ν_V as a constant is reasonable since the total strains were on the order of 10 percent. Therefore, assuming small strain theory, the strain rate is given by

$$\dot{E}_{IJ} = \begin{bmatrix} -\dot{g} & 0 & 0 \\ 0 & \nu_V \dot{g} & 0 \\ 0 & 0 & \nu_V \dot{g} \end{bmatrix} \tag{215}$$

The elastic strains for this test represented only 5 percent of the total strain and may be neglected. Therefore, from Equations 192-194 the rate of change of λ during loading is given by

$$\dot{\lambda} = \dot{a}\, L \ . \tag{216}$$

This equation may be used in conjunction with the kinetic evolution equation for λ given by Equation 174 to determine the stress.

A value of Y=4.7 as opposed to Y=4.5 was used in the yield function given by Equation 188 in an attempt to match the yield point of the experimental data. This indicates the snow was weaker than "normal." This result is consistent in that the sample was in the early stages of temperature gradient metamorphism which results in an overall weakening of the material.

The stress relaxation phase is governed by the differential equation

$$\dot{P} = -C\,P \ , \tag{212}$$

where $P(t_1) = P^*$.

Noting Equations 209 and 213 the form of the coefficient C becomes

$$C = -K \frac{\mathrm{tr}\,(\underset{\sim}{E})}{\dot{a}\, L} A \exp(-a_1 \,\mathrm{erf}(a_2 \,(\frac{L}{\lambda + L} - \frac{1}{2\, a_o})) \ . \tag{217}$$

From conservation of mass, the density ratio may be expressed in terms of the Green deformation tensor as

$$\det \underset{\sim}{C} = \left(\frac{a}{a_o}\right)^2 , \tag{218}$$

$$\text{where} \quad \underset{\sim}{C} = 2\underset{\sim}{E} + \underset{\sim}{1} = \begin{bmatrix} 1-2g & 0 & 0 \\ 0 & 1+2\nu_v g & 0 \\ 0 & 0 & 1+2\nu_v g \end{bmatrix}$$

Differentiating Equation 218 with respect to time and rearranging terms gives

$$\dot{a} = \left(\frac{a_o^2}{a}\right)[-(1+2\nu_v g)^2 + (1-2g)(1+2\nu_v g)\,2\nu_v]\,\dot{g} . \tag{219}$$

Therefore, substituting Equations 215 and 219 into Equation 217, the form of the coefficient C for unconfined compression becomes

$$C = -K \frac{2\nu_v - 1}{\left(\frac{a_o^2}{a}\right)[-(1+2\nu_v g)^2 + (1-2g)(1+2\nu_v g)\,2\nu_v]}$$

$$A \exp\left(-a_1 \operatorname{erf}\left(a_2 \left(\frac{L}{\lambda + L} - \frac{1}{2a_o}\right)\right)\right) , \tag{220}$$

where A is given by Equation 211.

Finally, the following elastic material coefficients were chosen from Mellor (1974).

$E_0 = 42$ MPa ,

$E_1 = 55$ MPA ,

and $\nu = 0.22$,

where E_0 = Young's modulus at t=0,

and E_1 = Young's modulus at t=900 s.

These values are approximate and could actually vary significantly.

Based on the elastic properties, the coefficient C given by Equation 220 was found to be

$$C = 6.8\,(10)^{-2}\ s^{-1} .$$

Hence, from Equation 214 the pressure distribution in the relaxation phase is given by

$$P(t) = P^* \exp[-0.068\,(t - t_1)]\ ,\ (t \geqslant t_1)\ . \tag{214}$$

Figure 18 shows a comparison of the theoretical results and the experimental data for the test in question. The results are excellent for the loading region. However, the theory predicts a significantly faster relaxation rate than the experimental data. A possible explanation for this lies in the assumption where the rate of change of the mean grain size, L, was neglected.

Recall, from Equation 126, the expression for the density ratio in terms of the internal state vector.

$$a = \frac{\lambda + L}{L} \tag{126}$$

Differentiating this expression with respect to time gives

$$\dot{a} = \frac{\dot{\lambda}}{L} - \frac{\lambda \dot{L}}{L^2}\ . \tag{221}$$

Under high rate deformation of low to medium density snow, it was assumed $\dot{\lambda} \gg \dot{L}$. Hence, Equation 221 reduced to

$$\dot{a} = \frac{\dot{\lambda}}{L}\ . \tag{222}$$

However, during stress relaxation, the density ratio is approximately a constant. Changes in a as defined by Equation 126 are balanced by changes in the elastic strains. Furthermore, these changes occur over a significant time span, e.g., on the order of minutes. Therefore, under these conditions

$$\dot{a} \ll 1\ .$$

Based on this result, it may not be valid to neglect $\dot{L}$ in Equation 221. In fact, it is possible that pressure sintering ($\dot{L}$) dominates intergranular glide ($\dot{\lambda}$) during relaxation. This hypothesis must be checked experimentally.

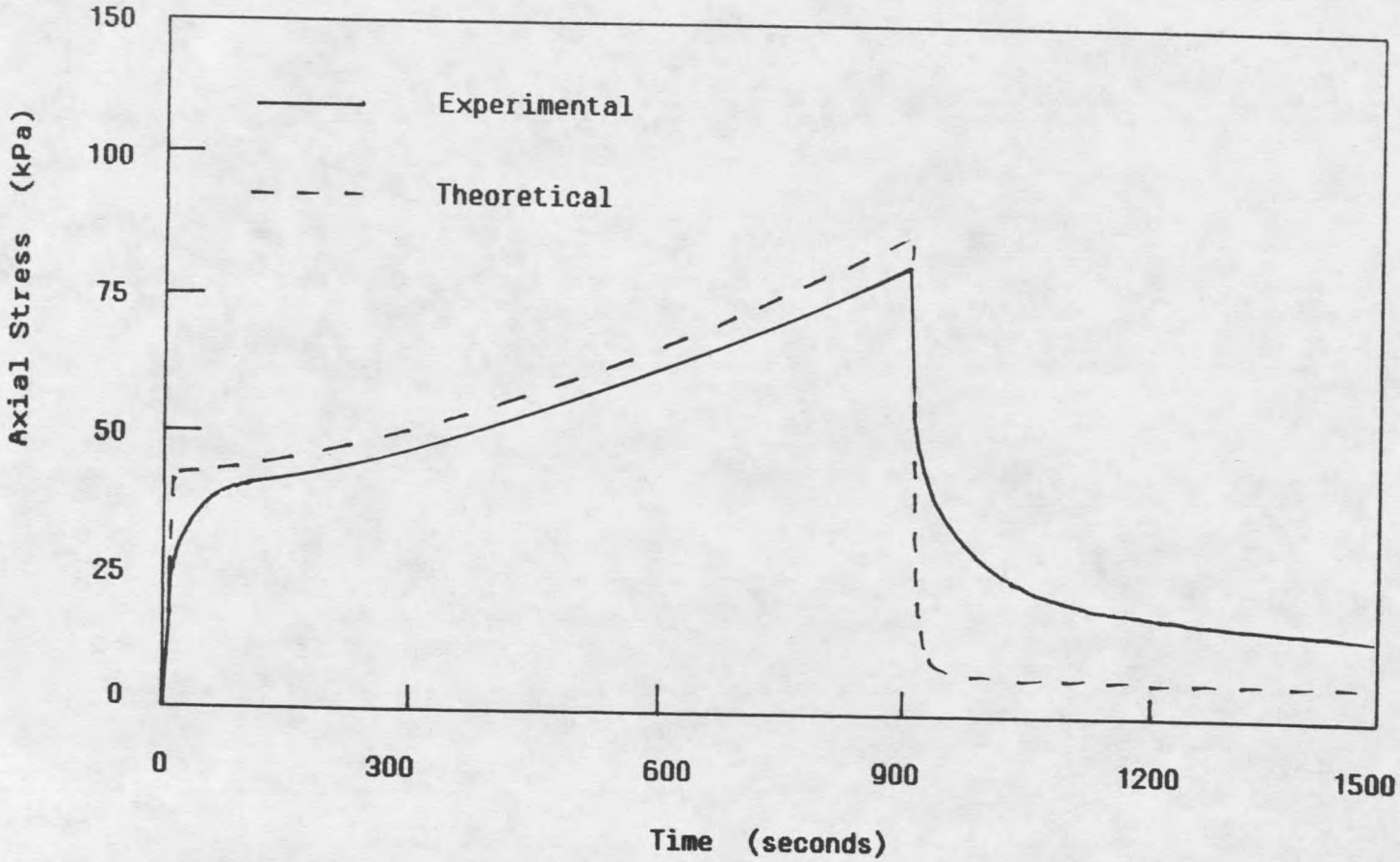

Figure 18. Comparison of theoretical loading and stress relaxation curves with experimental data (test No. RC-8-5-08.08.73-10).

It should be noted that changing the yield function merely altered the initial point of yield. This does not change the fundamental behavior of the curve of Figure 18. Furthermore, the fact that the snow was in the early stages of temperature gradient metamorphism suggests a drop in the yield. This again points out the significance of microstructural properties in snow.

Specific comparisons of theory and experiment must be tempered with the fact that the elastic coefficients are only approximate values. However, it is clear that the theory is capable of characterizing the material response during both loading and relaxation phases.

Combined Compression and Shear

The constitutive theory developed in this work has been shown to reflect the behavior of snow under a variety of uniaxial stress and strain conditions. However, the true value of the theory lies in the fact that it is valid for fully multiaxial stress and deformation conditions. Therefore, consider a combined compression and shear test for snow as shown in Figure 19. This is significantly more complicated than the previous deformations in that it involves "off diagonal" terms in the stress and deformation tensors. A direct consequence of this is that the second Piola-Kirchhoff stress is no longer a scaler multiple of the Cauchy stress but instead behaves according to the following.

$$\underset{\sim}{S} = \frac{\rho_o}{\rho} \underset{\sim}{F}^{-1} \underset{\sim}{t} \underset{\sim}{F}^{-1T} \tag{222}$$

Based on the coordinate system shown in Figure 19, the deformation is given by

$$x_1 = X_1 - X_1 \, g(t) \sin \Omega \ ,$$

$$x_2 = X_2 - X_1 \, g(t) \cos \Omega \ ,$$

$$\text{and} \quad x_3 = X_3 \ . \tag{223}$$

The deformation gradient for this particular test is given by

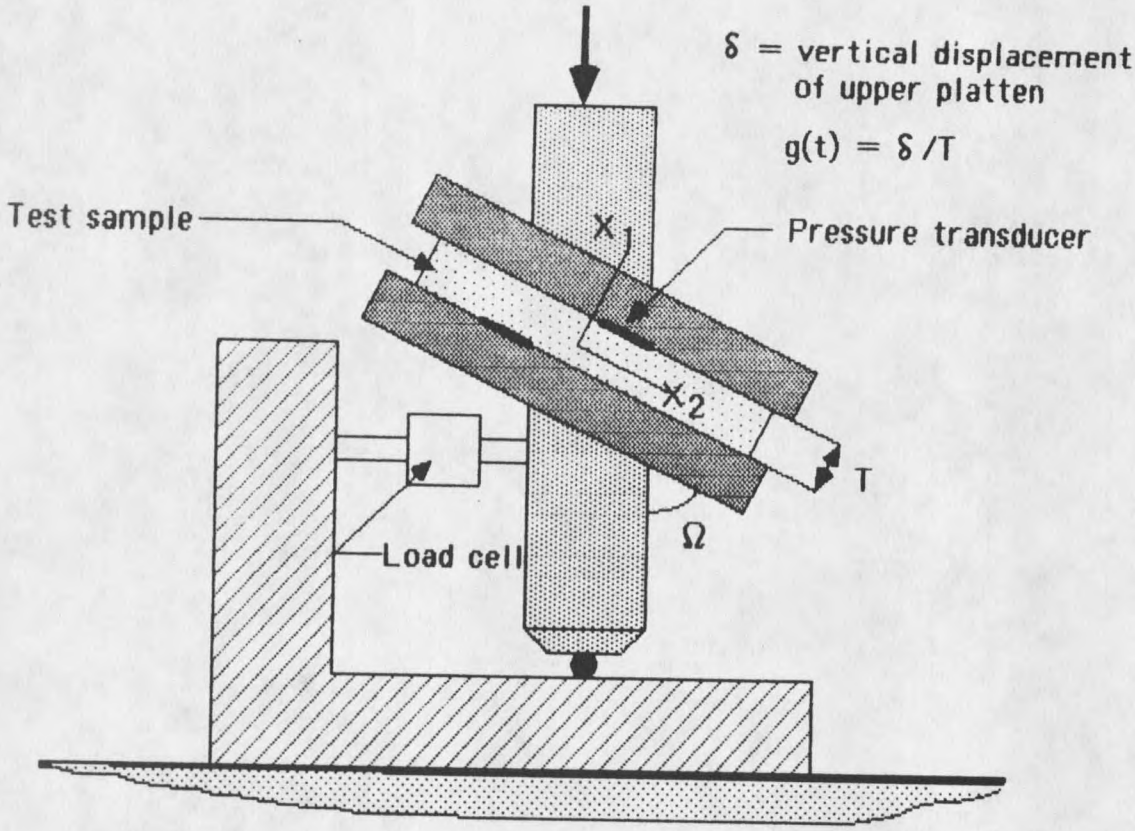

Figure 19. Schematic of a combined compression and shear test.

$$F_{iJ} = \frac{\partial x_i}{\partial X_J} = \begin{bmatrix} 1 - g(t)\sin\Omega & 0 & 0 \\ g(t)\cos\Omega & 1 & 0 \\ 0 & 0 & 1 \end{bmatrix} . \tag{224}$$

For finite deformations, the rate of change of λ takes the following form from Equations 191 and 192.

$$\dot{\lambda} = \dot{a}\, L \,, \tag{225}$$

Equation 225 in conjunction with the kinetic evolution equation given by Equation 174 allows one to determine the pressure, P. However, the full second Piola-Kirchhoff stress is needed to use the constitutive law in the solution of a boundary value problem.

The form of the second Piola-Kirchhoff stress is given by Equation 154.

$$\underset{\sim}{S} = d_1(\underline{\xi})\left[\frac{\partial \underset{\sim}{E}}{\partial a} + d_2(\underline{\xi})\,\mathrm{tr}\left(\frac{\partial \underset{\sim}{E}}{\partial a}\right)\underset{\sim}{1}\right]$$

$$= d_1\, L\left[\frac{\partial \underset{\sim}{E}}{\partial \lambda} + d_2\,\mathrm{tr}\left(\frac{\partial \underset{\sim}{E}}{\partial \lambda}\right)\underset{\sim}{1}\right] \tag{226}$$

As mentioned previously, the specific form of $d_2(\underline{\xi})$ is dependent on the microstructure. In the absence of such data, the form of d_2 will be taken from Equations 196 and 197 where it was assumed,

$$d_2 = \frac{\nu_V}{1 - 2\nu_V} \quad \text{and} \quad \nu_V = 0.73\, a - 0.06 \,.$$

The equation for ν_V was taken from data given by Mellor (1974).

The Cauchy stress may be expressed in terms of the second Piola-Kirchhoff stress as follows.

$$\underset{\sim}{t} = \frac{\rho}{\rho_o}\, \underset{\sim}{F}\, \underset{\sim}{S}\, \underset{\sim}{F}^T \tag{227}$$

Substituting Equation 226 into the above expression gives

$$\underset{\sim}{t} = d_1 L\, \frac{\rho}{\rho_o}\left[\underset{\sim}{F}\, \frac{\partial \underset{\sim}{E}}{\partial \lambda}\, \underset{\sim}{F}^T + d_2\,\mathrm{tr}\left(\frac{\partial \underset{\sim}{E}}{\partial \lambda}\right) \underset{\sim}{F}\, \underset{\sim}{F}^T\right] . \tag{228}$$

Taking the trace of the above equation and expressing tr $(\underset{\sim}{t})$ in terms of the pressure there follows,

$$P = -\frac{1}{3}\,\mathrm{tr}\,\underset{\sim}{t} = -\frac{1}{3}\,d_1 L\,\frac{\rho}{\rho_o}\,[\mathrm{tr}\,(\underset{\sim}{F}\,\frac{\partial \underset{\sim}{E}}{\partial \lambda}\,\underset{\sim}{F}^T)$$

$$+\,d_2\,\mathrm{tr}\,(\frac{\partial \underset{\sim}{E}}{\partial \lambda})\,\mathrm{tr}\,(\underset{\sim}{F}\,\underset{\sim}{F}^T)]\ . \qquad (229)$$

Equations 174 and 229 can be used to solve for the unknown constant, $d_1 L$. This in turn defines the complete second Piola-Kirchhoff stress tensor through Equation 226.

There is virtually no experimental data to verify any of the theoretical solutions to be discussed. The results are presented in an attempt to show the expected behavior of snow under multiaxial deformation. However, a series of combined compression and shear tests are scheduled to be run at Montana State University during the winter of 1985-1986. This will allow specific comparisons of the theory to experimental data.

Figure 20 shows the diagonal components of the second Piola-Kirchhoff stress plotted against the E_{11} component of the Lagrangian strain. The cross head angle, Ω, shown in Figure 19 was 60 degrees and the deformation rate was given by, $\dot{g}=1\ s^{-1}$. The initial and final densities were 200 and 400 kg/m^3 respectively.

The results are interesting in that they show the components S_{22} and S_{33} to be equal throughout the loading history. One would not expect this based on the asymmetry of the deformation. This points out the difficulty of interpreting the second Piola-Kirchhoff stress under complex deformations.

Figure 21 compares the t_{22} and t_{33} components of the Cauchy stress with the respective components of the second Piola-Kirchhoff stress. The results show the Cauchy stress diverging as expected. Furthermore, for very low strains, all the stress components are the same. This again represents a correct behavior as the Piola stress and the Cauchy stress are identical assuming small strain theory.

Figure 22 plots the S_{12} component of the second Piola-Kirchhoff stress versus its conjugate Lagrangian strain component. The results indicate a near exponential response

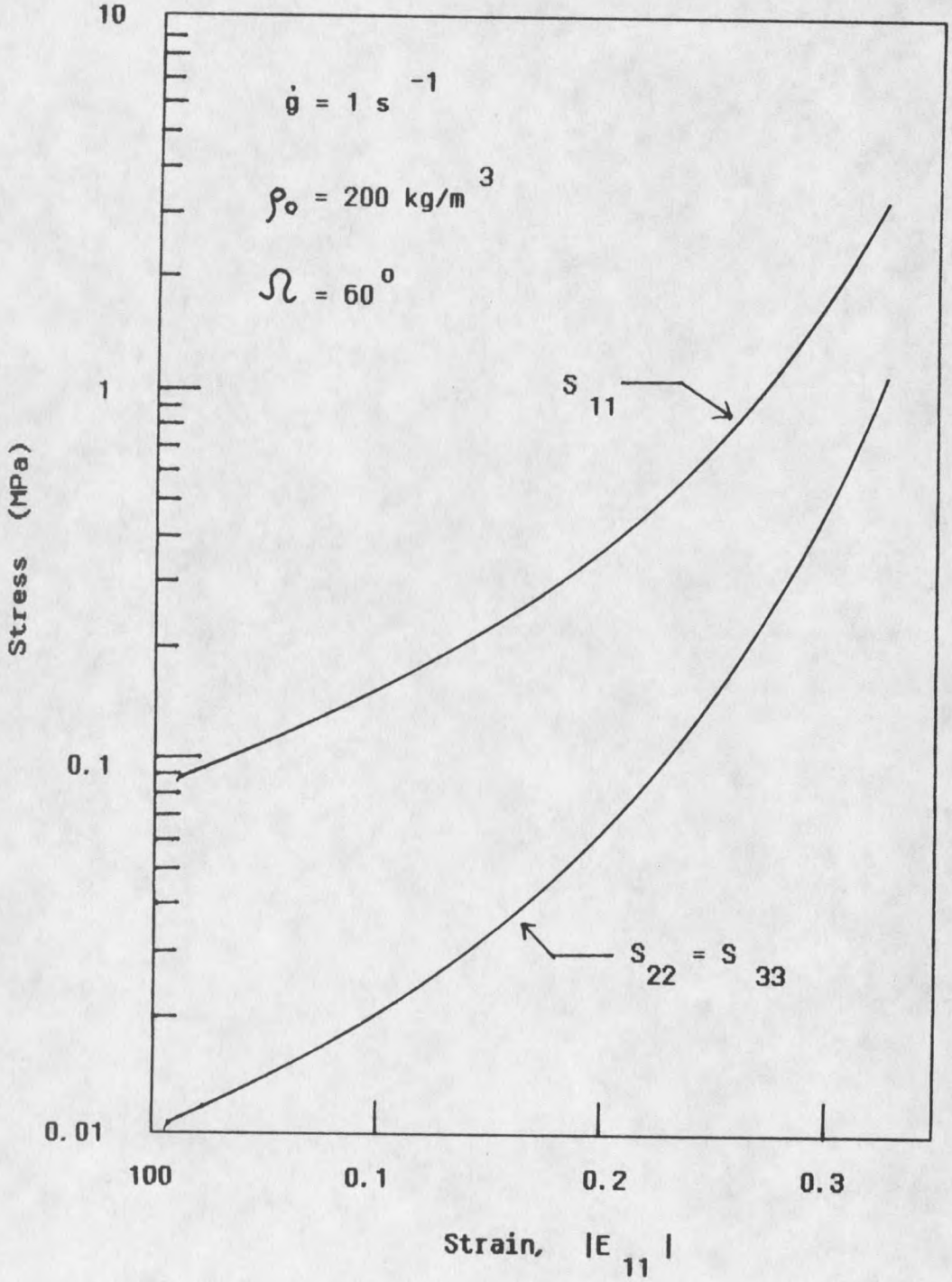

Figure 20. Stress distribution of the diagonal components of the second Piola-Kirchhoff stress versus the E_{11} component of the Lagrangian strain.

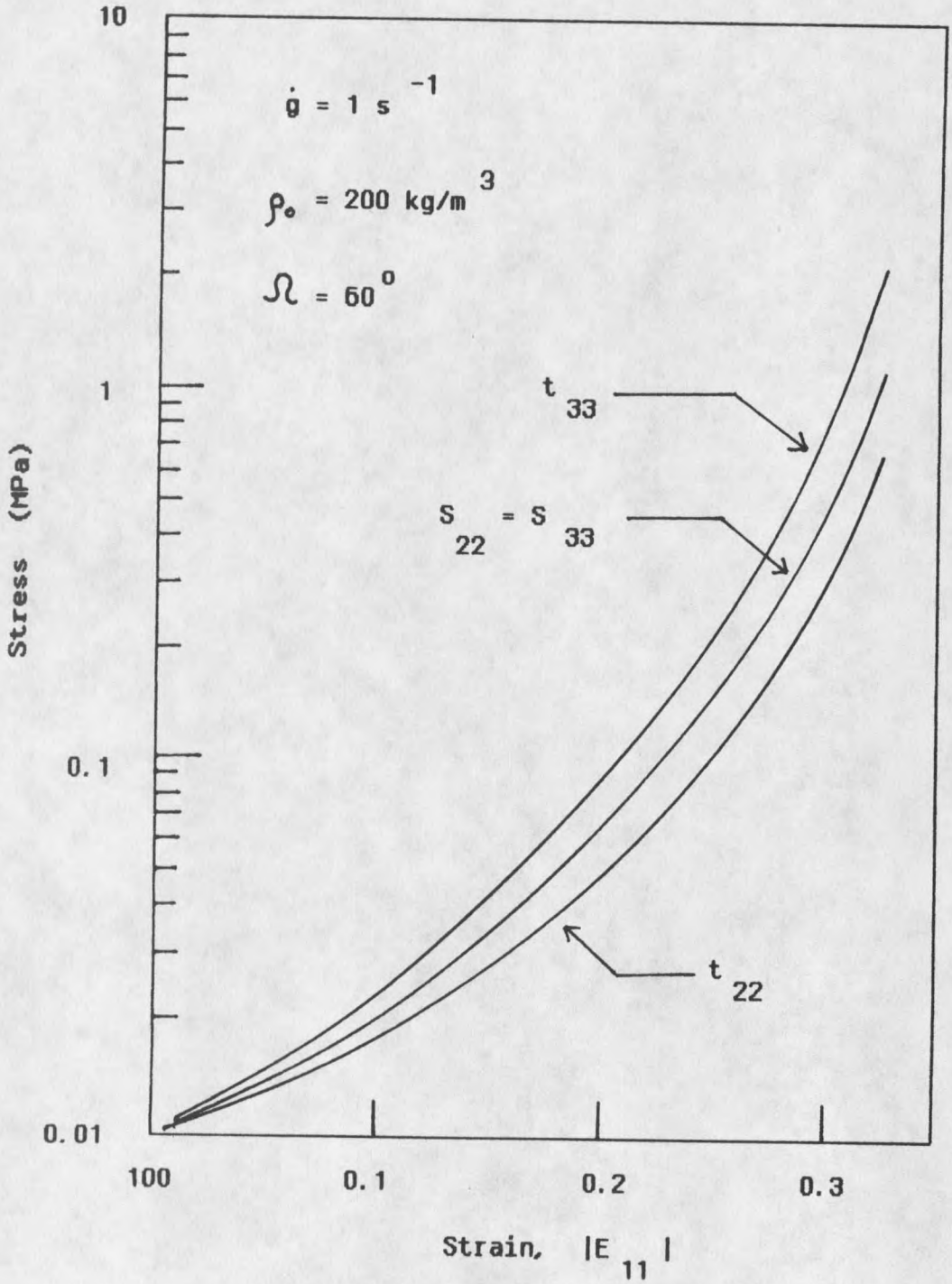

Figure 21. Comparison of the t_{22} and t_{33} components of the Cauchy stress versus the respective components of the second Piola-Kirchhoff stress.

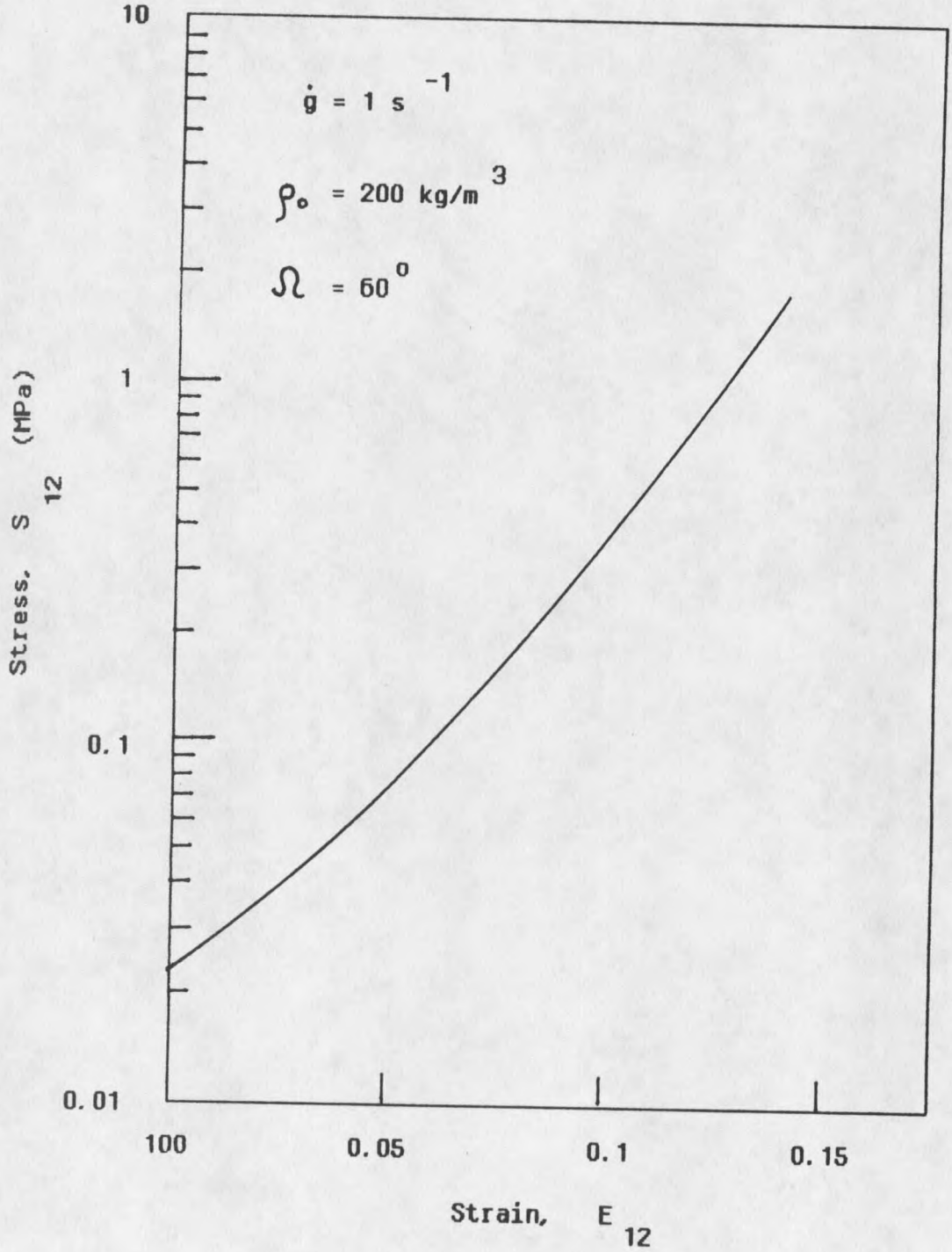

Figure 22. Stress strain curve for the conjugate variables S_{12} and E_{12}.

similar to that observed for the "diagonal" components. However, it should be emphasized that this particular stress/strain component cannot be associated with a pure shear effect as it contains volumetric effects as well. This is another difficulty inherent in large deformation theory.

The theory presented does not take into account the possible fracturing of the snow sample. Fracture will occur at some critical deformation angle, Ω, which may depend on the microstructure of the sample. This type of failure must be addressed through a fracture criteria for snow, e.g., Brown (1977). Finally, all of the multiaxial results presented exhibit a rate dependent response similar to that observed under uniaxial conditions.

CHAPTER 8

DISCUSSION

Developing a new constitutive theory for a material whose behavior is nonlinear is a difficult task. The procedure involves taking a physical theory and attempting to predict an observed material response. When this is done, the question often arises as to whether one is simply curve fitting experimental data or actually modeling the response. At the same time, all constitutive theories require some empirical data to determine material coefficients. The true test is to see if one can extrapolate existing data to characterize the material behavior under a variety of loading conditions.

The paradoxical problem discussed above is alleviated to some extent by the general theories of constitutive relations. These theories are extremely useful in that they set limitations on the forms individual theories can take. For instance, the first law of thermodynamics was used to determine the proper conjugate stress tensor for a given strain. The Second Law places restrictions on possible forms of the functional dependence of the independent variables. The principles of equipresence, frame indifference, and material isotropy were also invoked in developing the theory. All of these results were useful in that they placed limitations on a very general theory.

The use of internal state variables is significant in that it enabled the microstructural properties of the material to be incorporated into a continuum theory. This is essential if one is to actually model the response quantitatively. The results of Chapter 5 demonstrated the ability to measure internal state variables for snow at the granular level.

The results of Chapter 7 were presented to show the ability of this theory to characterize the response of snow under multiaxial deformation and a variety of loadings. Experimental comparisons were limited primarily by the lack of multiaxial data as well as microstructural information. However, the theory clearly accounts for many of the unique phenomological properties of snow. Furthermore, this approach lends significant promise to future efforts in micromechanical constitutive theories.

Suggested Experimental Research

The groundwork for a constitutive theory for snow based on internal state variables at the granular level has been laid. Clearly, the most important experimental research at this point is to obtain multiaxial test data which involves microstructural measurements. Two specific tests of interest are the uniaxial confined compression tests and the combined compression and shear tests discussed in previous chapters. A wealth of microstructural response data could be obtained by taking surface sections before and after each test. This would provide valuable information on the evolution of the microstructural variables.

The significance of pressure sintering versus intergranular glide at very low strain rates should be investigated for low to medium density snow. This is necessary to determine the importance of pressure sintering during stress relaxation. A possible test for consideration would be slow compression of snow over a long period of time. Surface sections taken before and after such a test should provide some insight into the degree of pressure sintering.

Stress wave experiments in the field should also be performed. This would allow one to investigate alterations in the microstructure under intense loads. Furthermore, the effect of pore pressure on the material response could be determined. Preliminary stress wave studies by Brown and Hansen (1985) indicate that the pore pressure is significant to the bulk pressure.

Suggested Theoretical Research

The primary analytical emphasis should be to develop evolution equations which accurately reflect the microstructural response. For instance, the effect of deviatoric stresses on intergranular glide and the yield function should be determined. Temperature effects should also be studied. This does not imply a full blown thermodynamic theory need be developed. Rather, the effects of temperature as an isothermal parameter could be explored. Finally, the effects of internal state variables other than density on material properties should be examined. This could explain much of the scatter in data which is plotted as a function of density. All of the analytical work described complements the experimental work. Indeed, the theory is very useful in determining what to measure in future experiments.

The general theory developed could be applied to many of the problems in snow requiring multiaxial states of stress. These include vehicle mobility, wave propagation, and projectile penetration among others. The theory in its current state is available for use provided the limitations on the density range are observed.

Conclusions

A multiaxial constitutive theory for inelastic deformation of snow has been developed. The theory is significant in that it is valid for finite deformations and is rate dependent. Both of these properties are necessary to successfully model the behavior of snow.

Equally significant is the inclusion of microstructural properties in the formulation while maintaining a continuum theory. The internal state variables provide a powerful method of characterizing the plastic state of the material.

Finally, although this work was directed towards snow mechanics, it is felt that the theory presented is applicable to the field of granular materials in general, the main difference being the selection of an appropriate internal state vector.

REFERENCES CITED

REFERENCES CITED

Abele, G. and J. Gow, 1975, "Compressibility Characteristics of Undisturbed Snow," CRREL Research Report 336.

Abele, G. and J. Gow, 1976, "Compressibility Characteristics of Compacted Snow," CRREL Report 76-21.

Adams, E. E. and R. L. Brown, 1983, "Metamorphism of Dry Snow as a Result of Temperature Gradient Metamorphism and Vapor Density Differences," *Annals of Glaciology,* Vol. 4.

Aitken, G. W., 1978, "Terminal Ballistics in Cold Regions Materials," Proc. 4th International Symposium on Ballistics, Monterey, CA.

Albert, D. G., 1983, "Review of the Propagation of Inelastic Pressure Waves in Snow," CRREL Report 83-13.

Anderson, G. D., 1968, "The Equation of State of Ice and Composite Frozen Soil Material," CRREL Research Report 257.

Bataille, J. and J. Kestin, 1979, "Irreversible Processes and Physical Interpretation of Rational Thermodynamics," *Jour. Non-Equilib. Thermodyn.,* Vol. 4.

Berger, R. H. and W. L. Harrison, 1976, "The Critical State Approach to Snow Mechanics," CRREL Technical Note.

Bowen, R. M., 1976, "Theory of Mixtures," Part I of A. C. Eringen, ed., *Continuum Physics III,* Academic, New York, New York.

Bradley, C. C., R. L. Brown, and T. R. Williams, 1977, "Gradient Metamorphism, Zonal Weakening of the Snow-Pack and Avalanche Initiation," *Journal of Glaciology,* Vol. 19, No. 81.

Brown, R. L., 1977, "A Fracture Criterion for Snow," *Journal of Glaciology,* Vol. 19, No. 81.

Brown, R. L., 1979a, "A Volumetric Constitutive Law for Snow Subjected to Large Strains and Strain Rates," CRREL Report 79-20.

Brown, R. L., 1979b, "A Study of Vehicle Performance in Snow," *Journal of Terramechanics,* Vol. 16, No. 4.

Brown, R. L., 1980a, "A Volumetric Constitutive Law Based on a Neck Growth Model," *Journal of Applied Physics,* Vol. 51, No. 1.

Brown, R. L., 1980b, "Stress Waves in Snow," *Journal of Glaciology,* Vol. 25, No. 91.

Brown, R. L., 1980c, "An Analysis of Non-Steady Pressure Waves in Snow," *Journal of Glaciology,* Vol. 25, No. 92.

Brown, R. L., 1980d, "Propagation of Stress Waves in Alpine Snow," *Journal of Glaciology,* Vol. 26, No. 94.

Brown, R. L., 1981a, "An Analyses of Vehicle Power Requirements in Deep Snowpack," *Journal of Terramechanics,* Vol. 18, No. 3.

Brown, R. L., 1981b, "A Method for Evaluating Shockwave Propagation in Snow," *Cold Regions Science and Technology,* Vol. 5.

Brown, R. L. and A. C. Hansen, 1985, "Field Studies on Stress Waves in Natural Snow Cover," Workshop in Snow Property Management, Lake Louise Chateau, B. C., Canada.

Carrol, M. and A. Holt, 1972, "Static and Dynamic Pore-Collapse Relations for Ductile Porous Materials," *Journal of Applied Physics,* Vol. 43.

Coleman, B. D. and W. Noll, 1960, "An Approximation Theorem for Functionals with Applications in Continuum Mechanics," *Arch. Rational Mech. Anal.,* Vol. 6.

Coleman, B. D. and W. Noll, 1961, "Foundations of Linear Viscoelasticity," *Reviews of Modern Physics,* Vol. 33.

Coleman, B. D. and W. Noll, 1963, "The Thermodynamics of Elastic Materials with Heat Conduction and Viscosity," *Arch. Rational Mech. Anal.,* Vol. 13.

Coleman, B. D., 1964, "Thermodynamics of Materials with Memory," *Arch. Rational Mech. Anal.,* Vol. 17.

Coleman, B. D. and V. J. Mizel, 1966, "Norms and Semi-Groups in the Theory of Fading Memory," *Arch. Rational Mech. Anal.,* Vol. 23.

Coleman, B. D. and M. E. Gurtin, 1967, "Thermodynamics with Internal State Variables," *Journal of Chemical Physics,* Vol. 47, No. 2.

DeHoff, R. T., 1964, "The Determination of the Geometric Properties of Aggregates of Constant-Size Particles from Counting Measurements Made on Random Plane Sections," *AIME,* Vol. 230.

DeHoff, R. T., 1965, "The Estimation of Particle-Size Distributions from Simple Counting Measurements Made on Random Plane Sections," *AIME,* Vol. 233.

Duvall, G. E. and G. R. Fowles, 1963, "Shock Waves," Ch. 9 of R. S. Bradley, ed., *High Pressure Physics and Chemistry 2,* Academic, New York, New York.

Ericksen, J. L., 1960, "Tensor Fields," *Encyclopedia of Physics,* S. Flugge, ed., Vol. 3.1.

Fullman, R. L., 1953, "Measurement of Particles Sizes in Opaque Bodies," *AIME*, Vol. 197.

Gaffney, E. S., 1985, "Hugionot of Water Ice," Proceedings of the NATO Symposium, NATO Advance on Ices in the Solar System, Reidel, Dorderecht, Netherlands.

Good, W., 1974, "Numerical Parameters to Identify Snow Structure," IASH-AISH Publication No. 114.

Goodman, M. A., 1969, "A Continuum Theory for the Dynamical Behavior of Granular Materials," Ph.D. Dissertation, Tulane University.

Goodman, M. A. and S. C. Cowin, 1972, "A Continuum Theory for Granular Materials," *Arch. Rational Mech. Anal.*, Vol. 44.

Gow, A. J., 1969, "On the Rates of Growth of Grains and Crystals in South Polar Firn," *Journal of Glaciology*, Vol. 8, No. 53.

Gubler, H., 1978, "Determination of the Mean Number of Bonds per Snow Grain and of the Dependence of Tensile Strength of Snow on Stereological Parameters," *Journal of Glaciology*, Vol. 20, No. 83.

Hansen, A. C. and R. L. Brown, 1985, "The Effect of Ice Fracture on Energy Dissipation of Plastic Waves in Snow," *Cold Regions Science and Technology* (Submitted).

Harrison, W. L., R. H. Berger, and S. Takagi, 1975, "On the Applications of Critical State Soil Mechanics to Dry Snow," CRREL Internal Report 473.

Hilliard, J. E., 1968, "Direct Determination of the Moments of the Size Distribution of Particles in an Opaque Sample," *AIME*, Vol. 242.

Hobbs, P. V., 1974, *Ice Physics*, Clarendon Press, Oxford, Great Britain.

Kinosita, S., 1967, "Compression of Snow at Constant Speed," International Conference on Physics of Snow and Ice, Hokkaido University, Japan.

Kry, P. R., 1975a, "Quantitative Stereological Analysis of Grain Bonds in Snow," *Journal of Glaciology*, Vol. 14, No. 72.

Kry, P. R., 1975b, "The Relationship Between the Visco-Elastic Properties and Structure of Fine-Grained Snow," *Journal of Glaciology*, Vol. 14, No. 72.

Lubliner, J., 1972, "On the Thermodynamic Foundations of Non-Linear Solid Mechanics," *Int. Journal of Non-Linear Mechanics*, Vol. 7.

Malvern, L. E., 1969, *Introduction to the Mechanics of a Continuous Medium*, Prentice Hall, Englewood Cliffs, New Jersey.

Martin, J. B., 1975, *Plasticity*, MIT Press, Cambridge, Massachusetts.

Mellor, M., 1965, "Explosions in Snow," CRREL Monograph III-A3a.

Mellor, M., 1968, "Avalanches," CRREL Monograph III-A3d.

Mellor, M., 1974, "A Review of Basic Snow Mechanics," *IAHS-AISH* Publication No. 114.

Mellor, M., 1977, "Engineering Properties of Snow," *Journal of Glaciology,* Vol. 19, No. 81.

Napadenski, H., 1964, "Dynamic Response of Snow to High Rates of Loading," CRREL Research Report 119.

Nunziato, J. W. and E. W. Walsh, 1980, "On Ideal Multiphase Mixtures with Chemical Reactions and Diffusion," *Arch. Rational Mech. Anal.,* Vol. 73.

Passman, S. L., 1974, "Mechanics and Thermodynamics of a Mixture of a Granular Material with a Fluid," University of Wisconsin, Mathematics Research Center, Technical Summary Report No. 1391.

Passman, S. L., 1977, "Mixtures of Granular Materials," *Int. Jour. Engng. Sci.,* Vol. 15.

Perla, R., 1982, "Preparation of Section Planes in Snow Specimens," *Journal of Glaciology,* Vol. 28, No. 98.

Read, H. E., J. A. Trangenstein, and K. C. Valanis, 1981, "An Endochronic Soil Model with Critical State," Electric Power Research Institute, NP-1388.

Reid, C. R., 1984, "A Continuum Approach to Sintering Kinetics," M.S. Thesis, Montana State University.

Rice, J. R., 1971, "Inelastic Constitutive Relations for Solids: An Internal Variable Theory and its Application to Metal Plasticity," *Jour. Mech. Phys. Solids,* Vol. 19.

Rice, J. R., 1975, "Continuum Mechanics and Thermodynamics of Plasticity in Relation to Microscale Deformation Mechanisms," Ch. 2 in A. S. Argon, ed., *Constitutive Equations in Plasticity,* MIT Press, Cambridge, Massachusetts.

St. Lawrence, W. F., 1977, "A Structural Theory for the Deformation of Snow," Ph.D. Dissertation, Montana State University.

Swinzow, G. K., 1972, "Terminal Ballistics in Ordinary Snow," CRREL Technical Report 238.

Truesdell, C. and R. Toupin, 1960, "Principles of Classical Mechanics and Field Theory," *Encyclopedia of Physics,* S. Flugge, ed., Vol. 3.1.

Truesdell, C. and W. Noll, 1965, "The Non-Linear Field Theories of Mechanics," *Encyclopedia of Physics,* S. Flugge, ed., Vol. 3.3.

Truesdell, C., 1965, *The Elements of Continuum Mechanics,* Springer-Verlag, New York, New York.

Underwood, E. E., 1970, *Quantitative Stereology,* Addison-Wesley, Reading, Massachusetts.

Valanis, K. C., 1966, "Thermodynamics of Large Viscoelastic Deformations," *Jour. Math. and Physics,* Vol. 45.

Valanis, K. C., 1971a, "A Theory of Viscoplasticity Without a Yield Surface. Part I," *Archives of Mechanics,* Vol. 23, No. 4.

Valanis, K. C., 1971b, "A Theory of Viscoplasticity Without a Yield Surface. Part II," *Archives of Mechanics*, Vol. 23, No. 4.

Valanis, K. C. and H. E. Read, 1980, "New Endochronic Plasticity Model for Soils," Electric Power Research Institute, SSS-R-81-4926.

Wakahama, G. and A. Sato, 1977, "Propagation of a Plastic Wave in Snow," *Journal of Glaciology,* Vol. 19, No. 81.

APPENDICES

APPENDIX A

MATERIAL FRAME INDIFFERENCE

The properties of a material are *intrinsic properties*, in that the manner in which a material responds to a process depends on the material itself. Consequently, the material should look the same to two different observers (frames of reference), i.e., an origin and a coordinate system $(O, \underline{x})$. The material cannot change by changing the reference system. This gives rise to a subtle but important principle called the principle of material frame indifference (objectivity). Before proceeding further, it is necessary to define some quantities.

Definition: Let a particle X contained in a body β occupy the region $\underline{x}$ at time t. The ordered pair $(\underline{x}, t)$ is called an *event*.

Definition: Two frames of reference, $(O, \underline{x})$, $(O^*, \underline{x}^*)$ are said to be *equivalent* if they agree about:

a. Distance between points in a body.

b. Order in which events occur.

c. The orientation of a line segment.

d. The time interval between two events.

Based on this last definition, any reference frames $(O^*, \underline{x}^*)$ obtained by a time dependent rigid transformation from the frame $(O, \underline{x})$ are equivalent. These frames are related in the manner,

$$\underline{x}^* = \underline{c}(t) + \underset{\sim}{Q}(t)\,\underline{x} \ , \tag{229}$$

$$t^* = t - a \ ,$$

where $\underline{c}(t)$ and $\underset{\sim}{Q}(t)$ are smooth functions of time and $\underset{\sim}{Q}(t)$ is orthogonal.

$$\underset{\sim}{Q}^T = \underset{\sim}{Q}^{-1} \tag{230}$$

Definition: Any quantity which depends only on the orientation of the reference frame and not on any other aspect of the motion of the frame (translational velocity, translational acceleration, angular velocity) is said to be *objective*. Therefore,

if f, $\underline{v}$, and $\underset{\sim}{t}$ are objective scalers, vectors, and tensors, these are related under two equivalent reference frames by:

a. $f^* = f$,

b. $\underline{v}^* = \underset{\sim}{Q}\,\underline{v}$,

c. $\underset{\sim}{t}^* = \underset{\sim}{Q}\,\underset{\sim}{t}\,\underset{\sim}{Q}^T$, (231)

where f, $\underline{v}$, and $\underset{\sim}{t}$, are defined with respect to $(O, \underline{x})$,

and f^*, $\underline{v}^*$, and $\underset{\sim}{t}^*$ are defined with respect to $(O^*, \underline{x}^*)$.

An exception to the tensor transformation law shown above is the deformation gradient. This is a two point tensor which transfers similar to a vector, i.e.,

$$\underset{\sim}{F}^* = \underset{\sim}{Q}\,\underset{\sim}{F} \tag{232}$$

The reason for this is as follows. Consider the deformation gradient in two frames.

$$d\underline{x} = \underset{\sim}{F}\,d\underline{X} \;;\; d\underline{x}^* = \underset{\sim}{F}^*\,d\underline{X}^* \tag{233}$$

I can choose equivalent frames such that $\underline{X}^* = \underline{X}$, i.e., the reference frame of each system is the same. This does not affect the generality of the results. Hence, I can write

$$d\underline{x}^* = \underset{\sim}{F}^*\,d\underline{X} \tag{234}$$

Also, from Equation 231 there follows,

$$d\underline{x}^* = \underset{\sim}{Q}\,d\underline{x} = \underset{\sim}{Q}\,\underset{\sim}{F}\,d\underline{X} \tag{235}$$

Comparing this expression with Equation 234 gives

$$\underset{\sim}{F}^* = \underset{\sim}{Q}\,\underset{\sim}{F} \;.$$

Objectivity of the Stress Tensor

Consider the internal contact forces in a body β. These forces depend only on the configuration of β and not on the configuration of external masses. Hence, internal contact forces are formally invariant under changes of frame. This requirement means that the Cauchy stress tensor is objective and must transform according to

$$\underset{\sim}{t}^* = \underset{\sim}{Q}\,\underset{\sim}{t}\,\underset{\sim}{Q}^T \tag{236}$$

Principle of Material Frame Indifference

The principle of material frame indifference states that the material properties are independent of the observer. This means mathematically that constitutive equations must be invariant under changes of frame. That is, if a constitutive equation is satisfied for a process with a motion and a symmetric stress tensor given by

$$\underline{x} = \underline{\chi}\,(\underline{X}, t) \quad , \quad \underset{\sim}{t} = \underset{\sim}{t}\,(\underline{X}, t) \ ,$$

then it must be satisfied for any equivalent process $(\underline{\chi}^*, \underset{\sim}{t}^*)$ where the motion and the stress are related by

$$\underline{x}^* = \underline{c}(t) + \underset{\sim}{Q}\,\underline{x} \ ,$$

$$\underset{\sim}{t}^* = \underset{\sim}{Q}(t)\,\underset{\sim}{t}\,\underset{\sim}{Q}(t)^T \ ,$$

and $t^* = t - a$.

It is interesting to note that this principle has little connection with the laws of mechanics but rather expresses an invariance of the material response. However, the restrictions developed from the principle have a pronounced effect on the form of the constitutive equations developed.

Constitutive Law

Now consider the constitutive law given by

$$\dot{\underset{\sim}{E}} = \frac{1}{\rho_o}\,\frac{\partial^2 \Psi}{\partial \underset{\sim}{S}\,\partial \underset{\sim}{S}} : \dot{\underset{\sim}{S}} + \frac{1}{\rho_o}\,\frac{\partial^2 \Psi}{\partial \underset{\sim}{S}\,\partial \Theta}\,\dot{\Theta} + \frac{\partial \underline{f}}{\partial \underset{\sim}{S}} \cdot \dot{\underline{\xi}} \ , \tag{238}$$

where $\underset{\sim}{E}$ = the Lagrangian strain tensor,

$\underset{\sim}{S}$ = the second Piola stress tensor,

$\underline{\xi}$ = an internal state vector consisting of n objective scalers,

Θ = the temperature,

Ψ = the complementary energy,

and $\underline{f} = \dfrac{\partial \Psi}{\partial \underline{\xi}}$ = the thermodynamic conjugate to the internal state vector.

I would like to show this equation satisfies the principle of material frame indifference.

Recall the following transformations which hold under an arbitrary change of frame.

$$\underset{\sim}{F}^* = \underset{\sim}{Q}\,\underset{\sim}{F} \quad , \quad \underset{\sim}{t}^* = \underset{\sim}{Q}\,\underset{\sim}{t}\,\underset{\sim}{Q}^T$$

From these definitions the transformation laws for numerous other tensors can be developed. The details are shown below.

Lagrangian Strain ($\underset{\sim}{E}$)

The Lagrangian strain is defined by the following expression.

$$\underset{\sim}{E} = \frac{1}{2}(\underset{\sim}{F}^T \underset{\sim}{F} - \underset{\sim}{1})$$

Hence,

$$\underset{\sim}{E}^* = \frac{1}{2}(\underset{\sim}{F}^{T*} \underset{\sim}{F}^* - \underset{\sim}{1}^*)$$

$$= \frac{1}{2}(\underset{\sim}{F}^T \underset{\sim}{Q}^T \underset{\sim}{Q}\,\underset{\sim}{F} - \underset{\sim}{1})$$

$$= \frac{1}{2}(\underset{\sim}{F}^T \underset{\sim}{F} - \underset{\sim}{1}) .$$

Therefore,

$$\underset{\sim}{E}^* = \underset{\sim}{E} . \tag{239}$$

Second Piola Stress ($\underset{\sim}{S}$)

The Second Piola Stress is given by

$$\underset{\sim}{S} = \frac{\rho_o}{\rho}\,\underset{\sim}{F}^{-1}\,\underset{\sim}{t}\,(\underset{\sim}{F}^{-1})^T .$$

The density is a scaler invariant, i.e.,

$$\rho^* = \rho \ .$$

Therefore,

$$\underset{\sim}{S}^* = \frac{\rho_o}{\rho} \underset{\sim}{F}^{-1*} \underset{\sim}{t}^* (\underset{\sim}{F}^{-1})^{T*}$$

$$= \frac{\rho_o}{\rho} (\underset{\sim}{F}^{-1} \underset{\sim}{Q}^T)(\underset{\sim}{Q} \underset{\sim}{t} \underset{\sim}{Q}^T)(\underset{\sim}{Q} \underset{\sim}{F}^{-1T})$$

$$= \frac{\rho_o}{\rho} \underset{\sim}{F}^{-1} \underset{\sim}{t} \underset{\sim}{F}^{-1T} \ .$$

This gives,

$$\underset{\sim}{S}^* = \underset{\sim}{S} \ . \tag{240}$$

<u>Time Derivative of the Second Piola Stress ($\dot{\underset{\sim}{S}}$)</u>

The time derivative of the Second Piola Stress is given by

$$\dot{\underset{\sim}{S}} = \frac{\rho_o}{\rho} \dot{\overline{\underset{\sim}{F}^{-1} \underset{\sim}{t} \underset{\sim}{F}^{-1T}}} - \frac{\rho_o \dot{\rho}}{\rho^2} \underset{\sim}{F}^{-1} \underset{\sim}{t} \underset{\sim}{F}^{-1T}$$

$$= \frac{\rho_o}{\rho} (\dot{\underset{\sim}{F}}^{-1} \underset{\sim}{t} \underset{\sim}{F}^{-1T} + \underset{\sim}{F}^{-1} \underset{\sim}{t} \dot{\underset{\sim}{F}}^{-1T} + \underset{\sim}{F}^{-1} \dot{\underset{\sim}{t}} F^{-1T})$$

$$- \frac{\rho_o \dot{\rho}}{\rho^2} \underset{\sim}{F}^{-1} \underset{\sim}{t} \underset{\sim}{F}^{-1T} \ . \tag{241}$$

The transformation laws for the derivatives of the deformation gradient are given by the following.

$$\dot{\underset{\sim}{F}}^* = \dot{\underset{\sim}{Q}} \underset{\sim}{F} + \underset{\sim}{Q} \dot{\underset{\sim}{F}}$$

$$\dot{\underset{\sim}{F}}^{T*} = \dot{\underset{\sim}{F}}^T \underset{\sim}{Q}^T + \underset{\sim}{F}^T \dot{\underset{\sim}{Q}}^T$$

$$\dot{\underset{\sim}{F}}^{-1*} = \dot{\underset{\sim}{F}}^{-1} \underset{\sim}{Q}^T + \underset{\sim}{F}^{-1} \dot{\underset{\sim}{Q}}^T$$

$$\dot{\underset{\sim}{F}}^{-1T*} = \dot{\underset{\sim}{Q}} \underset{\sim}{F}^{-1T} + \underset{\sim}{Q} \dot{\underset{\sim}{F}}^{-1T}$$

Also,

$$\dot{\underset{\sim}{t}}^* = \dot{\underset{\sim}{Q}}\,\underset{\sim}{t}\,\underset{\sim}{Q}^T + \underset{\sim}{Q}\,\dot{\underset{\sim}{t}}\,\underset{\sim}{Q}^T + \underset{\sim}{Q}\,\underset{\sim}{t}\,\dot{\underset{\sim}{Q}}^T .$$

Substituting the above results into Equation 241 gives

$$\dot{\underset{\sim}{S}}^* = \frac{\rho_o}{\rho}\,[\dot{\underset{\sim}{F}}^{-1}\,\underset{\sim}{t}\,\underset{\sim}{F}^{-1T} + \underset{\sim}{F}^{-1}\,\dot{\underset{\sim}{Q}}^T\,\underset{\sim}{Q}\,\underset{\sim}{t}\,\underset{\sim}{F}^{-1T} + \underset{\sim}{F}^{-1}\,\underset{\sim}{t}\,\underset{\sim}{Q}^T\,\dot{\underset{\sim}{Q}}\,\underset{\sim}{F}^{-1T}$$

$$+ \underset{\sim}{F}^{-1}\,\underset{\sim}{t}\,\dot{\underset{\sim}{F}}^{-1T} + \underset{\sim}{F}^{-1}\,\dot{\underset{\sim}{Q}}^T\,\underset{\sim}{Q}\,\underset{\sim}{t}\,\underset{\sim}{F}^{-1T} + \underset{\sim}{F}^{-1}\,\dot{\underset{\sim}{t}}\,\underset{\sim}{F}^{-1T}$$

$$+ \underset{\sim}{F}^{-1}\,\underset{\sim}{t}\,\dot{\underset{\sim}{Q}}^T\,\underset{\sim}{Q}\,\underset{\sim}{F}^{-1T}] - \frac{\rho_o\dot{\rho}}{\rho^2}\,\underset{\sim}{F}^{-1}\,\underset{\sim}{t}\,\underset{\sim}{F}^{-1T} . \qquad (242)$$

Now note the following identity.

$$\dot{\underset{\sim}{1}} = \dot{\overline{\underset{\sim}{Q}^T\,\underset{\sim}{Q}}} = \dot{\underset{\sim}{Q}}^T\,\underset{\sim}{Q} + \underset{\sim}{Q}^T\,\dot{\underset{\sim}{Q}} = \underset{\sim}{0}$$

Collecting terms and using the above identity, Equation 242 becomes

$$\dot{\underset{\sim}{S}}^* = \frac{\rho_o}{\rho}\,[\dot{\underset{\sim}{F}}^{-1}\,\underset{\sim}{t}\,\underset{\sim}{F}^{-1T} + \underset{\sim}{F}^{-1}\,\underset{\sim}{t}\,\dot{\underset{\sim}{F}}^{-1T} + \underset{\sim}{F}^{-1}\,\dot{\underset{\sim}{t}}\,\underset{\sim}{F}^{-1T}]$$

$$- \frac{\rho_o\dot{\rho}}{\rho^2}\,\underset{\sim}{F}^{-1}\,\underset{\sim}{t}\,\underset{\sim}{F}^{-1T} .$$

Comparing this expression with Equation 241 gives

$$\dot{S}^* = \dot{S} . \qquad (243)$$

<u>Complementary Energy</u> (Ψ)

The complementary energy (Ψ) is a scaler invariant, i.e.,

$$\Psi^* = \Psi .$$

Furthermore, Equation 240 shows that $\underset{\sim}{S}$ is an invariant tensor. Therefore, it follows that $\frac{\partial\Psi}{\partial\underset{\sim}{S}}$ must also be invariant. For instance, at equilibrium,

$$\frac{1}{\rho_o}\,\underset{\sim}{E} = \frac{\partial\Psi}{\partial\underset{\sim}{S}} ,$$

where $\underset{\sim}{E}$ is invariant by Equation 239. Hence, $\frac{\partial^2 \Psi}{\partial \underset{\sim}{S}\, \partial \underset{\sim}{S}}$ must also be invariant, i.e.,

$$\left(\frac{\partial^2 \Psi}{\partial \underset{\sim}{S}\, \partial \underset{\sim}{S}}\right)^* = \frac{\partial^2 \Psi}{\partial \underset{\sim}{S}\, \partial \underset{\sim}{S}} \quad . \tag{244}$$

By similar reasoning there follows,

$$\left(\frac{\partial^2 \Psi}{\partial \underset{\sim}{S}\, \partial \Theta}\right)^* = \frac{\partial^2 \Psi}{\partial \underset{\sim}{S}\, \partial \Theta} \quad . \tag{245}$$

Finally, the internal state vector is a collection of n objective scalers. Hence,

$$\underline{\xi}^* = \underline{\xi} \quad , \quad \dot{\underline{\xi}}^* = \dot{\underline{\xi}} \quad ,$$

and $$\left(\frac{\partial \underline{f}}{\partial \underset{\sim}{S}}\right)^* = \left(\frac{\partial^2 \Psi}{\partial \underset{\sim}{S}\, \partial \underline{\xi}}\right)^* = \frac{\partial^2 \Psi}{\partial \underset{\sim}{S}\, \partial \underline{\xi}} = \frac{\partial \underline{f}}{\partial \underset{\sim}{S}} \quad . \tag{246}$$

The constitutive equation of interest is given by

$$\dot{\underset{\sim}{E}} = \underset{\approx}{M} : \dot{\underset{\sim}{S}} + \underset{\sim}{A}\, \dot{\Theta} + \frac{\partial \underline{f}}{\partial \underset{\sim}{S}} \cdot \dot{\underline{\xi}} \; ;$$

where $$\underset{\approx}{M} = \frac{1}{\rho_o} \frac{\partial^2 \Psi}{\partial \underset{\sim}{S}\, \partial \underset{\sim}{S}} \quad ,$$

and $$\underset{\sim}{A} = \frac{1}{\rho_o} \frac{\partial^2 \Psi}{\partial \underset{\sim}{S}\, \partial \Theta} \quad .$$

The time derivative of the Lagrangian strain may be expressed in terms of the rate of deformation tensor D as follows.

$$\dot{\underset{\sim}{E}} = \underset{\sim}{F}^T \underset{\sim}{D}\, \underset{\sim}{F}$$

Hence,

$$\underset{\sim}{F}^T \underset{\sim}{D}\, \underset{\sim}{F} = \underset{\approx}{M} : \dot{\underset{\sim}{S}} + \underset{\sim}{A}\, \dot{\Theta} + \frac{\partial \underline{f}}{\partial \underset{\sim}{S}} \cdot \dot{\underline{\xi}} \; ,$$

or

$$\underset{\sim}{D} = (\underset{\sim}{F}^{T-1}) \left(\underset{\approx}{M} : \dot{\underset{\sim}{S}} + \underset{\sim}{A}\, \dot{\Theta} + \frac{\partial \underline{f}}{\partial \underset{\sim}{S}} \cdot \dot{\underline{\xi}}\right) \underset{\sim}{F}^{-1} \quad . \tag{247}$$

Now consider a change of reference frame.

$$\underset{\sim}{D}^* = (\underset{\sim}{F}^{T-1*})\,(\underset{\approx}{M}^* : \dot{\underset{\sim}{S}}^* + \underset{\sim}{A}^* \dot{\Theta}^* + (\frac{\partial f}{\partial \underset{\sim}{S}})^* \dot{\underline{\xi}}^*)\,\underset{\sim}{F}^{-1*} \tag{248}$$

From the previous discussion there follows,

$$\underset{\approx}{M}^* = \underset{\approx}{M} \;,\; \underset{\sim}{S}^* = \underset{\sim}{S} \;,\; \underset{\sim}{A}^* = \underset{\sim}{A} \;,\; (\frac{\partial \underline{f}}{\partial \underset{\sim}{S}})^* = \frac{\partial \underline{f}}{\partial \underset{\sim}{S}} \;,$$

$$\Theta^* = \Theta \;, \text{ and } \dot{\underline{\xi}}^* = \dot{\underline{\xi}} \;.$$

Using these results, Equation 248 becomes

$$\underset{\sim}{D}^* = \underset{\sim}{Q}\,\underset{\sim}{F}^{T-1}\,(\underset{\approx}{M} : \dot{\underset{\sim}{S}} + \underset{\sim}{A}\,\dot{\Theta} + \frac{\partial \underline{f}}{\partial \underset{\sim}{S}} \cdot \dot{\underline{\xi}})\,\underset{\sim}{F}^{-1}\,\underset{\sim}{Q}^T = \underset{\sim}{Q}\,\underset{\sim}{D}\,\underset{\sim}{Q}^T \tag{249}$$

The rate of deformation tensor is objective as shown by Malvern (1969). Therefore, the constitutive equation satisfies the principle of material frame indifference.

APPENDIX B

SURFACE SECTION TECHNIQUE AND IMAGE ANALYSES

This appendix briefly describes the technique used to obtain microstructural data from the field. This includes the surface section technique as well as the image analysis of the section.

Surface Section Preparation

The intent of a surface section is to provide an arbitrary two-dimensional picture of the microstructure for a given material. This picture can then be used to obtain three-dimensional microstructural information based on quantitative stereology. Briefly, the procedure for preparing a snow section is as follows.

A sample of snow is collected in a small metal container. A container on the order of 10 cm^2 is sufficient. The pore space of the sample is filled with a liquid whose temperature is below the melting point of ice thus preserving the microstructural integrity of the snow. Next, the specimen is frozen solid and microtomed to a smooth planar surface. Finally, the surface is polished and stained to enhance the ice/filller contrast in preparation for photographing. Perla (1982) provides an excellent review of preparation of section planes in snow specimens.

Obtaining a quality surface section is as much an art as it is a science. For instance, there is a wide variety of pore fillers and stains available. Each has its own unique characteristics and one must decide which of these is to be used. Furthermore, there are subtleties in the method which can significantly affect the results. For example, the degree of polishing as well as the amount of time the polished specimen is allowed to etch can affect the contrast. Finally, the difficulties are magnified when preparing sections in the field as opposed to the laboratory due to weather conditions and time constraints.

The chemical dimethyl phthalate (C_6H_4-1,2-($COOC_2H_5$)2) was chosen as a pore filler for the snow sections. This chemical is relatively inexpensive and has an approximate

melting point of +2°C. However, it is easily supercooled to temperatures below -5°C while experiencing no significant increase in viscosity.

Dry ice was used to freeze the sections in the field. This could usually be accomplished in 10 to 15 minutes. The specimens were then microtomed to a smooth surface and polished with lens tissue. Finally, the sections were allowed to etch a matter of minutes to bring out the edges of the ice/fillter interface.

One drawback to using dimethyl phthalate as a pore filler is that it is a colorless liquid. Therefore, oftentimes a dye is added to the liquid to enhance the photographic contrast between the ice and the filler. This did not prove to be successful for the dyes available so an alternative approach was sought. The solution was found by staining the surface of the sections with an "El Marko" pen in a manner similar to that in which one highlights a book. The pen would stain the dimethyl phthalate while leaving the ice alone. This proved to be a very quick and effective method. To prevent melting of the surface, the pens were cooled in dry ice while the sections were freezing. Various colors were tried with blue and black producing the best results.

An example of a section produced with this method is given in Figure 23. The section was photographed using a 55 mm macro lens on a standard 35 mm SLR camera. This is a critical step in the process and a larger macro lens would improve the image analysis procedure.

Image Analysis

The next step in the analysis procedure is to enhance the image (photograph) into three distinct phases as discussed in Chapter 5. For convenience, the three phases are repeated below.

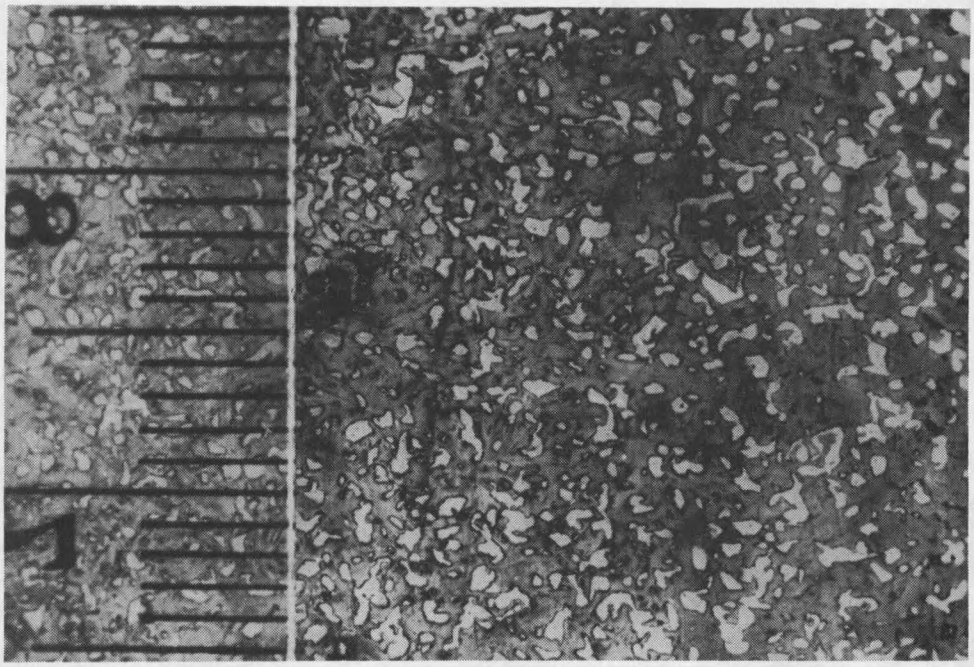

Figure 23. Photograph of a typical snow surface section.

α: ice grain phase

β: ice neck phase

γ: air phase

The image enhancement process is accomplished by digitizing the image on a high speed image analyzer and then numerically altering the digitized image. The enhancement of the digitized image is broken into two steps. First, the image is reduced from 256 gray levels to 2 gray levels representing either ice or air. Next, one must identify grain bonds in the section plane. Based on Kry's (1975a) operational definition of a grain bond, the following criteria are required to identify a bond.

1. A minimum constriction must exist in an ice grain cut by a section plane.
2. Both edges of the ice must show the constriction.
3. The notches must point approximately towards each other.

Once the bonds are identified, the neck regions are "painted" numerically on the image to represent the third phase. The neck region of a grain bond is defined as that area surrounding the bond where the grain surface goes from convex to concave with respect to an outward normal. A photograph of an enhanced surface section is shown in Figure 24.

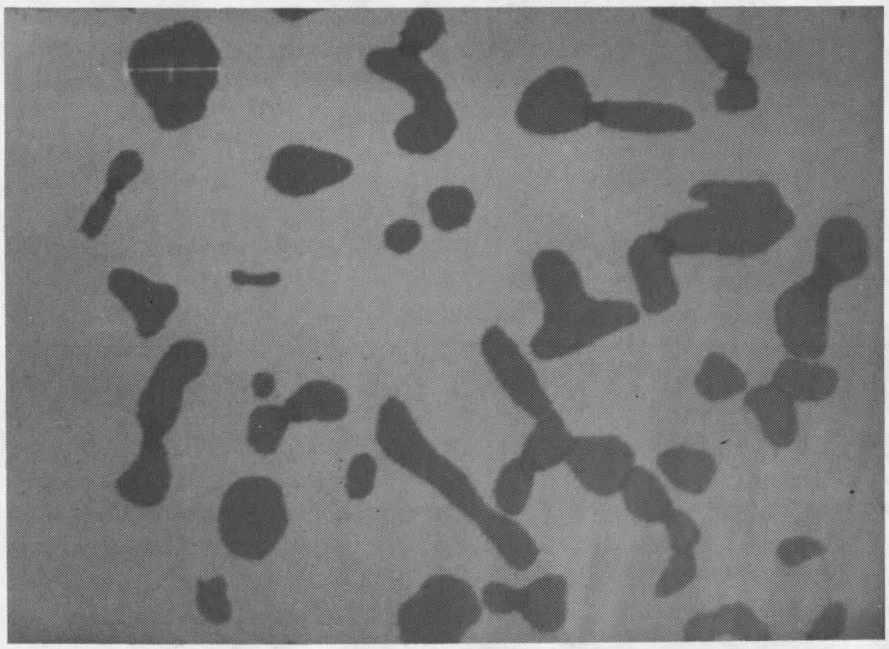

Figure 24. Photograph of a surface section after image enhancement.

Even with the above definitions, the actual determination of a grain bond is somewhat subjective. For instance, the area in question may be a grain bond or simply a necked down region of a single grain. However, in either case the areas in question represent similar microstructural features and will behave in a similar fashion under applied loads.

Once the image enhancement is complete, the actual image analysis is extremely easy as the theory of Chapter 5 has been written into a set of computer codes. The codes are not listed since a portion of them contain proprietary software. Furthermore, the codes are written explicitly for the specific image analysis system at Montana State University and would not be of use on alternate systems.